INVESTIGATION OF EQUILIBRIUM AND CHEMICAL KINETIC BEHAVIOUR OF DETONATION WAVES IN HYDROGEN-AIR MIXTURES AND AN EVALUATION OF THE OBLIQUE DETONATION WAVE AS THE COMBUSTOR FOR A SCRAMJET

by

Ahmed I. Sabet

A Thesis Submitted to the Graduate
Faculty of Rensselaer Polytechnic Institute
in Partial Fulfillment of the
Requirements for the degree of
MASTER OF ENGINEERING

Approved:

_____
Joseph E. Shepherd
Thesis Advisor

Rensselaer Polytechnic Institute
Troy, New York

May 1990

CONTENTS

LIST OF TABLES

LIST OF FIGURES

ACKNOWLEDGEMENT

I would like to express my deep gratitude to my advisor, Dr. Shepherd, for his patience and invaluable help in all aspects of this project, for giving me a sense of direction, and for making this portion of my educational career worthwhile.

I would also like to thank my mother and sister for all the moral support and encouragement they have given me through the years, and for providing me with a stable environment that has proven so valuable in this tumultuous world.

Last, and most important, I would like to thank Allah who taught me all I know.

ABSTRACT

Frozen and equilibrium Hugoniots were obtained for a variety of hydrogen-air detonations corresponding to different free stream compositions, temperatures, and pressures. The cross-over points were identified for each set of Hugoniots. For each set of Hugoniots, oblique detonation polars were generated which corresponded to various free stream Mach numbers. If possible, the deflection angle corresponding to the cross-over point was determined. As the free stream Mach number was increased, the cross-over point moved further along the polars in the direction of lower pressure ratio. The use of the flow deflection angle corresponding to the cross-over point as an upper bound instead of the maximum flow deflection angle severely restricts the range of useful flow deflection angles for oblique detonation waves.

Reaction zone structure was investigated for cases that corresponded to some of the generated polars. Comparison between the reaction zone structures obtained and those found in some of the recent literature indicates that some of the recent numerical analyses of detonations suffer from insufficient resolution of the reaction zone, which results in significant errors. The reaction zone structure is of the same form for the range of equilibrium states from the Chapman-Jouguet point to the cross-over point. The reaction zone structure for this regime consists

of a post-shock von-Neumann spike followed by a drop in pressure at a decreasing rate. The temperature jumps sharply after the shock wave, then remains constant in the short induction zone, then rises sharply in the reaction zone eventually leveling off to the equilibrium value. The range of equilibrium states above the cross-over point has a reaction zone structure similar in form to that at the cross-over point. For this regime, the reaction zone exhibits a von-Neumann "well" rather than a spike. The temperature drops at a decreasing rate behind the shock wave. The tendency of the flow to minimize the Gibbs free energy to reach equilibrium results in a drop in temperature in order that species of lower heats of formation may be formed. The thermal and kinetic components of energy are so high in this regime that the chemical energy release becomes negligible by comparison. Increasing the free stream Mach number within each of the two regimes results in a narrower reaction zone.

The location of the maximum rate of heat release should not be used for the determination of the reaction zone length for post-cross-over cases since it results in unrealistically long reaction zones.

The total pressure recovery factor across both plane and oblique detonation waves behaves in a manner similar to non-reacting shocks. The higher the normal component of the upstream Mach number, the more severe the total pressure

drop. The drop in the static pressure downstream of the wave outweighs the increase in total temperature across the wave, and the net result is therefore a lower total pressure downstream of the wave. A more rigorous analysis of the stagnation states across detonation waves should utilize the Gibbs free energy instead of the entropy since the flow through the wave is neither adiabatic nor frozen and thus both the chemical and thermal components of the enthalpy change across the wave.

A scramjet utilizing an oblique detonation for a combustor was designed for operation at a design point of 150,000 feet altitude and a flight Mach number of 20, using a stoichiometirc hydrogen-air mixture. A dissociative variable geometry inlet was designed. The inlet wedge angle for the design point is 9.576°, and the cowl further deflects the flow by 7.990°. The detonation wedge angle for the design point is 11.185°. The specific thrust is 274.67 m/s, and the air specific impulse is 28.01 sec, assuming equilibrium flow in the nozzle. For frozen nozzle flow, the specific thrust was 73.604 m/s. Various other design-points were considered. As the flight Mach number and altitude increased, the total pressure drop across the detonation and the specific thrust decreased, and the entropy rise across the inlet increased. The specific thrust increases with increasing loading factor.

If the flow in the nozzle is assumed to be frozen

then the specific thrust goes to zero at the cross-over point (overdrive parameter of 1.3843). If the flow in the nozzle is assumed to be in equilibrium then the specific thrust goes to zero at an overdrive parameter of 2.3. This indicates that the addition of fuel to hypersonic flows beyond the cross-over point and below a limiting value could be useful for thrust. The addition of fuel permits the formation of dissociation products which later recombine in the nozzle to form species of lower heats of formation. This reduces the enthalpy, and thus increases the nozzle exit velocity and specific thrust.

PART 1

INTRODUCTION AND HISTORICAL REVIEW

The study of supersonic combustion is very closely linked to developments in the field of hypersonic propulsion. Extensive investigations of the use of detonation waves and other supersonic combustion schemes were done in the late fifties and early sixties when hypersonic air-breathing propulsion systems were being considered to power single-stage-to-orbit vehicles. With the development of the Space Shuttle and the appearance of the energy crisis, funding for hypersonic research waned and activity in that field (at least in the United States) came to a halt. Interest in hypersonic propulsion was revived in the early eighties when the National Aerospace Plane (NASP) project was initiated.

One of the most important areas of supersonic combustion research is that of detonative combustion. A supersonic combustion ramjet (scramjet) utilizing a detonation wave as its engine was always a very attractive idea since the length of the combustor would be reduced to the order of magnitude of the thickness of the detonation wave. This results in a very short combustor (of the order of a few millimeters), which in turn reduces heat transfer, and relaxes the thermal stress requirements on the combustor material. An additional advantage would be that the free stream flow would not have to be diffused to very

low velocities since part of the compression process would be carried out by the detonation wave itself. Thus, the total pressure losses across the inlet diffuser are considerably reduced. This last advantage, however, is offset by the fact that there are large pressure losses across the detonation wave, mainly due to the shock wave that precedes the reaction zone.

Thus the need for both experimental and theoretical investigations of detonation wave phenomena was recognized very early on in hypersonic research. Although the general field of supersonic combustion was investigated as early as 1881 by LeChatelier, Berthelot, and Mallard, it was not until Chapman (1) and Jouguet (2) that concepts were put forth which permitted the mathematical solution of the detonation velocity problem. The next step was in the mid fifties when detonation waves were studied as means of providing a steady release of chemical energy in supersonic flow. Examples of such work are the studies made by Dorsh, Fletcher, et al. (3), and Nicholls, Dabora, and Gealer (4). Up until that time it was believed that the Chapman-Jouguet detonation was the only stable solution to the problem of a reactive shock wave (which is one way of modeling a detonation wave). This belief was supported by the fact that until the late fifties, only Chapman-Jouguet detonations were stabilized in laboratories. However, Gross and Chinitz (5) claim to have been able to stabilize both

plane and oblique strong detonation waves in experiments. More recently, Sichel et al (6) have conclusively shown that it is possible to stabilize oblique detonation waves. Although the existence of weak detonation waves is predicted by Chapman-Jouguet theory, it has not been possible, to this day, to stabilize a weak detonation wave. This is mainly due to the fact that weak detonation waves require a special relation between chemical kinetics and the dynamics of the flow (reference (7)).

Most of the work done in the fifties and sixties was restricted to simple geometries in conjunction with various simplifying assumptions such as perfect gas mixtures, constant molecular weight and ratio of specific heats across the wave, instantaneous heat addition, neglecting dissociation, and neglecting chemical kinetics. The need for such assumptions stemmed from the complexity of the problem. The increased availability of the digital computer has made it possible to relax some of those assumptions, although some of them are still kept in the interest of saving computational time and programming effort (reference (8)). In general, the ideal gas mixture assumption is a reasonable one, while the constant molecular weight and constant ratio of specific heats (γ) and the neglect of dissociation yield unreliable results. Chemical kinetics are typically used only to determine reaction zone structure, and thus are not considered in cases when only

the equilibrium gas composition is of interest.

As interest in hypersonic research was revived, a lot of recent papers have been devoted to investigations of oblique detonations and their application to scramjet propulsion. Most of this work consists of numerical simulations such as the work done by Pratt, Humphrey, and Glenn (9), Cambier, Adelman, and Menees (10), Chuck and Eberhardt (11), Fort and Pratt (12), and Eidelman, Grossman, and Lottati (13).

Some of the recent analyses present results that are at variance with steady, stationary oblique detonation wave theory, and most of them fail to model the reaction zone accurately. There is also some experimental work such as that carried out by Hertzberg et al (14), by Dabora, Wagner, and Desbordes (15), and Dabora and Wagner (16).

Most current and recent work on the application of detonation waves to propulsion assumes that there is no practical limit on how overdriven the waves could be.

This thesis has three objectives. The first is to investigate the effect of overdriving oblique detonation waves, and thus determine the practical limit on detonation wave overdrive for propulsion applications. This is done by means of constructing detonation wave polars of static pressure ratio versus flow deflection angle. This is done numerically by using the results of a chemical equilibrium computer code applied to some of the cases found in recent

literature, namely references (10) and (15). An analysis is first made using the free stream velocities given in those references, and then further analyses are made using higher free stream velocities.

The same cases are also used to investigate the reaction zone structure by utilizing a chemical kinetics computer code which uses the Zeldovich-von Neumann-Döring model. Of particular interest is the reaction zone length, and the temperature, pressure, and species profiles in the reaction zone.

The last objective is to apply the oblique detonation wave concept to propulsion using a simplified model of a scramjet. The emphasis in this case is on the total pressure drop across the detonation wave, and on engine performance parameters such as thrust per unit area, air specific impulse, specific fuel consumption, and thermal efficiency. It should be noted that Sargent and Gross (17) did similar work in 1959, but they neglected the effects of dissociation based on the argument that the rates of the chemical reactions compared to the velocity of the flow may not allow the attainment of equilibrium. Other differences from (17) are the use of hydrogen as fuel instead of a hydrocarbon, and the use of a design point that is at a higher altitude and higher Mach number to better approximate the possible design point of the NASP.

PART 2

THEORY

2.1 Overview of Detonation Wave Structure

A rigorous treatment of detonation waves requires a three-dimensional analysis. This is due to the cellular structure of detonation wave fronts. For a full discussion of the three-dimensional nature of detonations the reader is referred to Lee (18). However, it has been observed by (19) and others that as the detonation wave becomes very overdriven, the cell size becomes smaller. The cell size goes to zero for a value of the overdrive parameter (the ratio of the normal component of the free stream Mach number to the Chapman-Jouguet Mach number (M_{CJ})) of about 1.3 for hydrogen-oxygen mixtures. It is not yet clear whether the cellular structure actually disappears, or the cells just become so small that they can no longer be detected. This observation has been the primary motivation for the use of overdriven waves since the disappearance of the cellular structure allows a two-dimensional treatment of the wave and eliminates the inherent three-dimensional instability. Most of the cases discussed in this thesis have an overdrive parameter of 1.28 or higher, and thus it was felt that a two-dimensional treatment is justified. For a full treatment of detonation waves including their three-dimensional nature, the reader is strongly urged to consult chapter 9 of Strehlow (20). The following is a brief

summary of the nature of detonation waves.

2.2 The ZND Model and Oblique Detonation Polars

A simple yet powerful model of a two-dimensional detonation wave is the Zeldovich-von Neumann-Döring (ZND) model. In this model the detonation wave is treated as a non-reactive shock wave which serves to compress the flow and raise the temperature of the gases above the ignition point. This shock compression results in what is called the von-Neumann spike which can be seen in figure (1). Following the shock wave is an induction zone which is then followed by the reaction zone where most of the chemical heat release is obtained. The reaction zone is assumed to be steady and one-dimensional. The model also assumes that the C-J condition is asymptotically approached. The jump conditions across the normal detonation wave are obtained through the application of the conservation laws across the discontinuity. This yields:

$$\rho_1 w_1 = \rho_2 w_2 \tag{1}$$

$$p_1 + \rho_1 w_1^2 = p_2 + \rho_2 w_2^2 \tag{2}$$

$$h_1 + \frac{w_1^2}{2} = h_2 + \frac{w_2^2}{2} \tag{3}$$

where w denotes the normal velocity component. It should be noted that equation (3) merely states that the total enthalpy is conserved across the wave, a fact which shall be used later on in this thesis to compute the total pressure drop across the wave. The equations can be solved once an equation of state is selected and the enthalpies

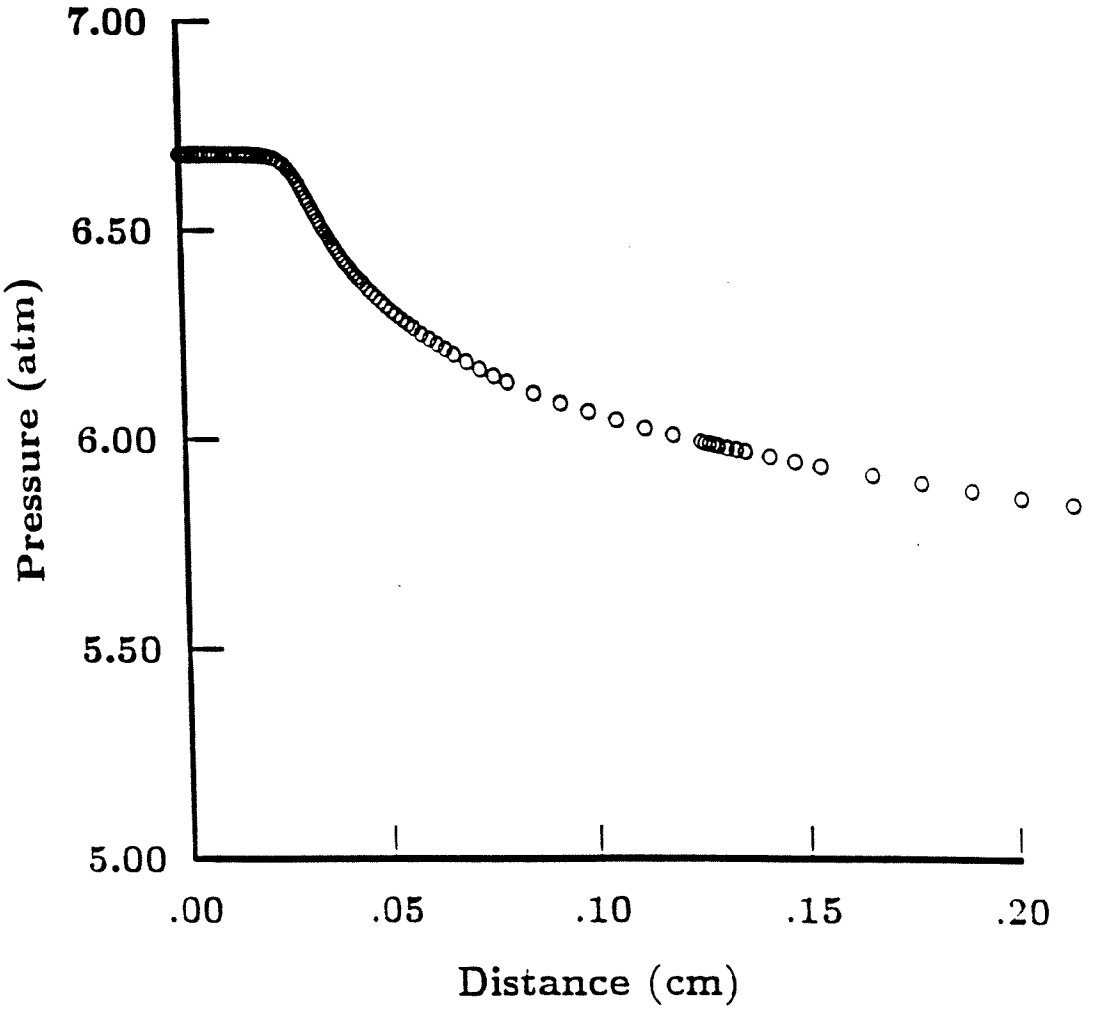

Figure 1. Typical pressure profile within the reaction zone of a detonation wave. Pressure at a distance of zero is the von-Neumann (post-shock) pressure. The plot is for case 2 of this thesis.

are expressed as a function of temperature and heat release. This yields four equations (conservation of mass, momentum, and energy, and equation of state), and four unknowns (pressure, density, enthalpy, and velocity). The equations are usually solved in terms of the upstream and downstream Mach numbers. The result is usually plotted on a P-v diagram and is referred to as a Hugoniot. Figure (2) shows a typical set of equilibrium and frozen Hugoniots. The frozen Hugoniot corresponds to the locus of possible states behind a non-reacting shock wave given the upstream conditions. Each point corresponds to a given upstream normal velocity. The equilibrium Hugoniot is similar except that the points now correspond to the various equilibrium states attainable behind the detonation wave given the upstream thermodynamic condition, composition, and normal velocity. The straight lines drawn on figure (2) are known as Rayleigh lines. They are lines that pass through the initial (upstream) state and cross both the equilibrium and frozen Hugoniots. The actual path from the initial state to the final equilibrium state is thus as follows. The non-reactive shock preceding the reaction zone corresponds to moving along the frozen Hugoniot from the initial state to the point of intersection between the Rayleigh line and the frozen Hugoniot. The reaction zone then corresponds to moving down along the Rayleigh line from the point of intersection with the frozen Hugoniot to the point of

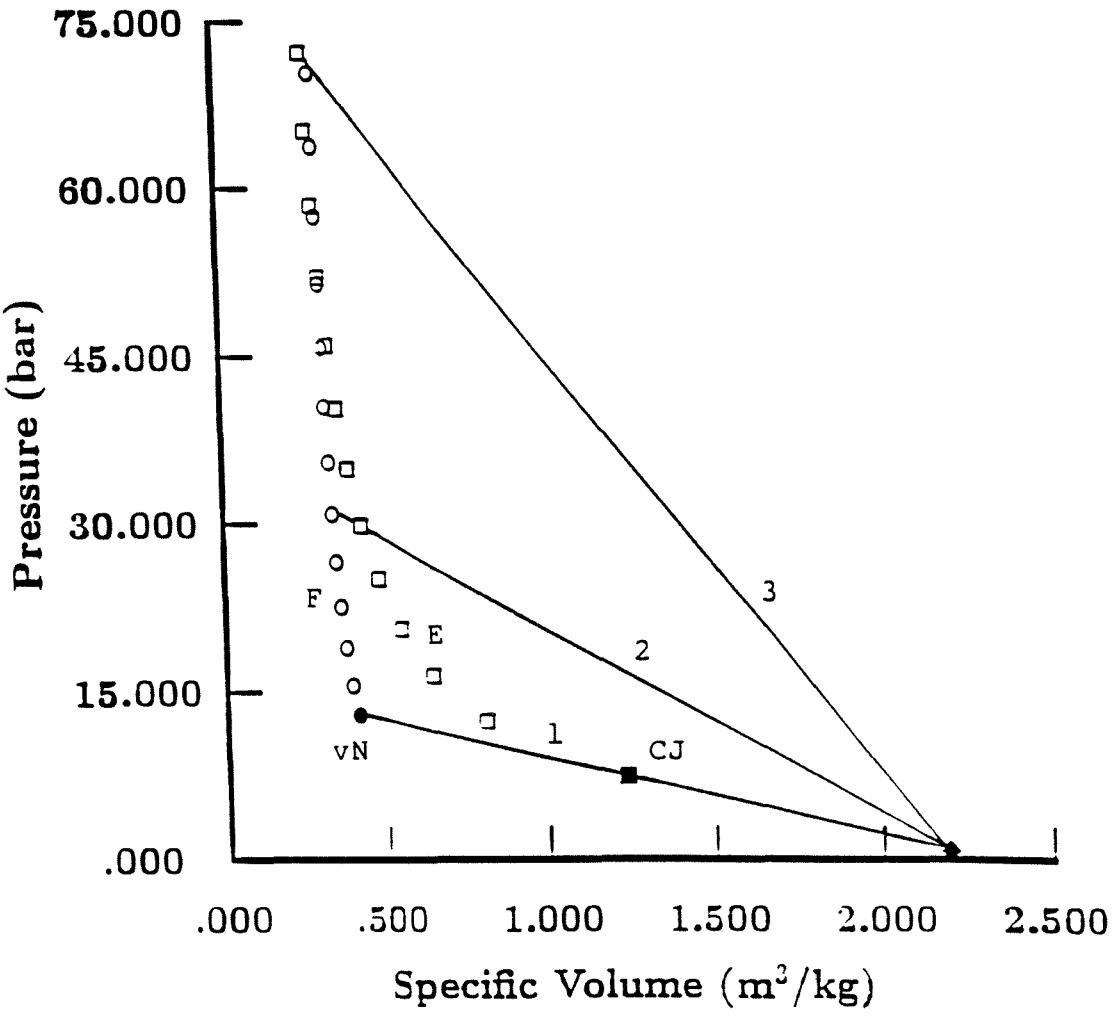

Figure 2. Typical frozen (F) and equilibrium (E) Hugoniots for a detonation wave, showing the various possible Rayleigh lines. The plot is for cases 6 through 13 of this thesis.

intersection with the equilibrium Hugoniot. Note that the Rayleigh line will always have two intersections with the equilibrium Hugoniot except in the limiting case when the Rayleigh line is actually tangent to the equilibrium Hugoniot. This is shown as line 1 in figure (2). When this is the case, the point of tangency corresponds to the minimum upstream normal Mach number that is required to reach the equilibrium Hugoniot. This minimum Mach number is referred to as the Chapman-Jouguet (CJ) Mach number (M_{CJ}), and is only a function of the mixture composition and the conditions at the upstream state. All other Rayleigh lines correspond to overdriven detonation waves where the upstream normal Mach number is larger than M_{CJ}. Such a line is shown in figure (2) as line 2. The figure shows only one intersection point which corresponds to the strong solution. In principle, there are two intersection points corresponding to two solutions, a "strong" one in which the flow behind the wave is subsonic, and a "weak" one in which the flow behind the wave is supersonic. The weak solution is possible in principle provided certain special relations between chemical kinetics and flow dynamics are met (reference (7)).

Figure (2) also shows that the equilibrium and frozen Hugoniots can actually cross, a fact which is overlooked by most people. Line 3 corresponds to an equilibrium state that is above the cross-over point.

In a simplified analysis where only the equilibrium final state is of interest, the rates of the chemical reactions are not important. Only the heats of reaction and equilibrium composition are required for the determination of the final state.

An oblique detonation can be treated as an equivalent normal detonation. This is done by considering an orthogonal frame of reference in which the wave lies along one of the axes. In this case only the normal component of velocity plays a role in the solution. The tangential velocity component remains unchanged. Note that for oblique detonation waves, the requirement becomes that the normal Mach number is larger than or equal to M_{CJ}. From figure (3) it is clear that the equations for the upstream and downstream normal velocity components are given by:

$$w_1 = u_1 \sin\beta \tag{4}$$

$$w_2 = u_2 \sin(\beta - \theta) \tag{5}$$

where w_1 and w_2 are the normal components of velocity upstream and downstream of the wave, respectively. The net velocities upstream and downstream of the wave are u_1 and u_2, respectively. β is the detonation wave angle, and θ is the flow deflection angle. Noting that the tangential component of velocity, v, does not change across the wave, one can write:

$$w_2 = v \tan(\beta - \theta) \tag{6}$$

$$w_2 = u_1 \cos\beta \tan(\beta - \theta) \tag{7}$$

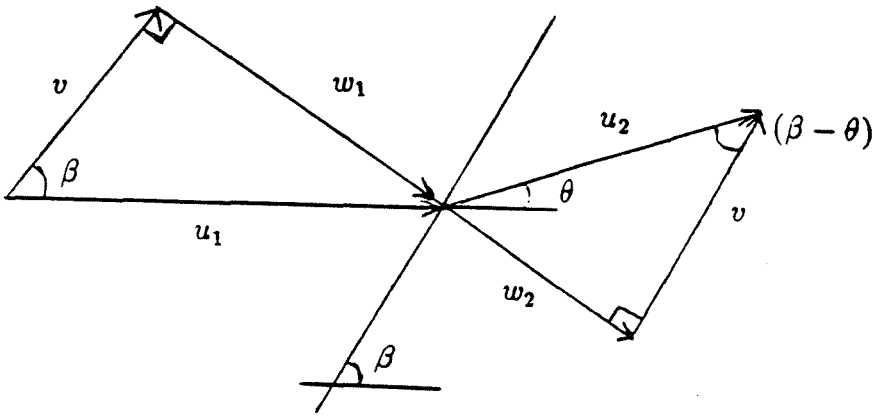

Figure 3. Velocity triangles upstream and downstream of an oblique detonation wave.

The detonation wave problem consists of finding w_2 given w_1. Once w_2 is known, the problem becomes that of finding β and θ given w_1 and w_2 through the following relations:

$$\beta = \sin^{-1}(w_1/u_1) \tag{8}$$

$$\theta = \beta - \tan^{-1}\frac{w_2}{u_1 \cos\beta} \tag{9}$$

Figure (4) shows a typical oblique detonation wave with two representative streamlines. It is interesting to note that while the flow deflects towards the wave as it goes through the adiabatic shock, it deflects away from the wave after passing through the reaction zone. This is due to the energy released by the chemical reactions. It should be pointed out that the flow does not deflect away from the wave through the reaction zone except for equilibrium states that fall below the cross-over point of the equilibrium and frozen Hugoniots. This is because the pressure gradient along the streamline becomes positive instead of negative for states above the cross-over point.

By solving the detonation problem for various values of w_1 (which corresponds to a constant u_1 and varying β), one can then obtain a detonation wave polar. It would be of interest to plot the equilibrium composition polar on the same set of axes as the frozen (non-reacting, adiabatic shock wave) polar. Figure (5) shows a typical pair of equilibrium and frozen polars. The frozen polar corresponds to the initial shock wave in the ZND model. An intersection of the two polars would indicate the point at which the

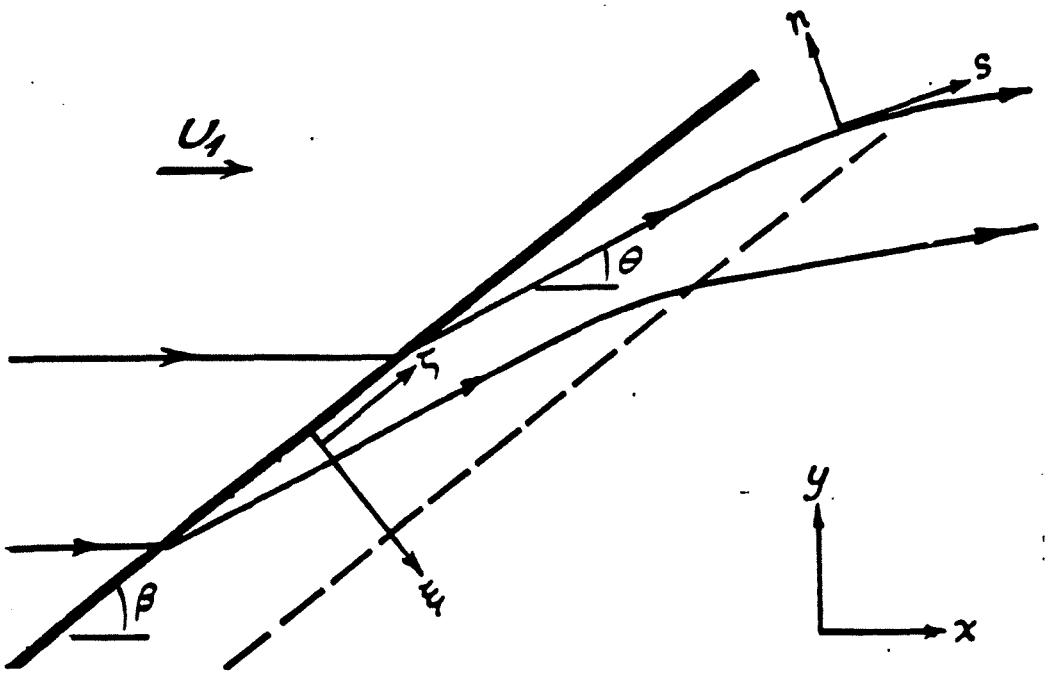

Figure 4. A schematic of an oblique detonation wave showing the deflection of two typical streamlines.

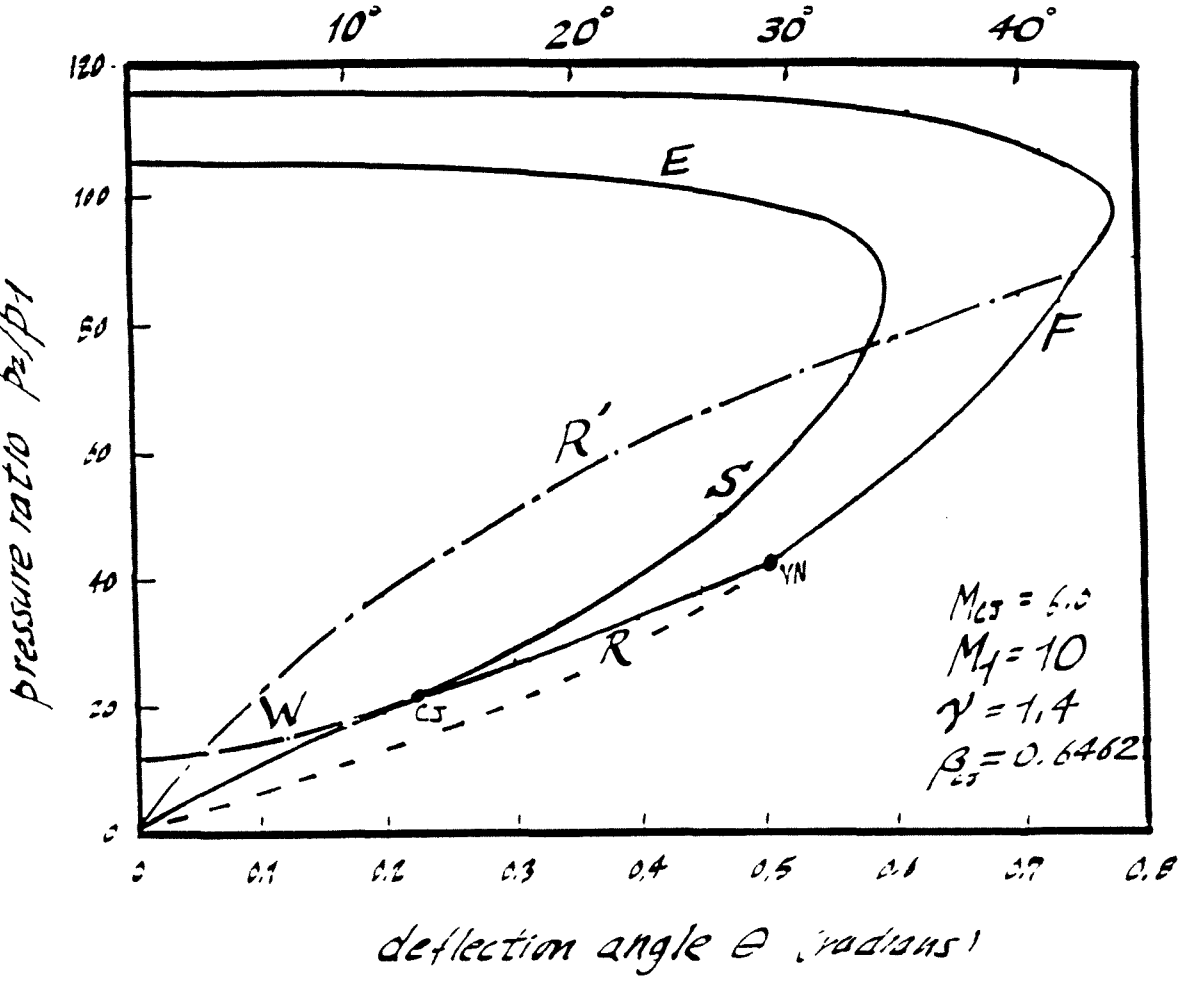

Figure 5. Typical equilibrium (E) and frozen (F) polars showing the CJ point and the von-Neumann point (vN). (S) denotes the strong branch, and (W) denotes the weak branch. (R) indicates the Rayleigh line. (M_{CJ}) is the CJ Mach number, (M_1) is the free-stream Mach number, (γ) is the ratio of specific heats, and (β_{CJ}) is the CJ detonation wave angle. The solution is for an ideal gas with constant ratio of specific heats and constant heat addition, q.

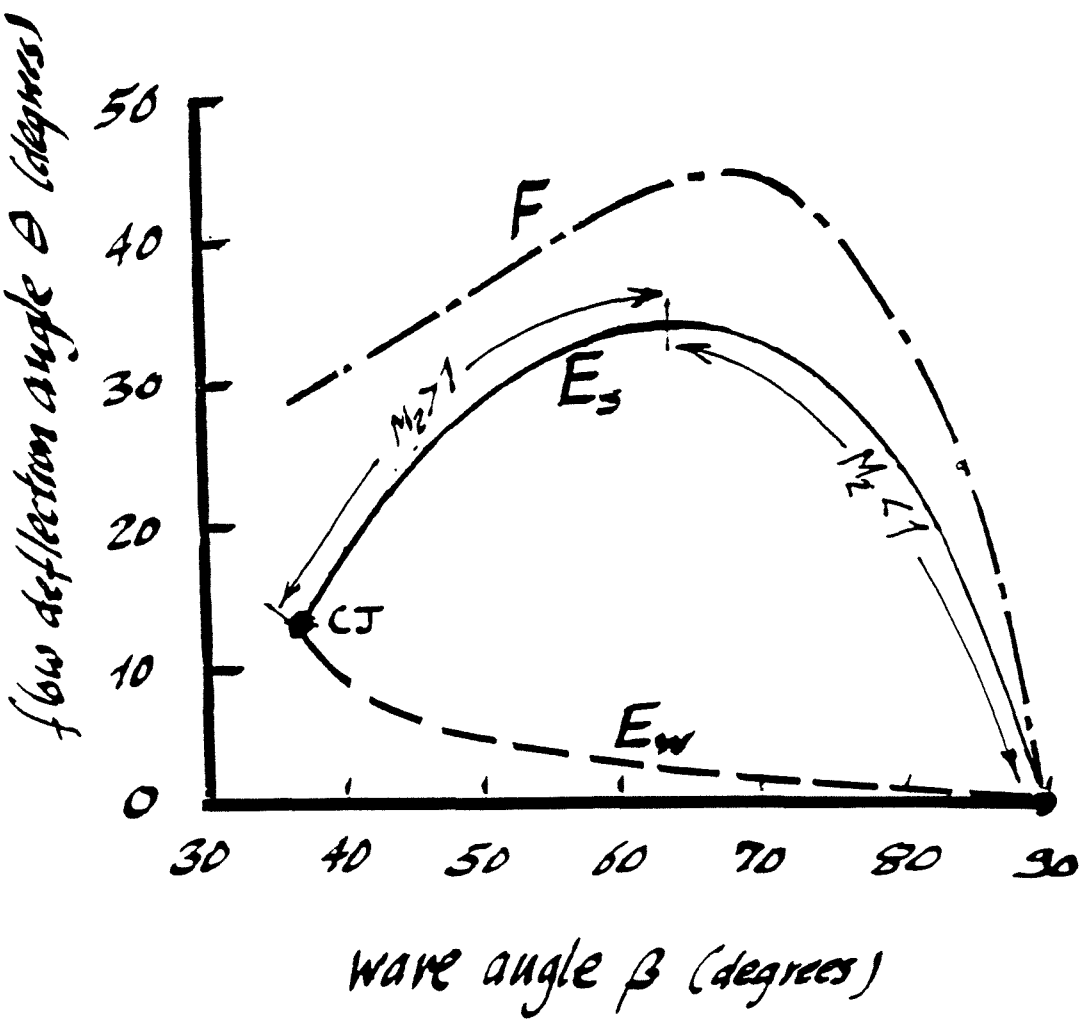

Figure 6. Plot of the flow deflection angle versus the wave angle for the polar set shown in figure (5). (F) denotes the frozen curve, (E_s) denotes the strong branch of the equilibrium curve, (E_w) indicates the weak branch of the equilibrium curve, and (CJ) denotes the CJ point.

detonation wave results in the same pressure and density as a non-reacting shock wave. This seems to indicate that the propulsive efficiency (or the specific thrust) of an engine using highly overdriven detonation waves would be much lower than what had been previously expected.

Figure (6) shows the plots of flow deflection angle versus wave angle corresponding to the polar set shown in figure (5). The figure clearly shows that the flow deflection angle varies from zero to the CJ flow deflection angle, and has a maximum in between. A flow deflection angle of zero corresponds to a normal detonation wave. The wave angle monotonically increases from the CJ value to 90 degrees which then corresponds to a normal detonation wave.

2.3 Reaction Zone Structure

The reaction zone of the detonation wave requires the introduction of a chemical kinetic mechanism. For two-dimensional flow, it is convenient to utilize curvilinear system of coordinates. In such a system, one axis (s) is along the streamline, and the other axis (n) is orthogonal to it. Using this coordinate system, one can then write the various conservation and process equations in a form that lends itself to numerical integration using a computer code. The following relations were taken from Shepherd (21).

The adiabatic change equation is given by reference (7) as:

$$\frac{\partial p}{\partial s} = a^2 \frac{\partial p}{\partial s} + \rho a^2 \sigma_k \frac{\partial y_k}{\partial s} \tag{10}$$

where a is the local speed of sound, the subscript 'k' denotes species 'k', and y_k is the mass fraction of species 'k'. The rate of change of y_k is given by:

$$\rho u \frac{\partial y_k}{\partial s} = W_k \omega_k \tag{11}$$

where u is the flow velocity, W_k is the molecular weight of species 'k', and ω_k is the net molar production rate of species 'k'. The conservation of momentum is given by the following two equations (reference (22)):

$$\rho u \frac{\partial u}{\partial s} = -\frac{\partial p}{\partial s} \tag{12}$$

$$\rho u^2 \frac{\partial \theta}{\partial s} = -\frac{\partial p}{\partial n} \tag{13}$$

where θ is the angle that the streamline makes with the direction of the flow upstream of the wave. The continuity equation takes the following form:

$$\frac{\partial (\rho u)}{\partial s} = -\rho u \frac{\partial \theta}{\partial n} \tag{14}$$

The flow can be assumed to be irrotational, and thus:

$$u \frac{\partial \theta}{\partial s} = \frac{\partial u}{\partial n} \tag{15}$$

Finally, it is necessary to make use of translational invariance along the wave as given by:

$$\frac{\partial}{\partial n} = \frac{-1}{\tan(\beta - \theta)} \frac{\partial}{\partial s} \tag{16}$$

Combining equations (15) and (13) yields:

$$\rho u \frac{\partial u}{\partial n} = -\frac{\partial p}{\partial n} \tag{17}$$

which when combined with equation (16) yields equation (12). Therefore, equation (13) can be replaced with equation (15). Combining equations (10) and (12), and using the following equation from (21):

$$\frac{\partial \rho}{\partial s} = -\frac{\rho}{u \sin^2(\beta - \theta)} \frac{\partial u}{\partial s} \tag{18}$$

yields:

$$\frac{\partial \rho}{\partial s} = \frac{\rho \sigma_k}{Z} \frac{\partial y_k}{\partial s} \tag{19}$$

$$Z = M^2 \sin^2(\beta - \theta) - 1 \tag{20}$$

But since:

$$M \sin(\beta - \theta) = M_n \tag{21}$$

where M_n is the normal Mach number downstream of the wave, therefore equation (18) becomes:

$$\frac{\partial \rho}{\partial s} = -\frac{\rho \sigma_k}{1 - M_n^2} \frac{\partial y_k}{\partial s} \tag{22}$$

Thus, the five equations that have to be solved are:

momentum:

$$\rho u \frac{\partial u}{\partial s} = -\frac{\partial p}{\partial s} \tag{23}$$

continuity:

$$\frac{\partial (\rho u)}{\partial s} = \frac{\rho u}{\tan(\beta - \theta)} \frac{\partial \theta}{\partial s} \tag{24}$$

irrotational:

$$u \frac{\partial \theta}{\partial s} = \frac{-1}{\tan(\beta - \theta)} \frac{\partial u}{\partial s} \tag{25}$$

adiabatic:

$$\frac{\partial p}{\partial s} = a^2 \frac{\partial \rho}{\partial s} + \rho a^2 \sigma_k \frac{\partial y_k}{\partial s} \tag{26}$$

species:

$$\rho u \frac{\partial y_k}{\partial s} = W_k \omega_k \tag{27}$$

where the five unknowns are ρ, u, p, y_k, and θ. These equations are usually programmed into a computer code and solved numerically. In most cases the numerical integration is done with time as the independent variable rather than spatial coordinates. The time-dependent equations are given in reference (23) as:

$$\frac{dp}{dt} = -\frac{u^2\sigma}{\eta} \tag{28}$$

$$\frac{d\rho}{dt} = -\frac{\sigma}{\eta} \tag{29}$$

$$\frac{dy_i}{dt} = \frac{W_i\omega_i}{\rho} \tag{30}$$

where sigma is the volume rate of change per unit mass due to reaction:

$$\sigma = -\sum_{i=1}^{N}\left(\frac{\partial\rho}{\partial y_i} + \frac{\rho}{c_pT}h_i\right)\frac{dy_i}{dt} \tag{31}$$

and η is the gas dynamic parameter:

$$\eta = 1 - M^2 \tag{32}$$

where M is the Mach number.

The following section describes how the relations discussed above can be incorporated within, and used in conjunction with computer codes to obtain detonation wave polars and reaction zone structure.

PART 3

METHOD OF PROCEDURE

3.1 Hugoniots and Oblique Detonation Polars

The relations developed in the previous section for the equilibrium final state for oblique detonation waves were employed to obtain detonation polars. This was done using the cases given in Cambier, Adelman, and Menees (10), and the case presented in Dabora, Wagner, and Desbordes (15). The initial conditions, mixture composition and CJ velocity for each of these cases are shown in table (1).

The procedure consisted of executing a FORTRAN computer code called STANJAN which was developed by Reynolds (24). The program is a chemical equilibrium computer code and relies on the basic fact that the equilibrium composition problem is one in which the Gibbs free energy for the entire mixture is minimized:

$$dG = 0 \tag{33}$$

For a complete discussion of the computer code and the principles behind it, the reader is referred to Reynolds (24).

A special version of the STANJAN program was created at Rensselaer Polytechnic Institute to perform the present analysis. Several modifications were made to the program during the course of this thesis to enable the analysis of highly overdriven detonations. This was necessary because for the frozen analyses, the temperatures immediately after

Table 1. Initial conditions, mixture compositions, and CJ velocities for the cases considered.

Case	Temperature (K)	Pressure (atm)	Composition (mol %)	CJ Velocity (m/s)
1	840.0	0.06	H_2: 20.1 O_2: 16.8 N_2: 63.1	1648.4
2	450.0	0.32	H_2: 20.1 O_2: 16.8 N_2: 63.1	1700.1
6	298.16	0.50	H_2: 24.03 O_2: 16.28 N_2: 59.69 (stoich.)	1824.2

the shock for the cases considered were sometimes in excess of the 6000 K limit which was set by Reynolds in the original code. Beyond 6000 K the code extrapolated specific heat data, which yielded unreliable results. Two new features were added to the RPI version of STANJAN. Data from the most recent NASA thermodynamic fits were used, so that the program can now handle product mixture temperatures of up to 20000 K. The thermodynamic curve-fits were obtained from McBride (25). The ability to compute the composition and state for a mixture that has the same entropy as the product mixture of a previous run, but with a specified enthalpy was added to the RPI version of STANJAN. This option enables the computation of stagnation properties.

The output of STANJAN consists of the thermodynamic properties of the mixture (such as temperature, pressure, specific volume, enthalpy, internal energy, and entropy), in addition to the mass fractions, specific heat at constant pressure and the ratio of specific heats. The program also outputs the post-shock velocity relative to the upstream velocity for the Chapman-Jouguet and shock wave options.

The first part of the work done in this thesis consisted of obtaining the equilibrium and frozen Hugoniots and polars for the above mentioned cases. The starting point was to execute the Chapman-Jouguet (C-J) option of

STANJAN to determine the C-J velocity. This would be the minimum normal velocity and would correspond to one set of end points on both the frozen and equilibrium Hugoniots. It also corresponds to the minimum flow deflection angle.

The next step consisted of a trial and error procedure in which the shock option of STANJAN was executed using a frozen composition. A frozen composition simply means that the product mixture was specified to contain only the reactants, which therefore corresponds to a non-reactive shock wave. The trial and error process was continued until the product mixture had a temperature of about 20000 K. This represented the upper limit on the normal component of velocity which in turn corresponds to the maximum possible free stream velocity, since the maximum upstream normal velocity is obtained for a flow deflection of zero which corresponds to a normal detonation and means that the the normal upstream velocity component is the free stream velocity. This maximum free stream velocity point also defines the other set of end points on both frozen and equilibrium Hugoniots. Note that the maximum free stream velocity point is just the result of the limitation on the temperatures that STANJAN can handle and yield reliable results (20000 K or less). The maximum free stream velocity for case 4 of Cambier, Adelman, and Menees (10) was 8100 m/s, and for the Dabora case (15) it was 8347 m/s.

Once the extreme points were determined the equilibrium and frozen Hugoniots were then obtained. The equilibrium Hugoniot was obtained by executing the shock option of STANJAN for the range of normal upstream velocity from the C-J velocity to the maximum free stream velocity while including every possible species in the product mixture. This included molecules, free radicals, atoms, ions, and electrons to account for chemical reaction, dissociation, and ionization. The species that were included in the equilibrium product mixture were: H_2, O_2, N_2, H, O, N, OH, H_2O, H_2O_2, HO_2, NO, H_2^+, O_2^+, N_2^+, H^+, O^+, N^+, H_2O^+, OH^+, NO^+, and electrons. The thermodynamic, composition, and velocity data for each point along the equilibrium Hugoniots considered in this thesis are included in Appendix A.

The frozen Hugoniot was obtained in a similar manner, except that the product mixture contained only the reactants. This corresponds to the desired non-reactive (frozen) shock wave. The thermodynamic and velocity data for each point along the frozen Hugoniots considered in this thesis are shown in Appendix B.

The next step was to plot the frozen and equilibrium Hugoniots on the same set of axes to determine the cross-over point. This is the point where the pressure and specific volume behind the reaction zone are the same as those behind the non-reactive shock wave.

Having obtained the frozen and equilibrium Hugoniots for each case, it was then possible to construct the equilibrium and frozen polars. Note that the Hugoniots obtained by the above procedure cover a much wider range of normal upstream velocities than that allowed by the free stream velocities stated in the cases under investigation. Thus it was possible to obtain various sets of polars which corresponded to various free stream velocities. One of those sets, of course, corresponded to the conditions given in the cases under study.

For each set of polars the procedure consisted of the following. If the Hugoniot data did not provide sufficient points (around twenty) for a w_2 versus w_1 relation, then additional runs of STANJAN were executed. This was the case for low free stream velocity polar sets, since the maximum free stream velocity for the Hugoniots was quite high.

Once sufficient points were available for a w_2 versus w_1 relation, the relation was obtained through a least-squares curve-fit.

The next step was to write a FORTRAN computer code (P.FOR) which enabled the computation of the flow deflection angle from equation (9), and the pressure ratio across the wave from equation (2) using the relation between w_2 and w_1 obtained above. A copy of P.FOR is included in Appendix C. The next step was to plot the equilibrium and frozen polars on the same set of axes and

determine the flow deflection angle which corresponds to the cross-over point.

Note that this procedure for obtaining the frozen and equilibrium polars is quite different from the technique used by Liou (8). Liou's procedure consists of establishing relations between the isentropic exponent and temperature downstream of a CJ detonation wave as functions of the upstream Mach number. Using those relations he then proceeds to determine the average ratio of specific heats downstream of the wave. From this it is then possible to compute the parameter F which is only a function of heat release, upstream Mach number, and the average ratios of specific heats upstream and downstream of the detonation wave. Once F is determined, then the density, pressure, and temperature ratios can be determined from the constant gamma heat addition model where the gamma is the CJ downstream gamma. Having the density ratio it is then possible to compute the flow deflection angle and wave angle and plot them as functions of the pressure ratio. The procedure presented in this thesis avoids the problem of having to approximate the downstream ratio of specific heats. This is done by avoiding any attempt to use a constant gamma model. The procedure makes use of curve-fits which relate the upstream and downstream normal velocity components. The points for those curve-fits are obtained as described above, by executing a chemical equilibrium code

for various upstream normal velocities. This does not put this procedure at any disadvantage compared to Liou's procedure since the latter also used a similar procedure to arrive at the functional relations between the isentropic exponents and the temperature as functions of the upstream Mach number. Once those velocities are known, the flow deflection and wave angles are immediately known. The momentum and mass conservation equations are then used to evaluate the pressure ratio. Thus there are no approximations involved. There is no need to base everything on the CJ point. In fact the only limitation of this approach is how good the curve-fits are. The coefficients for the curve-fits relating the upstream and downstream normal velocities for the cases considered in this thesis are given in Appendix D.

A modified version of P.FOR was used to obtain plots of the maximum, cross-over, and CJ flow deflection angles versus approach Mach number. A copy of the source code for this version (called MOD2.FOR) is enclosed in Appendix E. The program makes use of the fact that the normal upstream velocity for both the CJ case and the cross over case are known. The curve-fits of w_1 versus w_2 are then used to get the corresponding downstream normal velocities. Knowing the normal velocities and the free stream velocity it was then possible to compute the CJ and cross-over flow deflection angles for each free stream velocity. To compute the

maximum flow deflection angle it was necessary to obtain the derivative of the flow deflection angle with respect to the upstream normal velocity (using equation (9) from the theory section above). A root-solver was then used to solve for the value of the upstream normal velocity which would make this derivative zero. Once this was done, the downstream normal velocity was obtained using the curve-fits, and the maximum flow deflection angle was computed.

3.2 Reaction Zone Structure

The second part of the work done in this thesis consisted of using a detailed chemical mechanism for hydrogen-air combustion and a FORTRAN computer code to determine the ZND reaction zone structure. The code solves the system of ordinary differential equations which were given in part 2 above (equations (28) through (32)). In addition to those equations, the ideal gas equation of state is used:

$$p = \rho RT \tag{34}$$

The enthalpy is treated as a function of temperature only and is given by:

$$h = \sum_{i=1}^{N} y_i h_i(T) \tag{35}$$

where:

$$h(T) = \Delta h^0_{f,298} + \int_{298}^{T} c_p(T)\, dT \tag{36}$$

where JANNAF data are used for both h_f and c_p.

The reaction mechanism used is shown in table (2).

Table 2. Reaction mechanism used in the computer code ZND.FOR.

	REACTION	A	β	E
1.	$H_2 + O_2 \rightleftharpoons OH + OH$	1.70×10^{13}	0.00	47780.
2.	$OH + H_2 \rightleftharpoons H_2O + H$	1.17×10^{9}	1.30	3626.
3.	$H + O_2 \rightleftharpoons OH + O$	5.13×10^{16}	-0.82	16507.
4.	$O + H_2 \rightleftharpoons OH + H$	1.80×10^{10}	1.00	8826.
5.	$H + O_2 + M \rightleftharpoons HO_2 + M$	2.10×10^{18}	-1.00	0.
6.	$H + O_2 + O_2 \rightleftharpoons HO_2 + O_2$	6.70×10^{19}	-1.42	0.
7.	$H + O_2 + N_2 \rightleftharpoons HO_2 + N_2$	6.70×10^{19}	-1.42	0.
8.	$OH + HO_2 \rightleftharpoons H_2O + O_2$	5.00×10^{13}	0.00	1000.
9.	$H + HO_2 \rightleftharpoons OH + OH$	2.50×10^{14}	0.00	1900.
10.	$O + HO_2 \rightleftharpoons O_2 + OH$	4.80×10^{13}	0.00	1000.
11.	$OH + OH \rightleftharpoons O + H_2O$	6.00×10^{8}	1.30	0.
12.	$H_2 + M \rightleftharpoons H + H + M$	2.23×10^{12}	0.50	92600.
13.	$O_2 + M \rightleftharpoons O + O + M$	1.85×10^{11}	0.50	95560.
14.	$H + OH + M \rightleftharpoons H_2O + M$	7.50×10^{23}	-2.60	0.
15.	$H + HO_2 \rightleftharpoons H_2 + O_2$	2.50×10^{13}	0.00	700.
16.	$HO_2 + HO_2 \rightleftharpoons H_2O_2 + O_2$	2.00×10^{12}	0.00	0.
17.	$H_2O_2 + M \rightleftharpoons OH + OH + M$	1.30×10^{17}	0.00	45500.
18.	$H_2O_2 + H \rightleftharpoons HO_2 + H_2$	1.60×10^{12}	0.00	3800.
19.	$H_2O_2 + OH \rightleftharpoons H_2O + HO_2$	1.00×10^{13}	0.00	1800.
20.	$HO_2 + CO \rightleftharpoons CO_2 + OH$	5.80×10^{13}	0.00	22934.
21.	$CO + O + M \rightleftharpoons CO_2 + M$	3.20×10^{13}	0.00	-4200.
22.	$CO + OH \rightleftharpoons CO_2 + H$	1.51×10^{7}	1.30	-758.
23.	$CO + O_2 \rightleftharpoons CO_2 + O$	1.60×10^{13}	0.00	41000.

Reaction rate coefficients are in the form $k_f = AT^{\beta}\exp -E/RT$. Units are moles, cubic centimeters, seconds, Kelvins and calories/mole. Third body efficiencies: $k_5(H_2O) = 21k_5(Ar)$; $k_5(H_2) = 3.3k_5(Ar)$; $k_5(CO_2) = 5k_5(Ar)$; $k_5(CO) = 2k_5(Ar)$; $k_{12}(H_2O) = 6k_{12}(Ar)$; $k_{12}(H) = 2k_{12}(Ar)$; $k_{12}(H_2) = 3k_{12}(Ar)$; $k_{14}(H_2O) = 20k_{14}(Ar)$.

The reaction rate equations are of the modified Arrhenius form:

$$k = A[x_1]^{\nu_l}[x_m]^{\nu_m} T^n \exp(-E/RT) \qquad (37)$$

where the pre-exponential term A, the temperature exponent n, and the activation energy E are constants determined either theoretically or experimentally. The molar concentrations of the species are denoted by (x_i), and ν_l and ν_m are the stoichiometric coefficients of the species X_l and X_m in the elementary reaction formula:

$$\nu_l X_l + \nu_m X_m \longrightarrow \nu_i X_i + \nu_j X_j \qquad (38)$$

The reaction zone structure code has been used for previous ZND analyses (Shepherd 1985) and is based on the CHEMKIN interpreter and subroutine library which were developed by Kee, Rupley, and Miller (26). A stiff solver package based on LSODE by Hindmarsh (27) was used to find the solution to the system of ordinary differential equations.

The tolerances for the numerical integration scheme were adjusted so that no oscillations in the minor species profiles were observed near equilibrium.

The ZND structure was obtained for selected cases from references (10) and (15). Detailed profiles of all the possible species (excluding ionized species) plus temperature, pressure and sigma were generated for some of the considered cases. For the remaining cases, only the temperature, pressure, and sigma profiles were plotted.

Sigma is the rate of heat release which was defined in the equations in the theory section above.

3.3 Total Pressure Recovery Factor

The next part of this thesis was to evaluate the total pressure drop across detonation waves. To do this, Dr. Shepherd added a new option to STANJAN which allows the user to execute a run with the product mixture while keeping the entropy constant and specifying the enthalpy. Stagnation is, by definition, an isentropic deceleration. Therefore, once the specified enthalpy is set equal to the total enthalpy, the output of this new STANJAN option would correspond to the stagnation state. The total enthalpy could be evaluated upstream or downstream of the detonation wave since total enthalpy is conserved across the wave.

All of the total pressure drop computations were done using the upstream state and composition of the Dabora case. Total pressure recovery factor was obtained for normal detonation waves with a normal free stream velocity component that ranged from the C-J velocity (1824.2 m/s) to a value of 4200 m/s. In addition, total pressure recovery factor was computed along the equilibrium polar with the free stream Mach number of 10.68.

3.4 Scramjet Model

The final part of thesis work was to design a simplified scramjet model which uses an inviscid oblique detonation wave as a combustor. A stoichiometric

hydrogen-air mixture was used throughout this investigation. Figure (7) shows a schematic of the scramjet considered in this thesis with the various stations of interest. Station (0) represents the free-stream (ambient) condition.

The inlet of the scramjet was a single wedge which sets up an oblique shock wave which in turn sets up a reflected shock off the cowl. The condition downstream of the first shock wave corresponds to station (1') on figure (7), while the condition downstream of the reflected shock wave corresponds to station (1). Both the wedge and the cowl were assumed to be pivoted so that their angles could be varied to maintain a constant wave angle of 12^{o}. In practice the inlet of the NASP will be pivoted so as to make it possible to obtain design-point performance under various flight conditions. Thus, the constant wave angle does not constitute an unrealistic restriction, but simplifies the analysis immensely. Once the wave angle was fixed, it was then possible to compute the normal free stream velocity coming into the inlet. The shock option of STANJAN was then executed using this velocity, the free stream (ambient) condition, and air (nitrogen and oxygen). This is a lot more realistic than the constant mean ratio of specific heats which is often made. Knowing the conditions behind the first shock and the wave angle (12^{o}) for the second (reflected) shock, it was then possible to

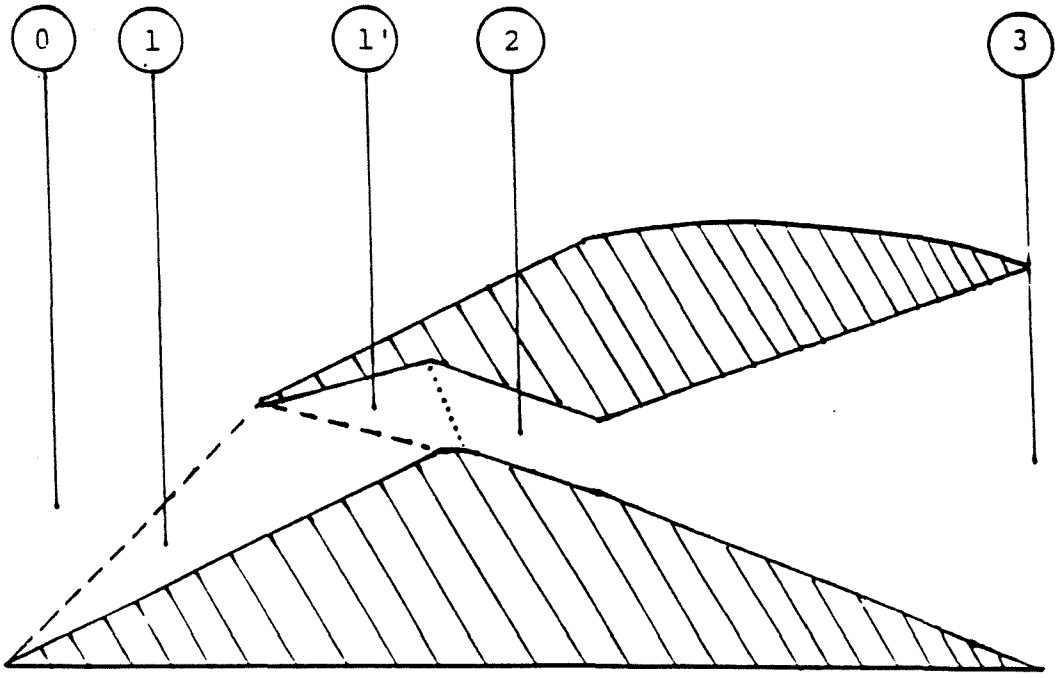

Figure 7. Schematic of a detonative scramjet showing the various stations used in the analysis of its performance. Station (0) is the free-stream state, station (1) is the state behind the first shock wave, station (1') is the condition behind the reflected shock and right before the detonation wave, station (2) is the condition downstream of the detonation wave, and station (3) denotes nozzle exit.

obtain the state, composition, and velocity of the air entering the combustion chamber (station (1')). It should be noted that once the wave angle, the pre-wave normal velocity, and the post-wave normal velocity are known, the deflection (wedge) angle can be easily found from equation (9).

For the design point, the C-J and cross-over points were determined for the post-inlet fluid, and a point midway between the two was selected as the operating point. The wedge angle corresponding to this point was computed. Of course, the C-J point would be the most desirable point at which to operate since it corresponds to the lowest total pressure drop across the wave and thus the highest specific thrust. But operating at a single point with no margin for error is not practical. If the normal component of the post-inlet velocity drops below the C-J velocity for the post-inlet mixture then no detonation would take place and the engine would stall.

Several off-design points along a typical trajectory of the NASP were also considered. In each case, the C-J and cross-over points were identified, a midway point was selected, and the the corresponding wedge angle was computed.

For each operating point, the post-detonation fluid (station (2)) was expanded to ambient pressure using the constant entropy/specified pressure option in STANJAN. Of

course this implies the use of a variable geometry nozzle, since for a fixed geometry nozzle the nozzle exit pressure is equal to the ambient pressure only at a single point. A fixed geometry nozzle could be designed along similar lines but would require iterating on the exit state until the conservation of both mass and total enthalpy are satisfied.

Once the nozzle exit state (station (3)) was obtained, the nozzle exit velocity was obtained by applying the conservation of total enthalpy between the nozzle throat and exit. Having the nozzle exit velocity, it was then possible to compute specific thrust, air specific impulse, and the nozzle exit-to-throat area ratio. The latter is obtained by applying the conservation of mass between the nozzle throat and exit.

Thus, a schedule of inlet wedge angles, detonation wedge angles, and nozzle exit-to-throat areas was obtained as a function of flight Mach number and altitude. Such a schedule could be programmed into an on-board computer. Using variable-geometry for the inlet, the detonation wedge, and nozzle would certainly make the engine very complex, but the payoff would be that the engine would always be operating at its design point.

The performance of the scramjet was also evaluated for operation beyond the cross-over point to determine if indeed this results in a much lower specific thrust.

No attempt was made to investigate the effect of

mixing the hydrogen with the air. Such an investigation would be quite complex and beyond the scope of this thesis.

All of the computations done in this thesis were done on a Zenith 286 computer using a Microsoft^{R} FORTRAN compiler. All of the plots were created on the same machine using the $T_{E}X$ typesetting program. The plots were then printed using a Hewlett-Packard laser printer.

PART 4

RESULTS

4.1 Introduction

This section is divided into three major parts. The first part deals with the Hugoniots, polars, and reaction structure, and is subdivided into the various cases considered in this thesis. Table (3) shows a capsule description of each case, the number assigned to it in the following discussion, the section and figures associated with it, whether a reaction zone structure was obtained for it, and if so whether species profiles were created. All cases from Cambier, Adelman, and Menees (10) are referred to as CAM cases, while all cases from Dabora, Wagner, and Desbordes are referred to as Dabora cases.

The second part presents the results of the total pressure recovery factor investigation using the Dabora cases.

The third part concerns the performance of the simplified scramjet model for various flight conditions and overdrive.

4.2 Hugoniots, Polars, and Reaction Zone Structures

4.2.1 Case 1

The curve-fits of w_2 as a function of w_1 for this case were not very good (correlation coefficients of about 0.8 with a fifth order curve-fit). It was therefore decided to use case 2 for a more rigorous analysis and generate

Table 3. Summary of the cases investigated, showing case description, case number, applicable sections and figures.

Case	Description	Sections	Figures	Reaction Zone (Y/N)	Species Profiles (Y/N)	Polars (Y/N)
1	case 1 of Table (1); M = 3.8	4.2.1 4.2.5	8-15	Y	Y	Y
2	case 2 of Table (1); M=5.0	4.2.2 4.2.5	16-24 30	Y	Y	Y
3	case 2; M=9.149	4.2.3 4.2.5	25-27 16,30	Y	N	Y
4	case 2; M=15	4.2.4 4.2.5	28 16,30	N	N	Y
5	case 2; M=19	4.2.4 4.2.5	29 16,30	N	N	Y
6	case 6 of Table (1); M=4.639	4.2.6 4.2.14	31-34 75	Y	N	N
7	case 6; M=5.086	4.2.7 4.2.14	35 31,75	N	N	Y
8	case 6; M=	4.2.8 4.2.14	36-43 31,75	Y	Y	Y
9	case 6; M=8.7	4.2.9 4.2.14	44-51 31,75	Y	Y	N
10	case 6; M=8.813	4.2.10 4.2.14	52-60	Y	Y	N
11	case 6; M=9.3	4.2.11 4.2.14	61-63 31,75	Y	N	N
12	case 6; M=10.172	4.2.12 4.2.14	64-73 31,75	Y	Y	Y
13	case 6; M=21.227	4.2.13 4.2.14	74 31,75	N	N	Y

only frozen and equilibrium polars for case 1. For this case the free-stream temperature, pressure, and Mach number were 840 K, 0.06 atm, and 3.8 respectively. The free stream composition along with the free-stream initial conditions are given in table (1) in section 3.1 above.

Figure (8) shows both the equilibrium and frozen polars for case 1. This case had the free stream conditions listed in table (1) in section 3.1 above for the CAM cases. The free stream normal Mach number was only 3.8, which corresponds to an overdrive parameter of 1.3392, where the overdrive parameter is the ratio of normal Mach number to M_{CJ}. Thus, this case was not highly overdriven. This is why the two polars do not intersect. Note that the entire equilibrium polar falls below the frozen polar. The polars have a shape similar to that for non-reactive shock waves (see reference (22)). They have a steep slope for the lower branch, and a very shallow slope for the upper branch. The maximum deflection angle is about 32^{o}, and thus the deflection angle of 31^{o} listed in reference (10) is possible. However, on figure (8), a deflection angle of 31^{o} corresponds to a pressure ratio (post-detonation to free stream static pressure ratio) of 8, as compared with the pressure ratio of 9.58 which could be computed from figure (6b) and free stream conditions of reference (10). Figures (9a) through (9c) show figures (6a) through (6c) from reference (10). The free stream conditions were given in

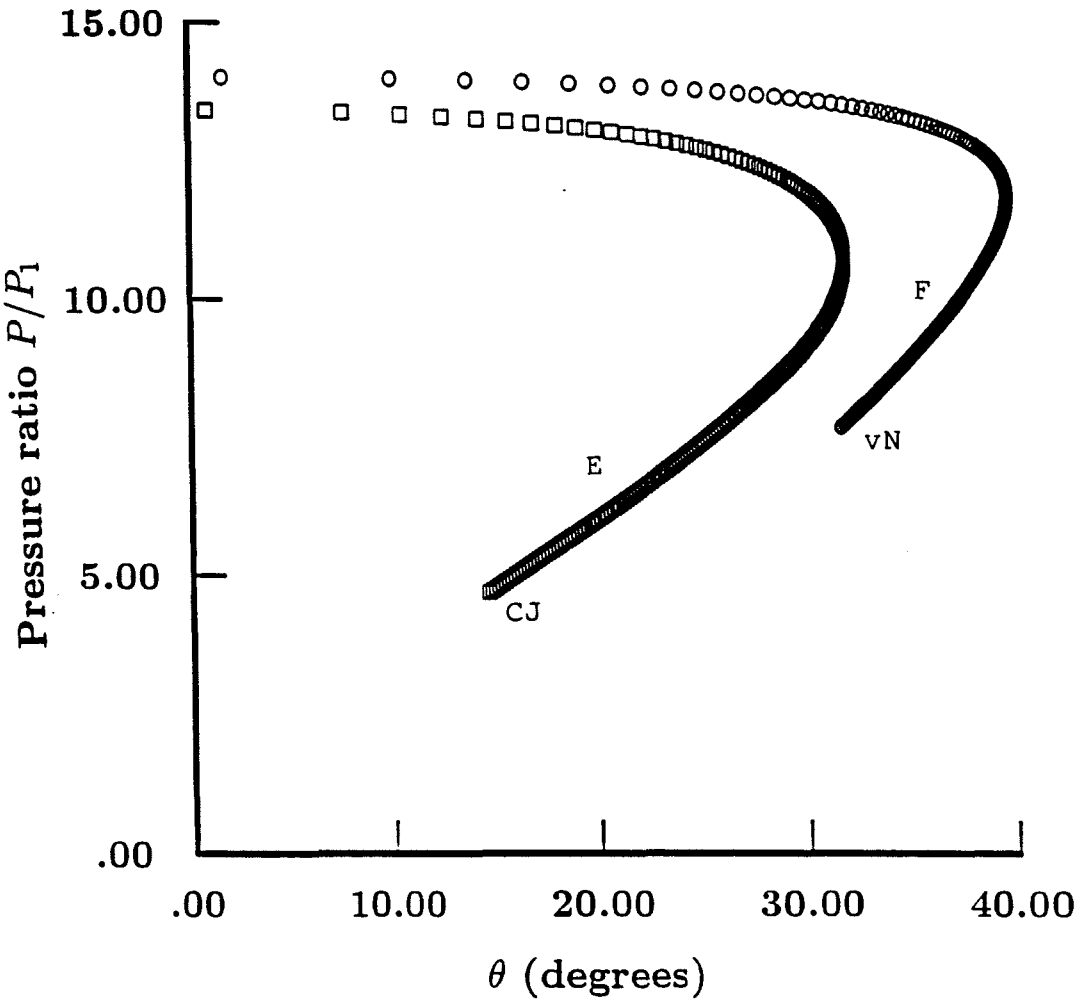

Figure 8. Frozen (F) and equilibrium (E) polars for case 1, showing the CJ point and the von-Neumann point (vN).

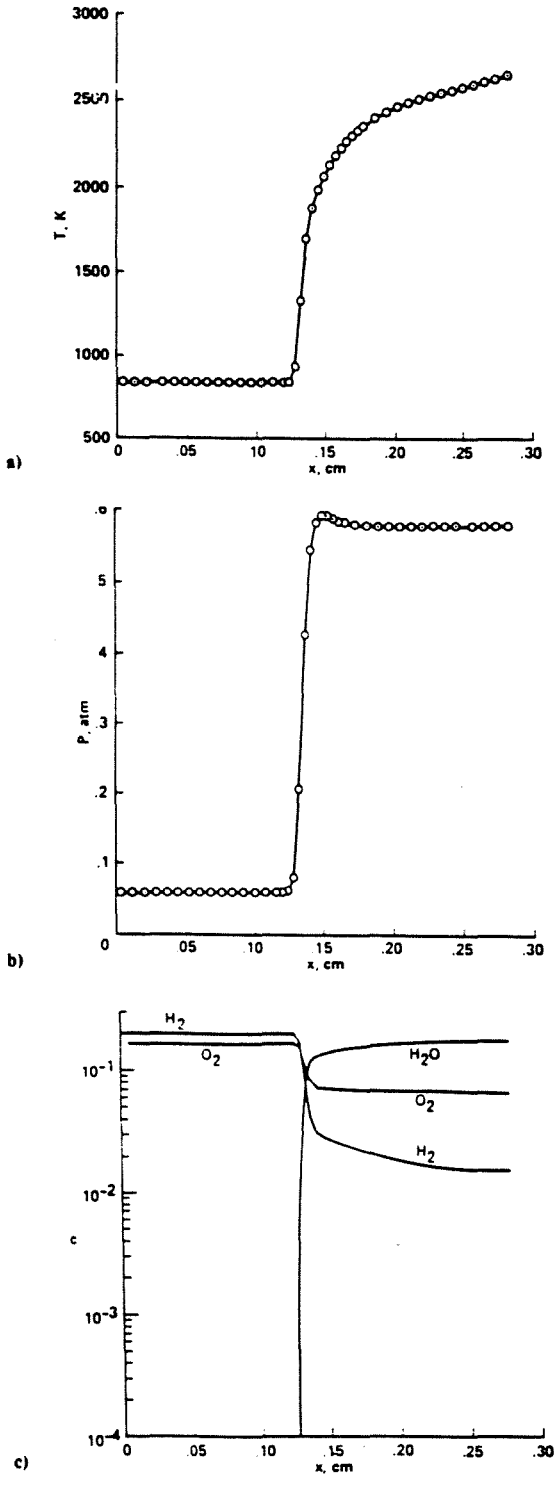

Figure 9. Temperature, pressure, and species profiles for case 1 as given in reference (10): a) temperature; b) pressure; c) species. These figures are given in reference (10) as figures (6a) through (6c).

table (1) in section 3.1 above.

Figures (10) and (11) show the temperature and pressure profiles within the reaction zone of case 1. It is not possible to compare those directly with figures (9a) and (9b) from reference (10) because the horizontal ordinate in that reference is not the same as the one used in this thesis. It seems to be a streamwise ordinate scaled down by some factor. However, it is possible to compare the peaks and behavior of the dependent variables. The equilibrium temperature is 2820.7 K as opposed to about 2700 K as stated in reference (10). There is also disagreement concerning pressures. Figure (11) shows a frozen pressure of 0.67 atm, while figure (9b) claims that the von-Neumann spike pressure is only 0.6 atm. The equilibrium pressures are also off: 0.597 atm as opposed to 0.575 atm as obtained from figure (9b). Even more perplexing about figures (9a) and (9b) is the fact that the major features of the two profiles do not coincide. While pressure seems to reach an equilibrium value, the temperature seems to be still rising. By contrast, the temperature and pressure level off at about the same location in figures (10) and (11).

Figures (12) through (15) show the species profiles within the reaction zone of case 1. Again, it is not possible to make rigorous comparisons with figure (9c) because of the different horizontal ordinates. However, a

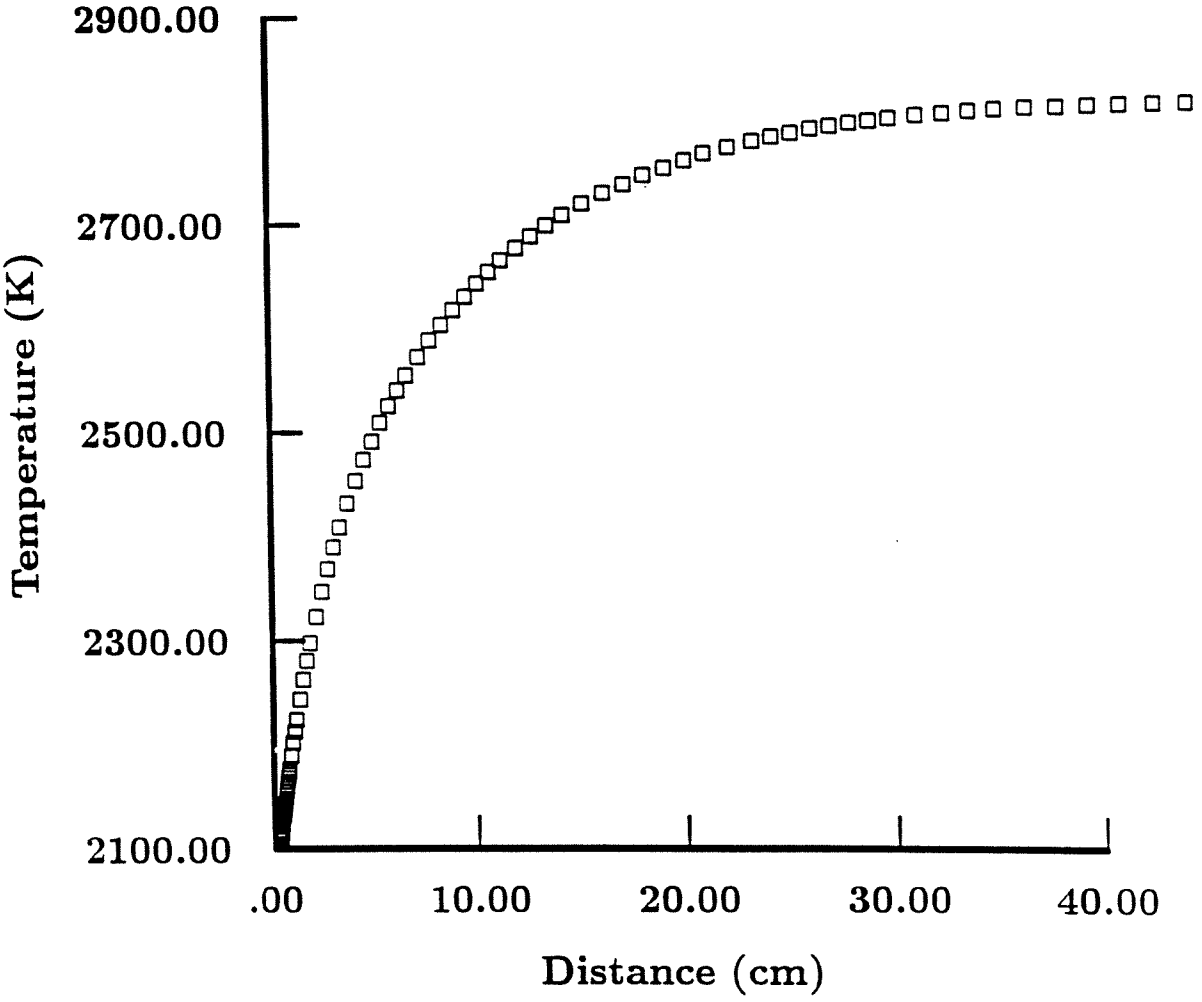

Figure 10. Temperature profile for the reaction zone of case 1.

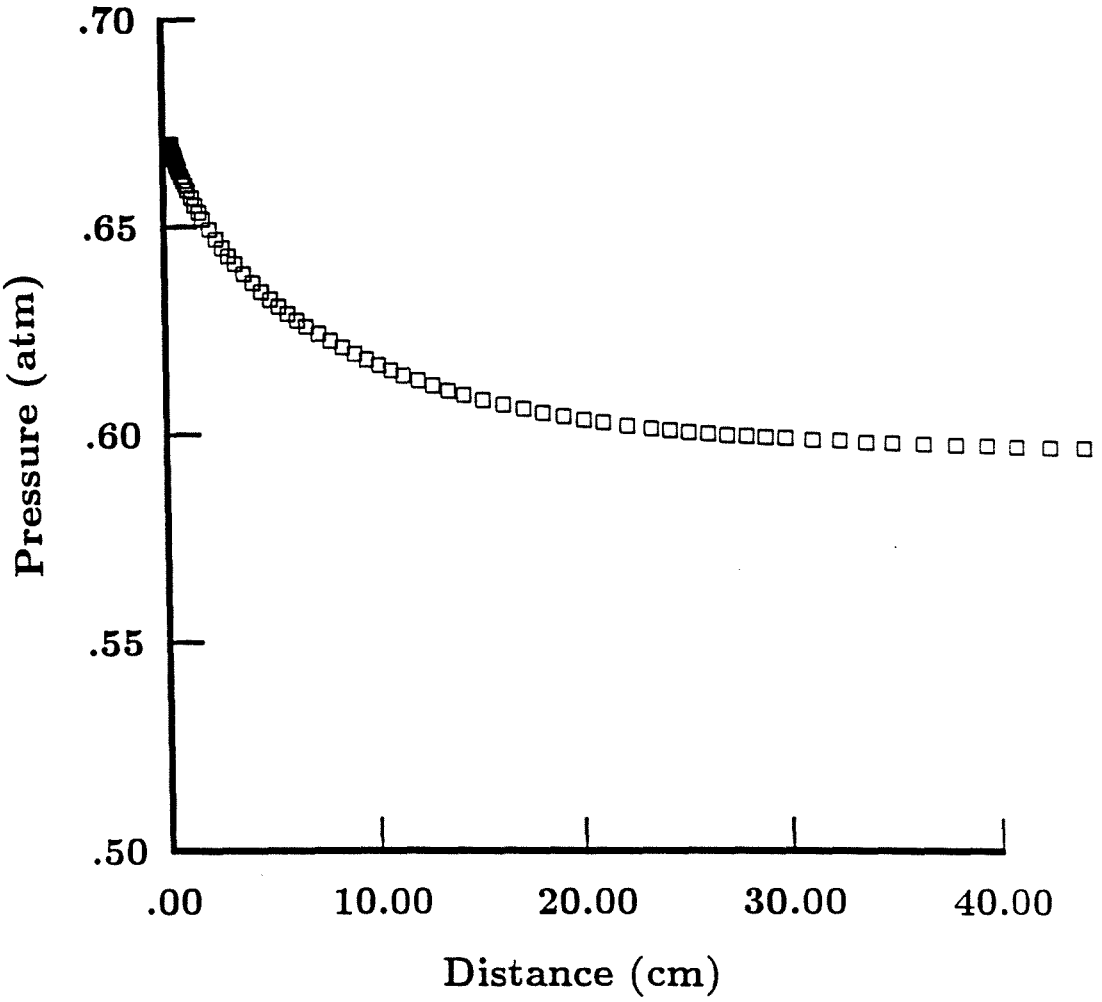

Figure 11. Pressure profile for the reaction zone of case 1.

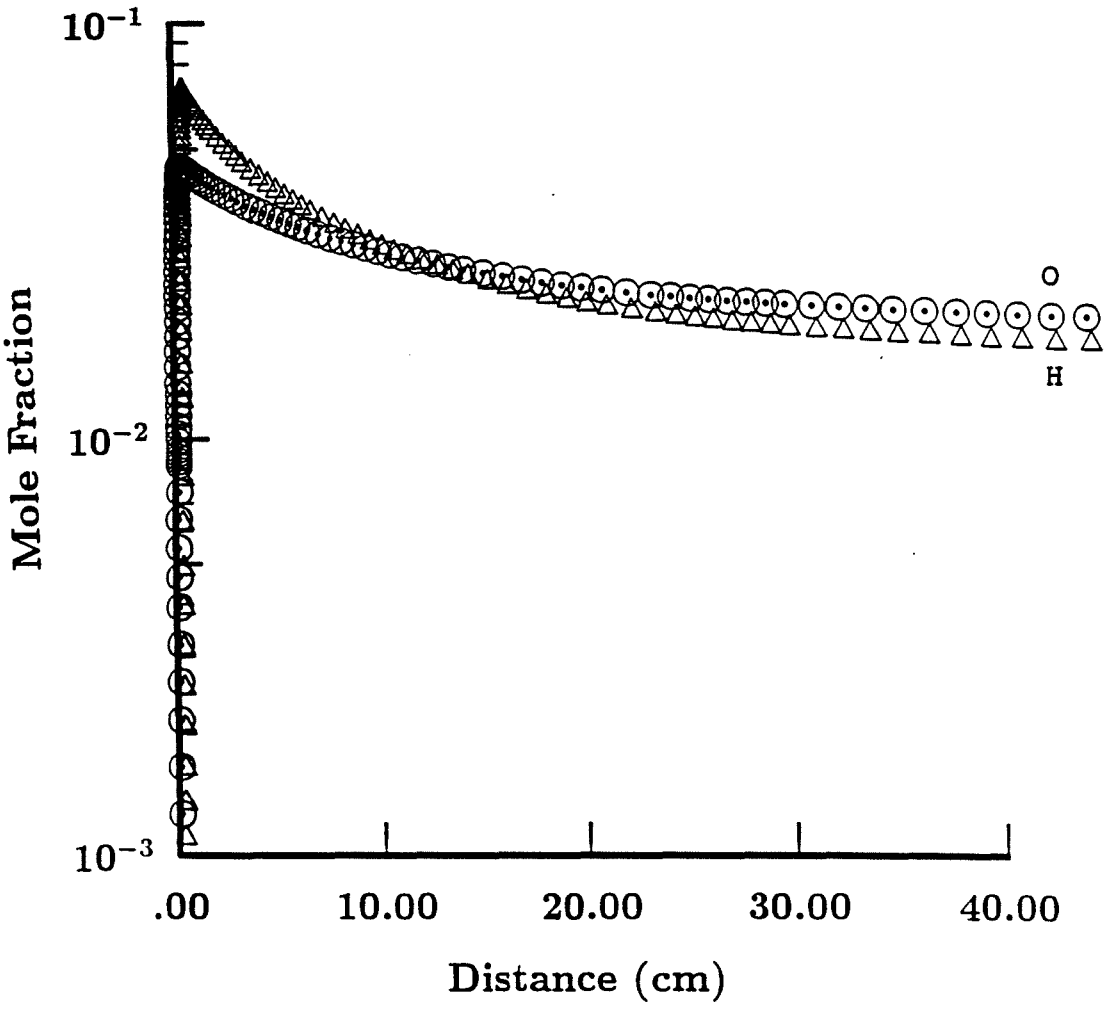

Figure 12. Mole fractions of H and O for the reaction zone of case 1.

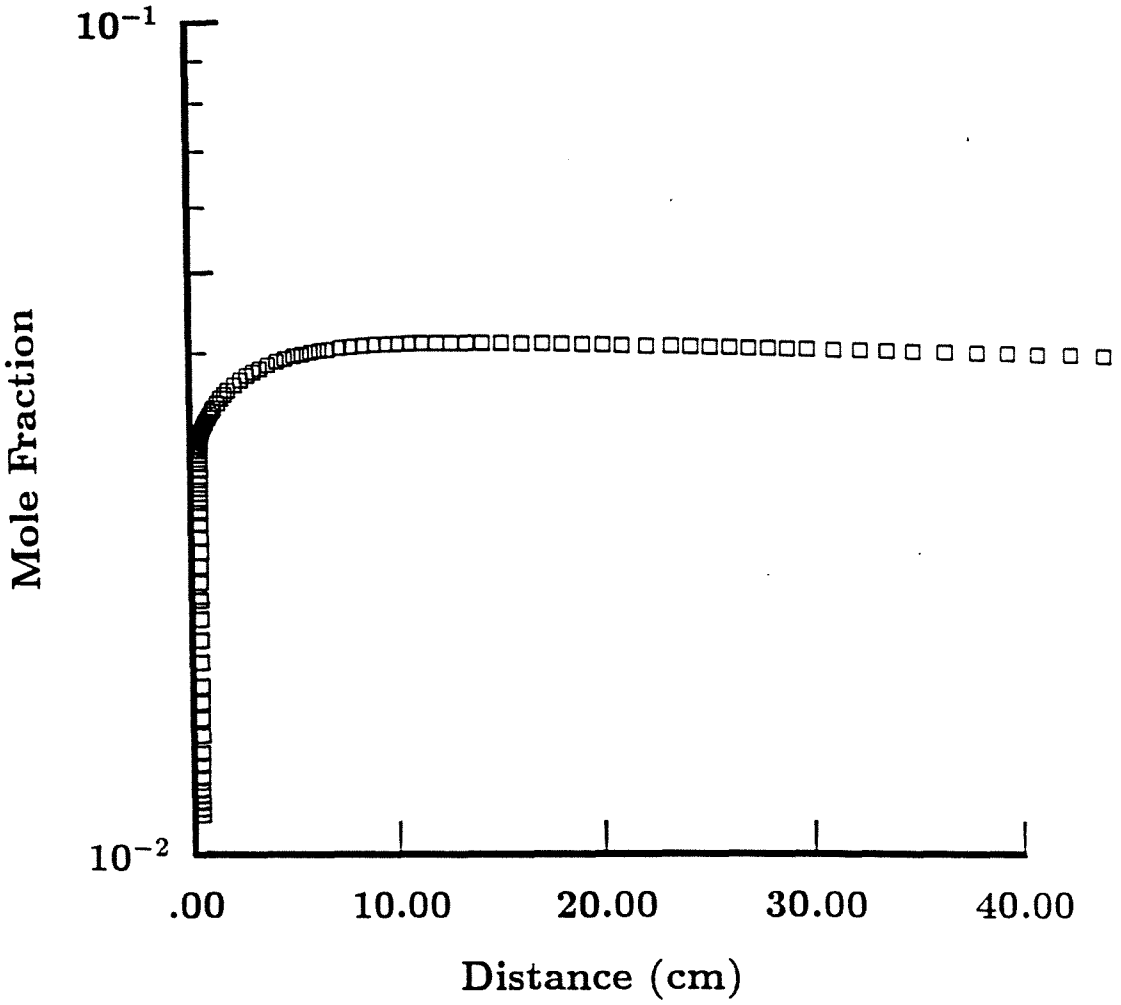

Figure 13. Mole fraction of OH for the reaction zone of case 1.

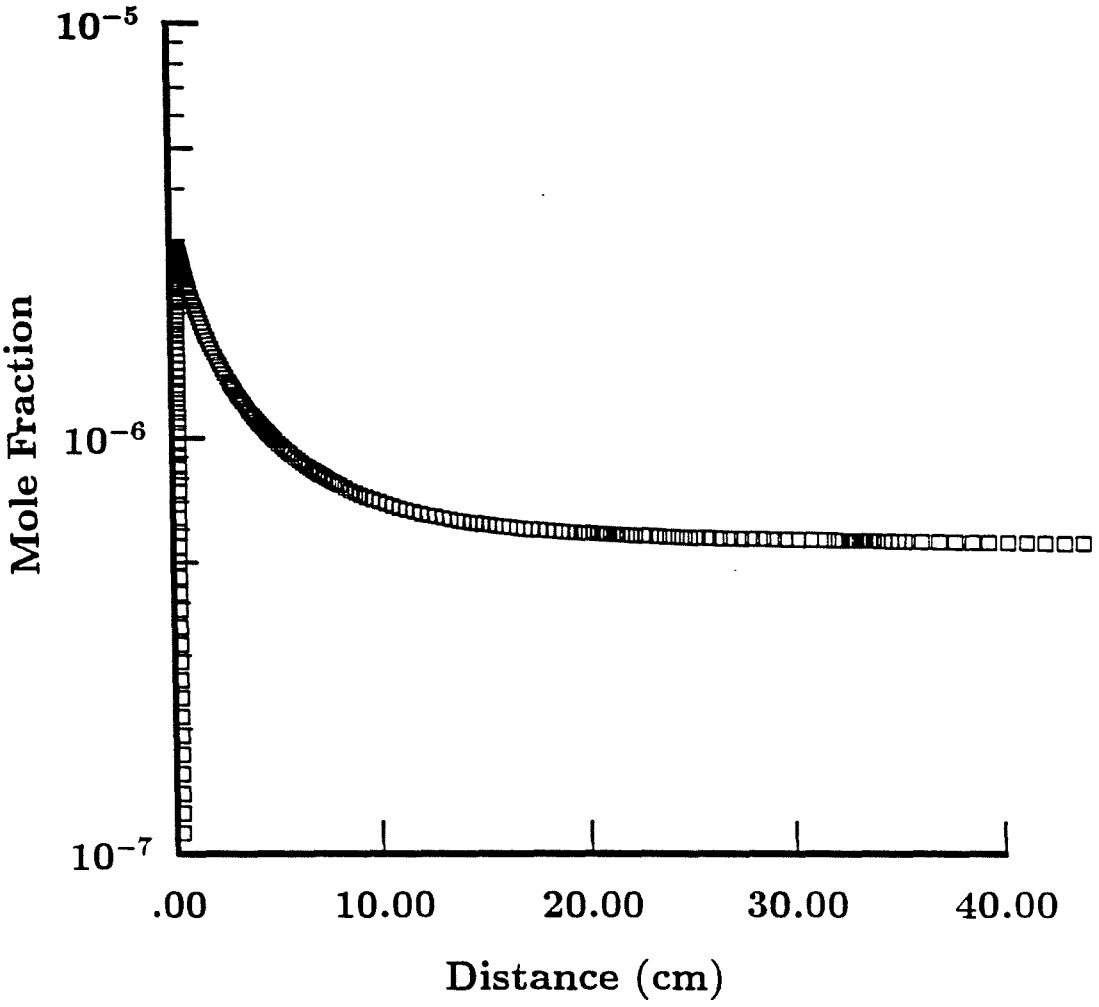

Figure 14. Mole fraction of H_2O_2 for the reaction zone of case 1.

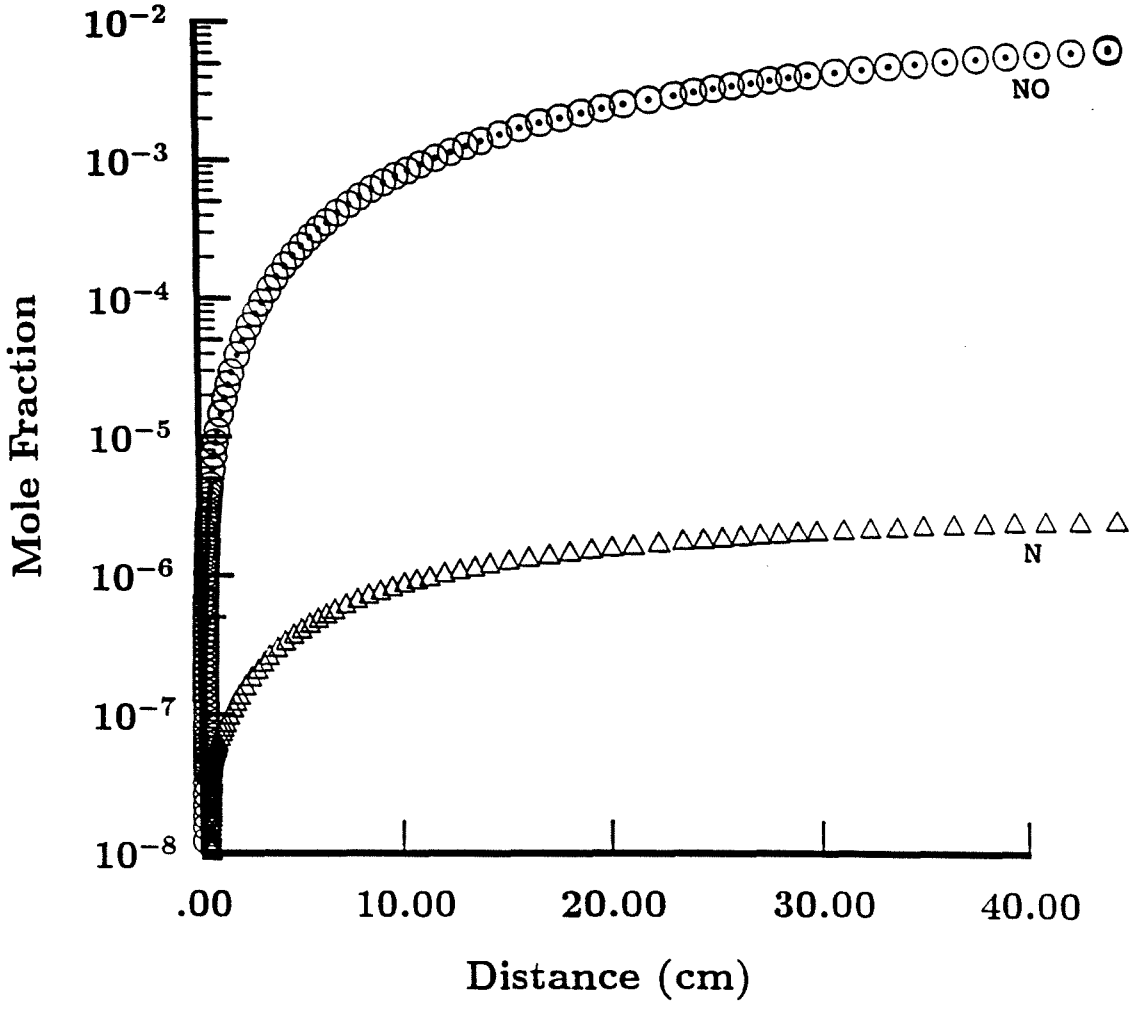

Figure 15. Mole fractions of N and NO for the reaction zone of case 1.

comparison of the peaks and trends of the profiles confirms the statements made above on the basis of the temperature and pressure profiles: the reaction zone is not sufficiently resolved to yield an accurate reaction zone structure.

A very interesting fact is that the equilibrium mixture contains a substantial quantity of dissociation products. This is in stark contrast with the assertion by Sargent and Gross (17) that inclusion of dissociation is unrealistic based on residence time arguments. The species concentrations level off after about 20 cm. This means that if a combustor that is at least 20 cm long is used, then the product gases will be in equilibrium. This is certainly not a very long combustor length.

Another interesting feature is the profiles of NO and N within the reaction zone as shown in figure (15). Although the mole fraction of both species is quite small, they do not level off in the same time scale as the other species. This is a generic feature of the Zeldovich mechanism for NO production. This might be advantageous, since it reduces the quantity of NO that is produced by the combustion process.

The reaction zone thickness based on the maximum rate of heat release is about 1.843 mm as given by ZND.FOR.

4.2.2 Case 2

Case 2 had the same free stream composition as case 1

but different initial conditions. The temperature was 450 K, pressure was 0.32 atm, and the Mach number was 5.0. Those conditions were also given in table (1) in section 3.1.

Figure (16) shows the equilibrium and frozen Hugoniots for case 2. The cross-over point is easily identifiable, and corresponds to a pressure of about 20 bars, and a specific volume of about 0.75 m^3/kg. The cross-over pressure ratio (ratio of cross-over pressure to free stream pressure) is therefore about 62.5. For this case, STANJAN was executed twice for the equilibrium Hugoniots: once with ionized species, and another time without ionized species. The maximum difference in temperature was 11.92 K for the most overdriven case which had an upstream normal velocity of 8500 m/s and an equilibrium temperature (with ionization) of 9423.19 K. The difference narrowed as the upstream normal velocity was decreased. Thus, the inclusion of ionized species in the product mixture does not have a substantial effect on the equilibrium temperature (a difference of 0.13% for the maximum upstream normal velocity of 8500 m/s).

Figure (17) shows the equilibrium and frozen polars for case 2. This case had a maximum free stream normal Mach number of 5.0, which yields an overdrive parameter of 1.2506, which is even less overdriven than case 2 of CAM. The maximum free stream normal Mach number is the one

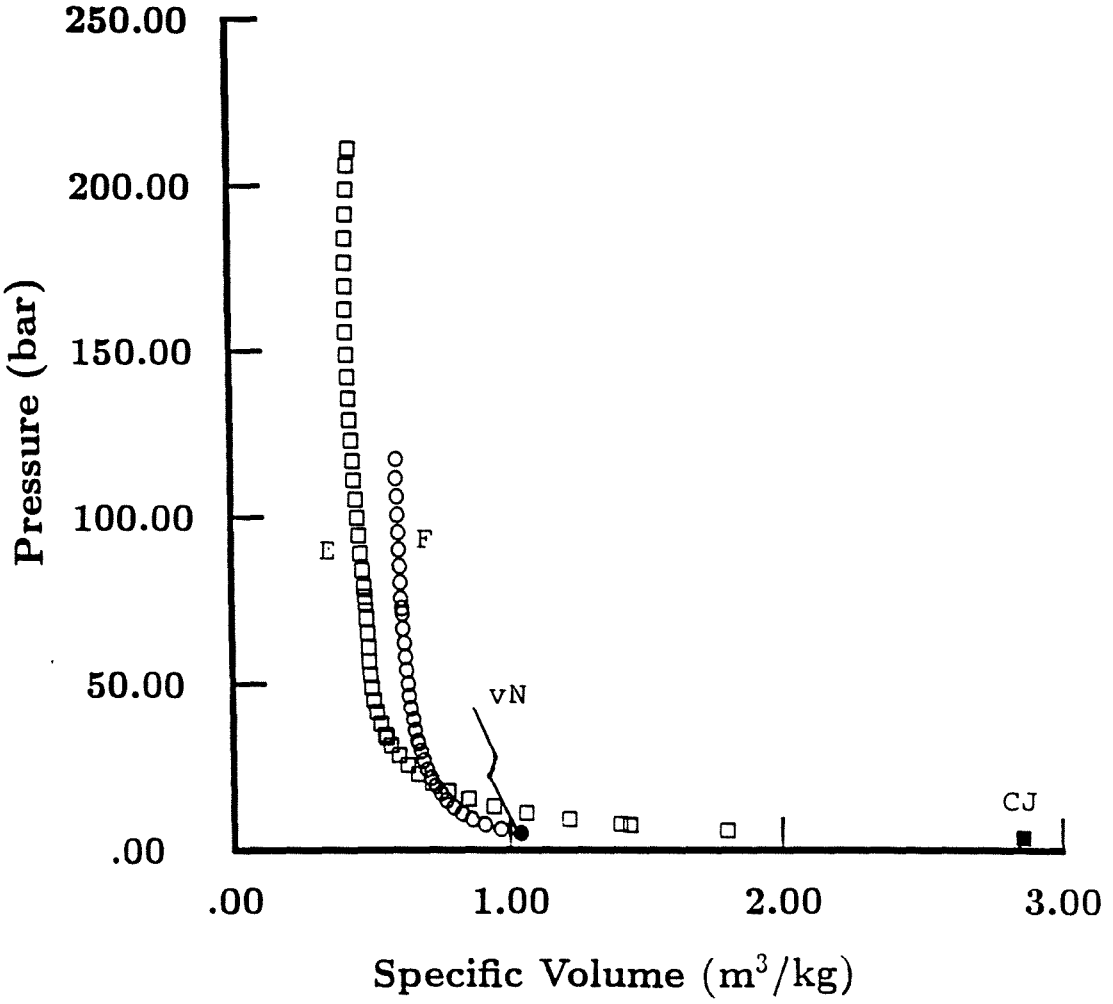

Figure 16. Frozen (F) and equilibrium (E) Hugoniots for cases 2 through 5.

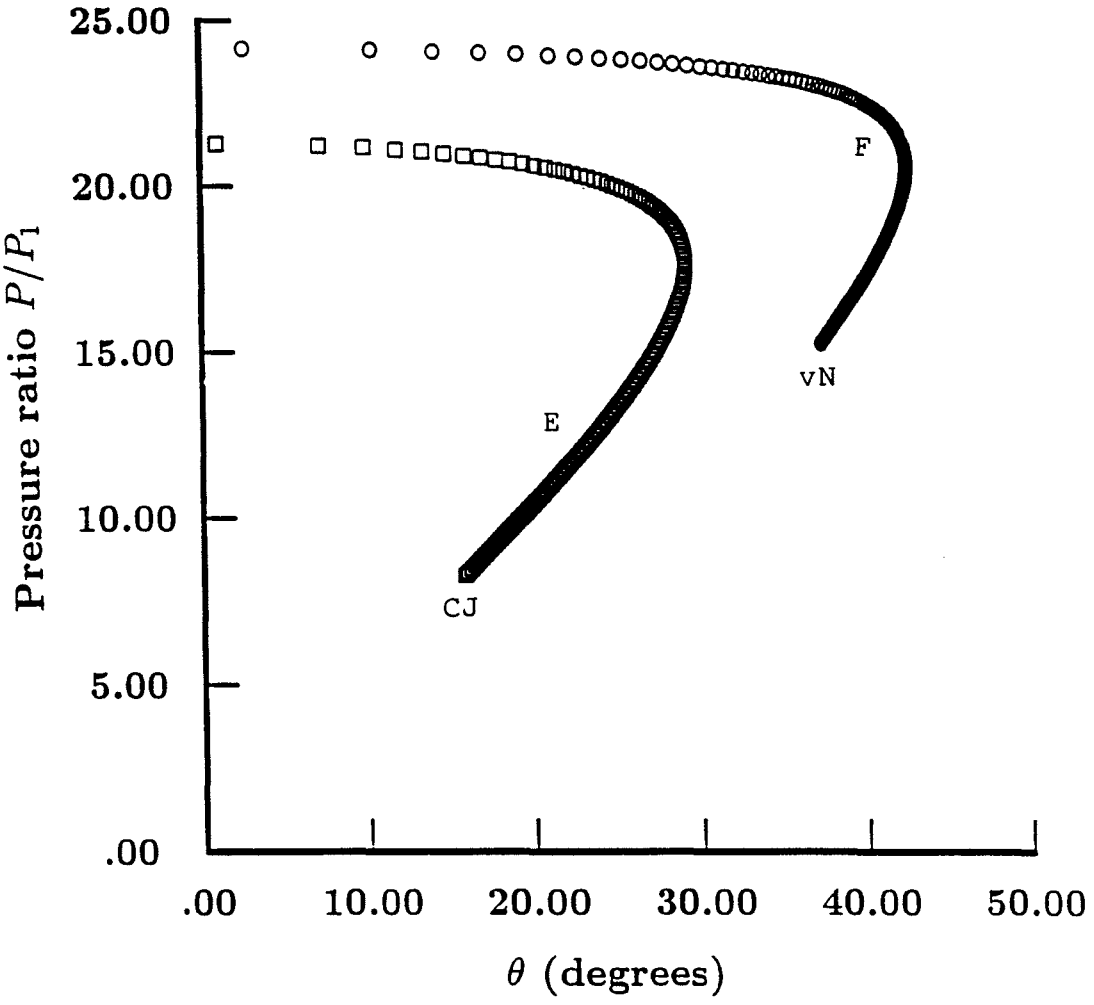

Figure 17. Frozen (F) and equilibrium (E) polars for case 2, showing the CJ point and the von-Neumann point (vN).

corresponding to the maximum wave angle. Thus, again the polars do not intersect. Note, however, that the maximum deflection angle on the equilibrium polar is about 28^{o}, while the deflection angle stated in reference (10) is 31^{o}. Thus the stated deflection angle cannot be achieved, and this raises considerable doubt concerning the validity of the results stated in reference (10).

Statements similar to those made about case 1 above can also be made about case 2 based on a comparison between figures (18) through (23) and figures (24a) through (24c) from reference (10). Both STANJAN and ZND yield equilibrium temperature and pressure of 2830.9 K and 5.601 atm respectively. This is in stark disagreement with the 2500 K and 4.5 atm shown in figures (24a) and (24b). The von-Neumann pressure is 6.681 atm as opposed to about 4.7 atm as obtained from figure (24b). One difference from case 1 is that the pressure and temperature in case 2 level off at about the same location. The reaction zone thickness based on maximum rate of heat release is about 0.317 mm. Overall, the results stated in reference (10) for case 2 seem more unreliable than those for case 1. The reason is probably that the stated deflection angle of 31^{o} is not attainable with the stated initial conditions.

4.2.3 Case 3

Figure (25) shows equilibrium and frozen polars for case 2 but with a higher maximum free stream normal Mach

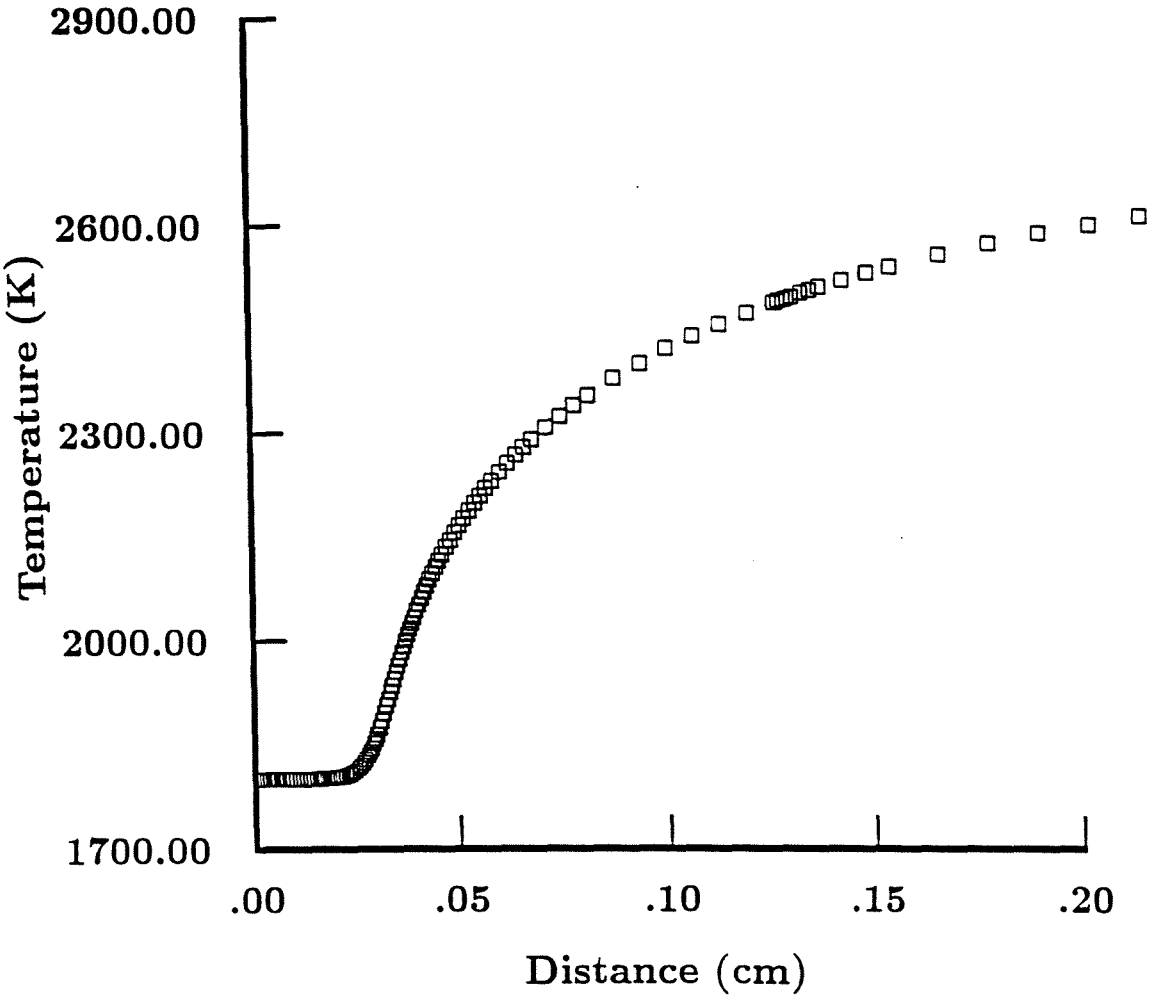

Figure 18. Temperature profile for the reaction zone of case 2.

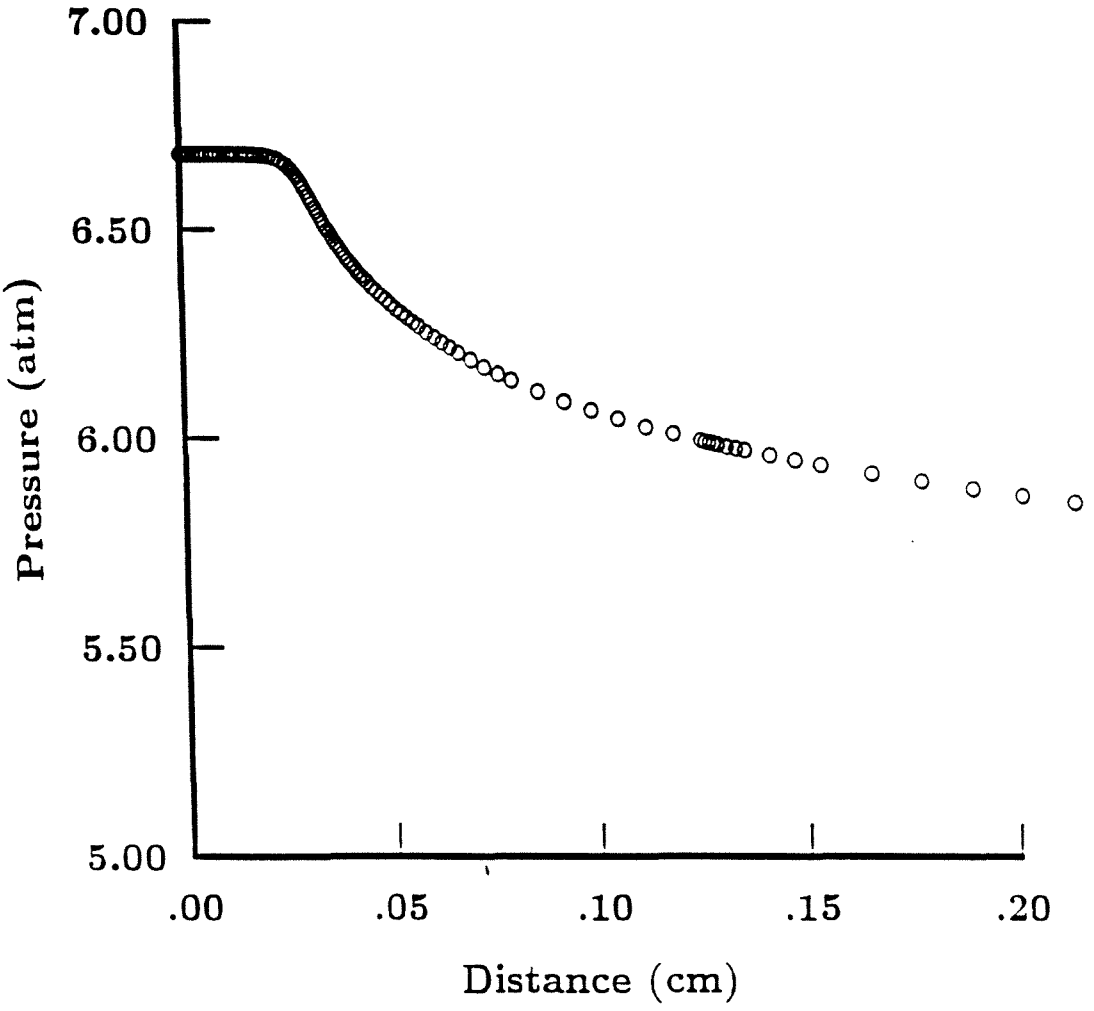

Figure 19. Pressure profile for the reaction zone of case 2.

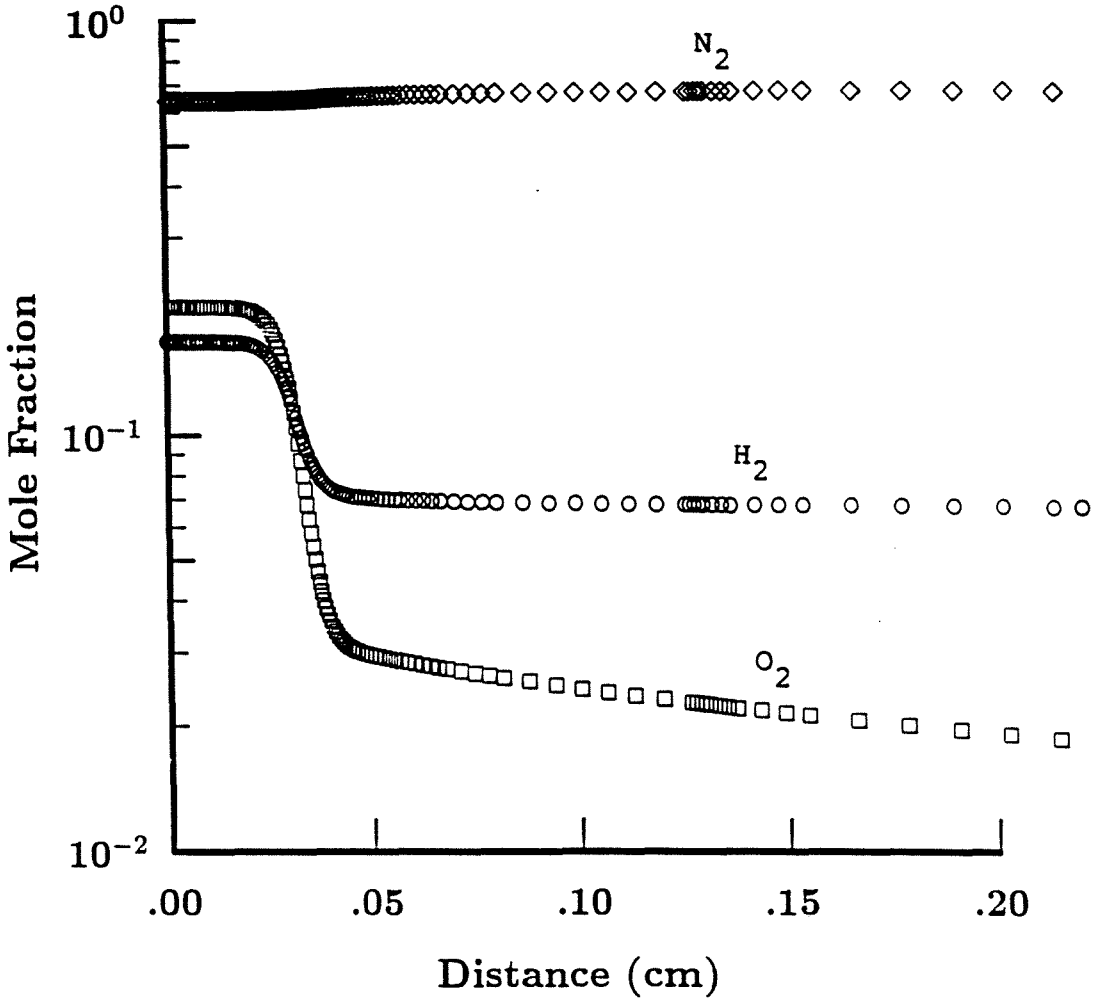

Figure 20. Mole fractions of H_2, O_2, and N_2 for the reaction zone of case 2.

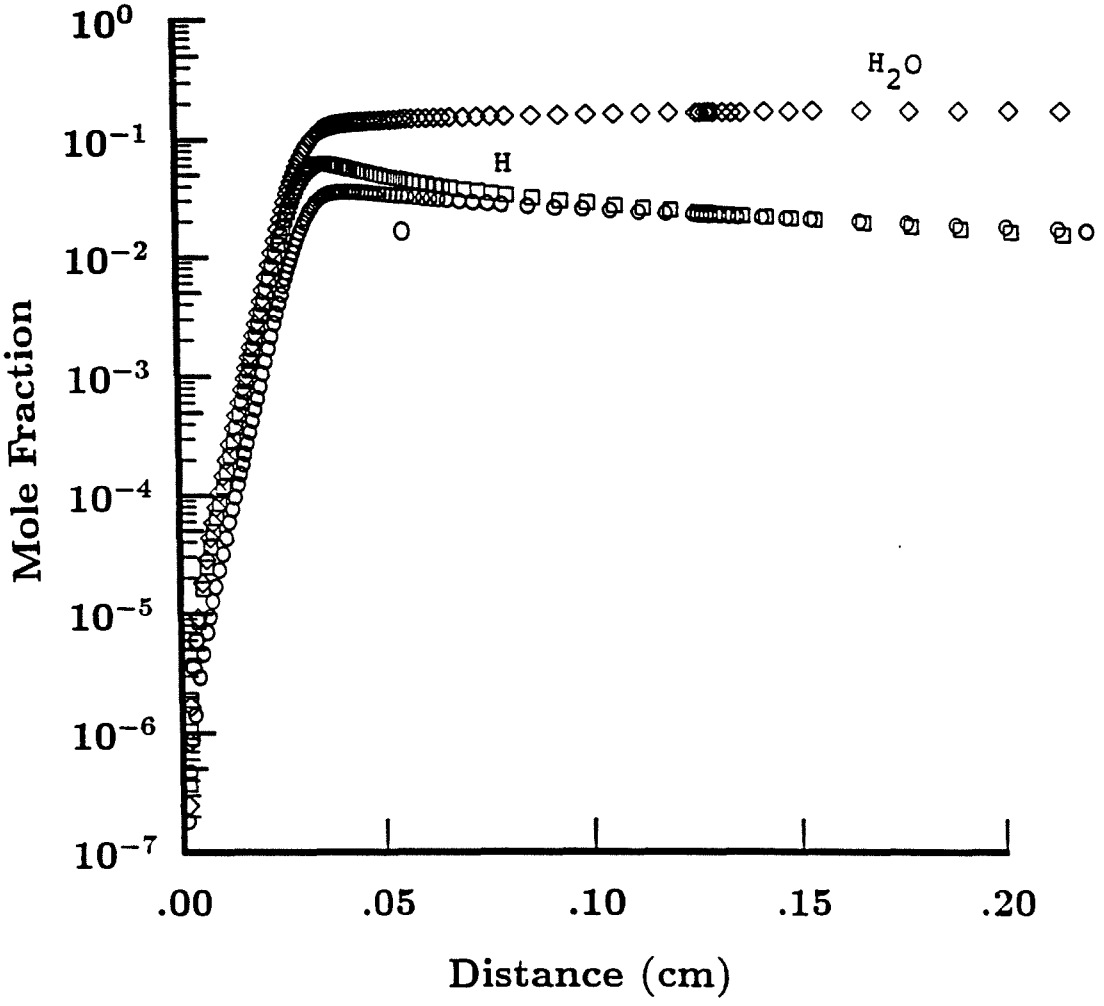

Figure 21. Mole fractions of H, O, and H_2O for the reaction zone of case 2.

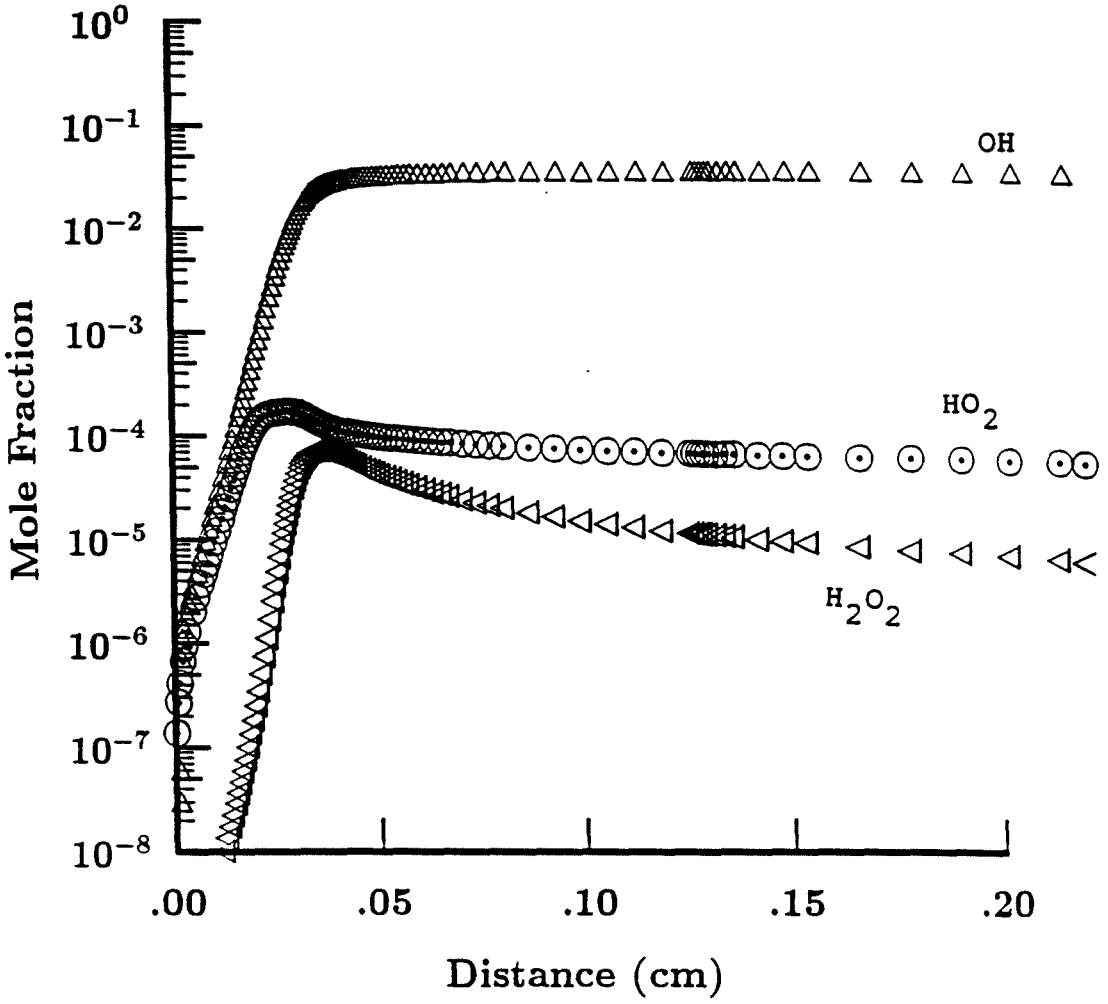

Figure 22. Mole fractions of OH, HO_2, and H_2O_2 for the reaction zone of case 2.

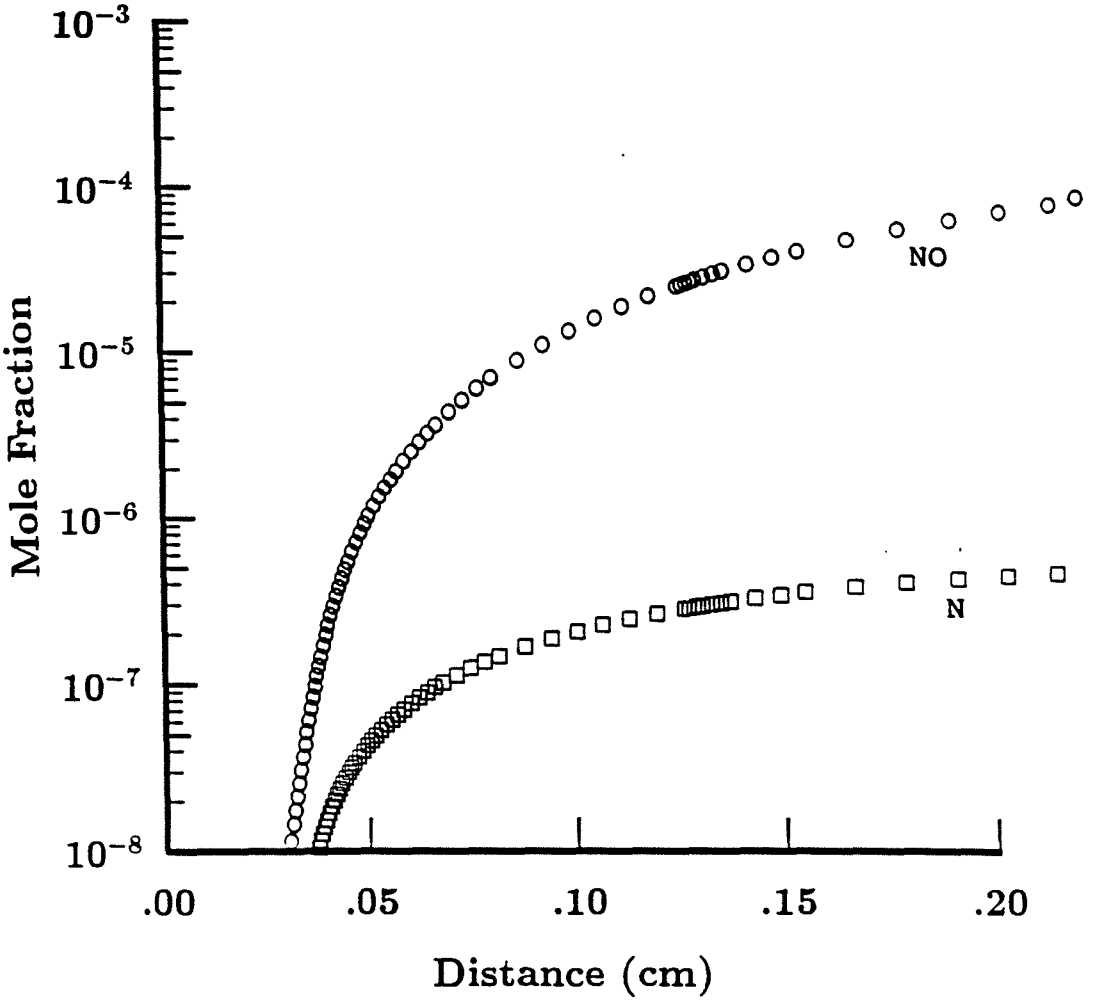

Figure 23. Mole fractions of N and NO for the reaction zone of case 2.

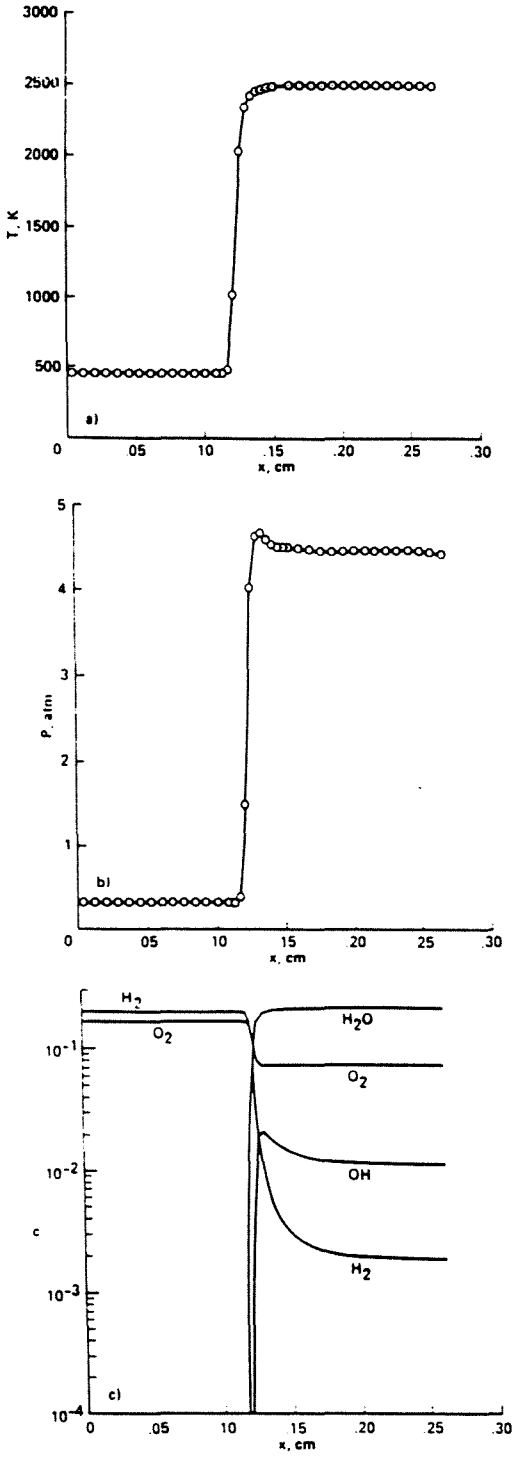

Figure 24. Temperature, pressure, and species profiles for case 2 as given in reference (10): a) temperature; b) pressure; c) species. These figures are given in reference (10) as figures (9a) through (9c).

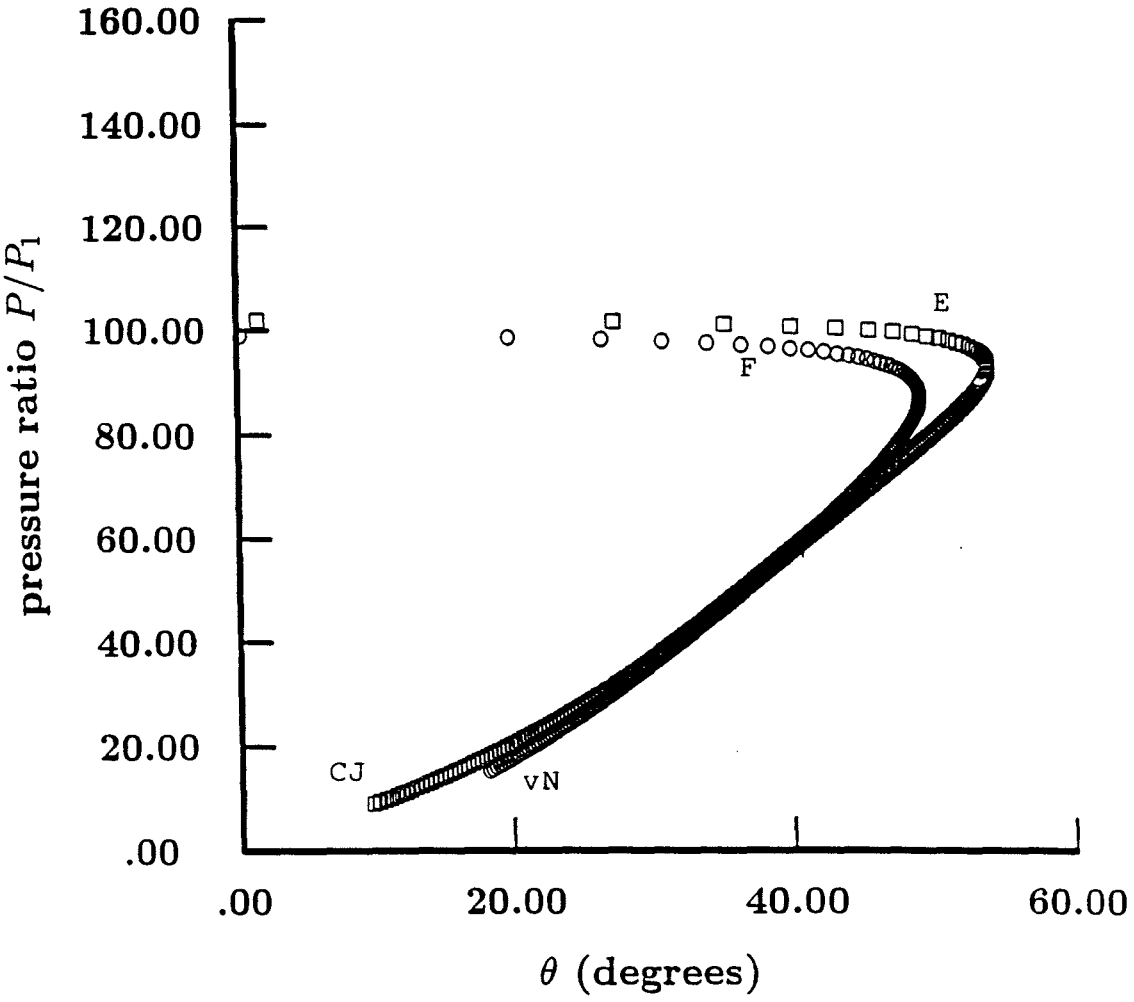

Figure 25. Frozen (F) and equilibrium (E) polars for case 3, showing the CJ point and the von-Neumann point (vN).

number of 9.64, which yields an overdrive parameter of 2.2881. This is quite overdriven and a cross-over point is obtained. The deflection angle corresponding to that cross-over point is about 40.9^{o}. If a deflection angle higher than 40.9^{o} is used, then the frozen pressure becomes lower than the equilibrium pressure. This means that instead of a von-Neumann spike, one obtains a von-Neumann "well". This is due to the fact that at angles above 40.9^{o} the frozen temperature becomes so high that the flow has to cool down instead of heat up due to chemical reaction.

Figures (26) and (27) show the temperature and pressure profiles for the reaction zone of case 3. This case corresponds to a point beyond the cross-over point, and therefore a von-Neumann "well" appears instead of a von-Neumann spike. Note that the temperature profile is the opposite of the two temperature profiles shown above for cases 1 and 2. The temperature after the non-reacting shock wave is so high (about 5700 K) that the flow cools down instead of heating up due to chemical reaction. In this case the chemical reaction adds nothing useful to the fluid from a propulsive standpoint. Fuel is wasted, since it does not result in a higher temperature. The reaction zone length for this case was 0.5562 mm based on the maximum rate of heat release.

4.2.4 Cases 4 and 5

Figure (28) shows another polar set for a more

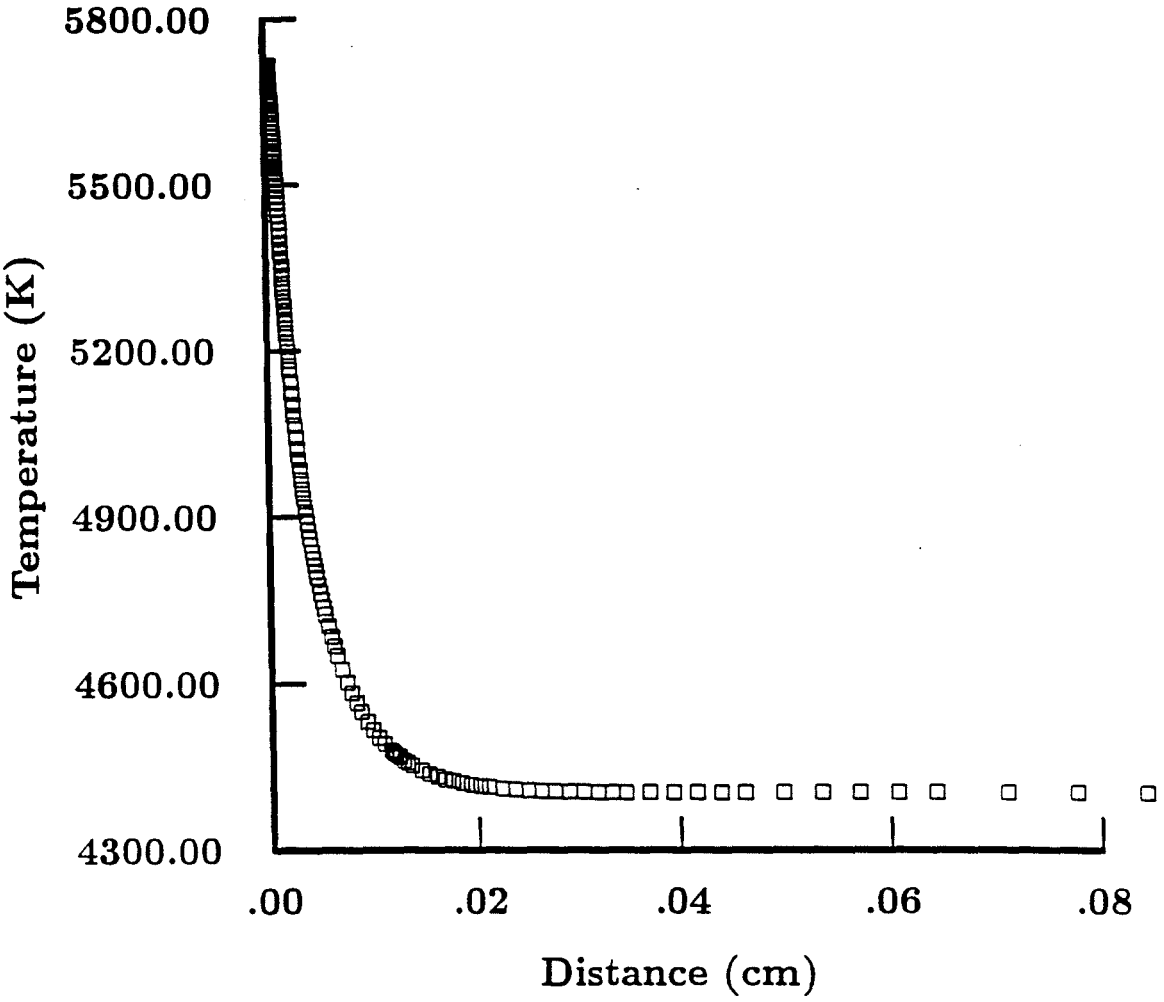

Figure 26. Temperature profile for the reaction zone of case 3.

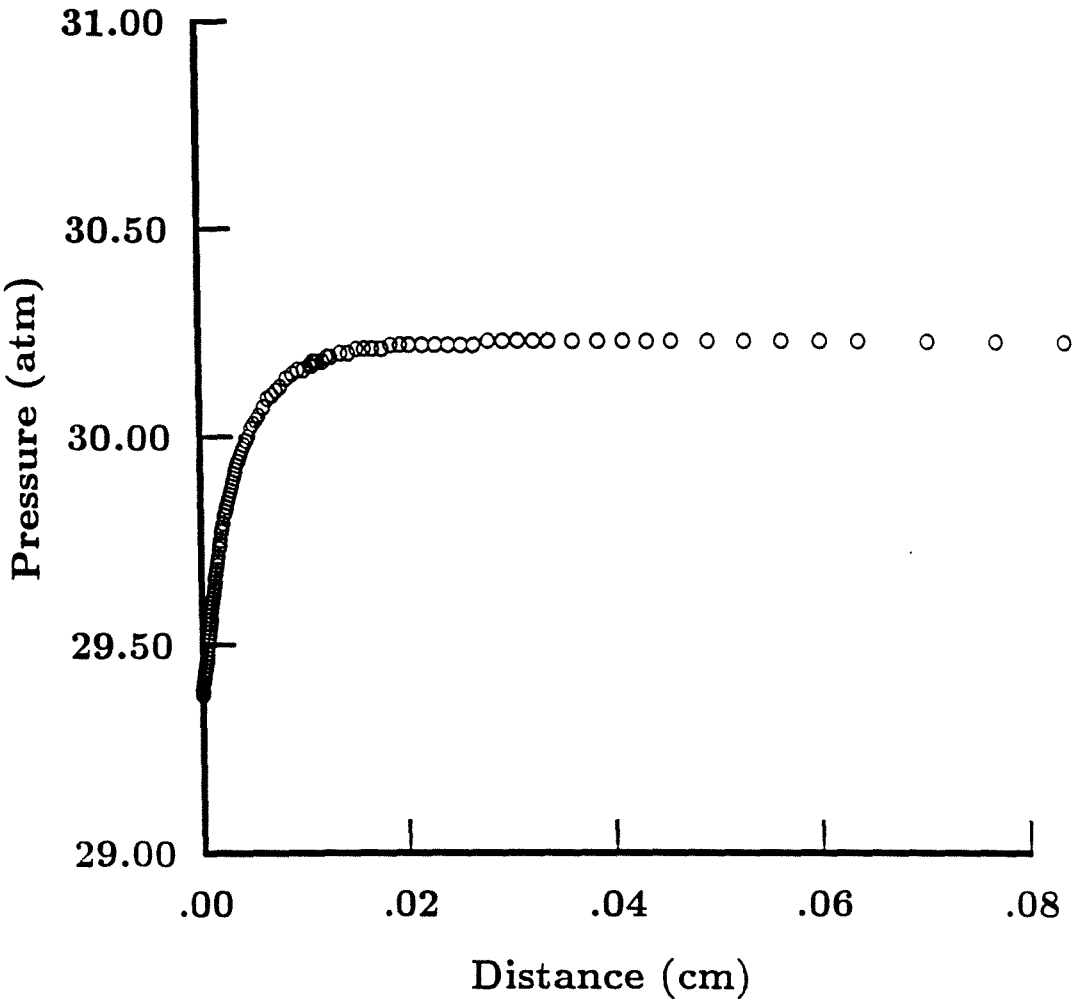

Figure 27. Pressure profile for the reaction zone of case 3.

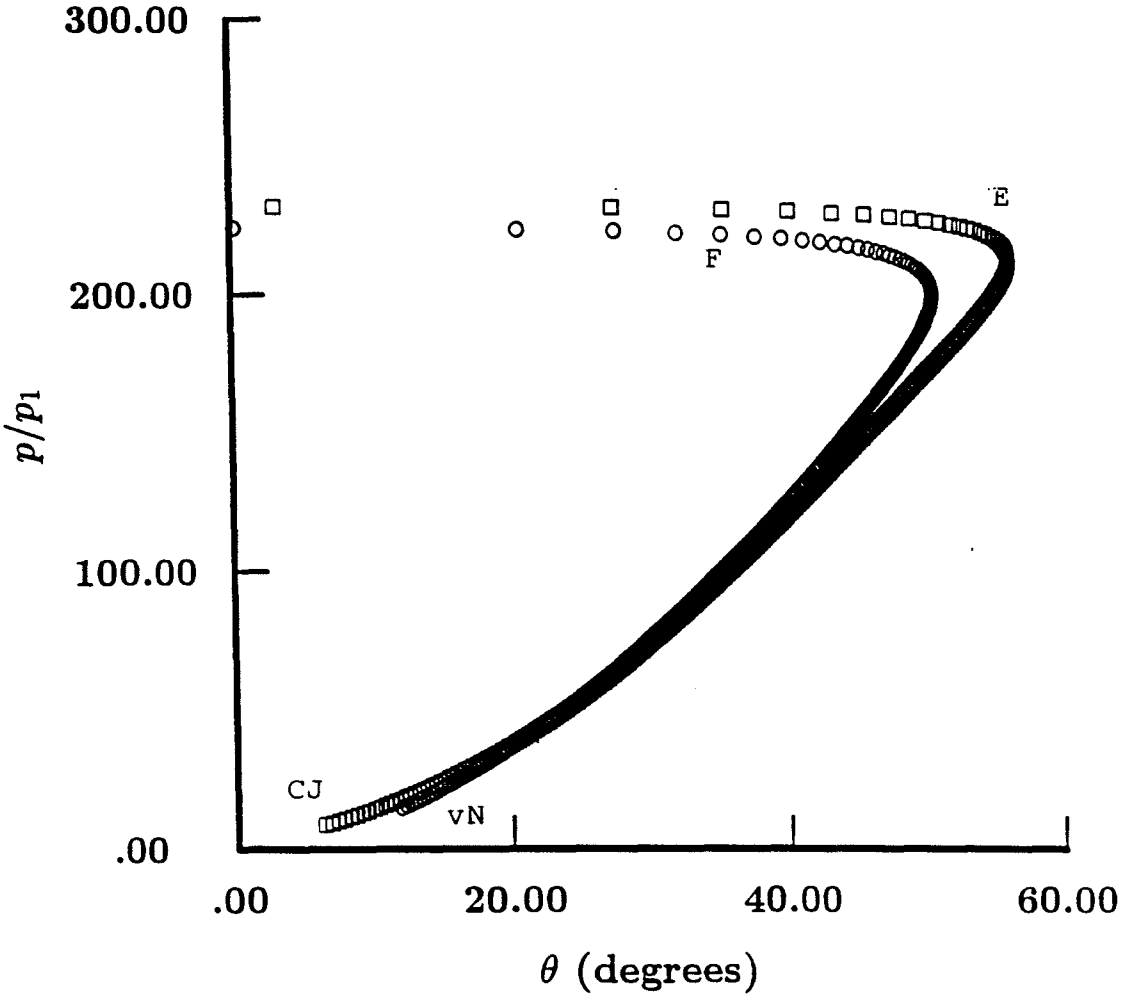

Figure 28. Frozen (F) and equilibrium (E) polars for case 4, showing the CJ point and the von-Neumann point (vN).

overdriven case from reference (10). The case has the same free-stream conditions and composition as case 2 but with a free-stream Mach number of 15. This gives an overdrive parameter of 3.7517. The effect of more overdrive is to push the cross-over point further down on the polars. The cross-over deflection angle now becomes about 21.25°.

The trend continues as is shown in figure (29) for a free stream Mach number of 19. This case has an overdrive parameter of 4.7522. The cross-over angle is now about 19°.

4.2.5 Summary of CAM Cases

Some general remarks can be made about the equilibrium concentrations as a function of the upstream normal velocity based on the STANJAN output which is enclosed in Appendix A. For the first CAM case (called case 2 in reference (10)), the ionized species have a very small mole fraction even at the highest normal upstream velocity of 8066 m/s. However, in going from the CJ velocity of 1648.4 m/s to the maximum normal upstream velocity the mole fraction of ionized species increases by as much as 13 orders of magnitude. The increase in the normal upstream velocity is also accompanied by a two orders of magnitude increase in the mole fraction of atomic species. In general, as the upstream normal velocity increases, so does the temperature behind the non-reactive shock which progressively promotes the formation of species with high heats of formation. The same trends are observed with the

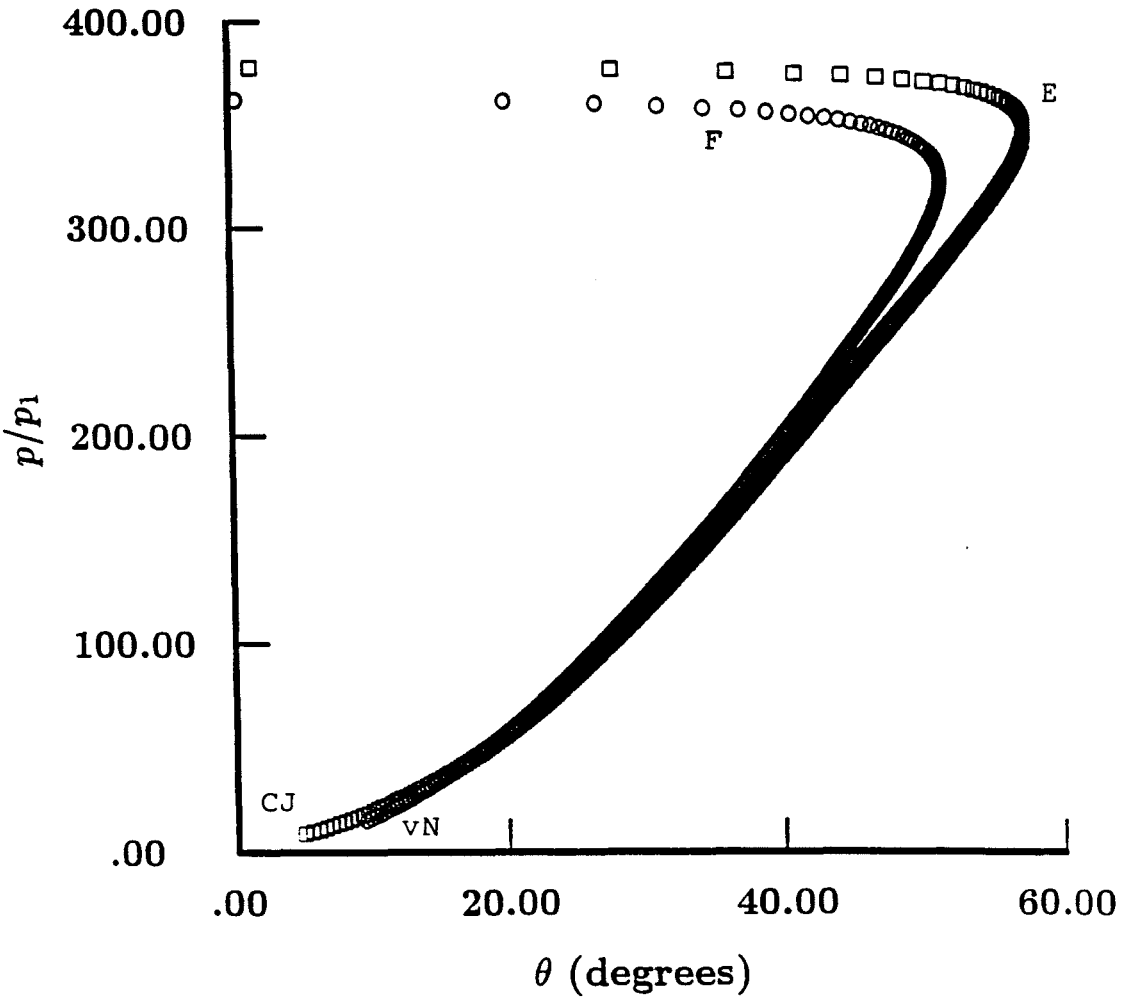

Figure 29. Frozen (F) and equilibrium (E) polars for case 5, showing the CJ point and the von-Neumann point (vN).

second case from reference (10) (called case 4 in that reference), except that dissociation is slightly inhibited by the fact that the initial pressure was higher than that for the other CAM case. The effect is only slight because the initial temperature is lower than for the other CAM case and thus acts to offset the effect of the lower pressure.

Although the mole fractions of ionized species are very small, one might expect a substantial effect on the equilibrium temperature, since the ionized species have very large positive heats of formation. This is not what was observed. When the equilibrium temperature was computed for case 2 with and without ionized species, the maximum difference was 0.13% for the most overdriven point with an upstream normal velocity of 8500 m/s.

Figure (30) shows a plot of the CJ, maximum, and cross-over flow deflection angles for the second case from reference (10) (called case 4 in that reference), for various free-stream Mach numbers. The cross-over curve exhibits a sharp rise to the left of a maximum point. This steep rise corresponds to the rapid movement of the cross-over point along the top branch of the polars. The maximum point corresponds to the case where the cross-over flow deflection angle coincides with the maximum flow deflection angle, and thus it is tangent to the maximum flow deflection angle curve. The part of the cross-over

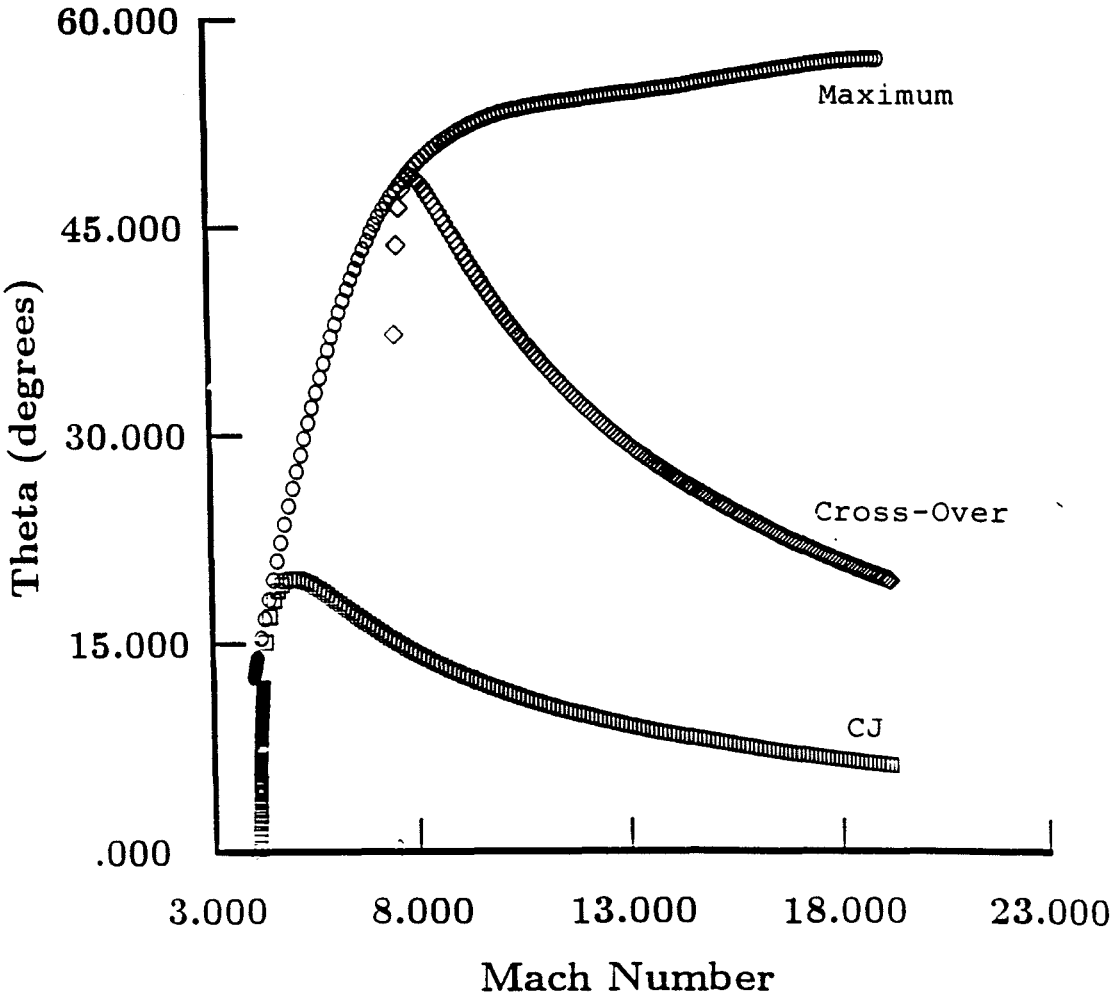

Figure 30. Maximum, CJ, and cross-over flow deflection angles versus free-stream Mach number for cases 2 through 5 (CAM case 4).

curve which is to the right of the maximum point corresponds to the slower movement of the cross-over point along the lower branch of the polars. Until now, most people were of the belief that the upper bound on the utility of oblique detonation waves for propulsion was the point corresponding to the maximum flow deflection angle (reference (9)). Based on the work done in this thesis, there is reason to believe that the upper bound is the cross-over point. Figure (30) clearly shows that the cross-over point is a much less favorable upper bound since it drastically reduces the range of utility of oblique detonation waves. Even more worrisome is the fact that the useful range of flow deflection angles shrinks as the Mach number is increased. The maximum useful range occurs for the free-stream Mach number when the cross-over point flow deflection angle coincides with the maximum flow deflection angle.

Since the reaction zone structure was investigated only for a limited number of cases from reference (10), it is not possible to make generalizations at this point about the effect of overdrive on the reaction zone structure. However, a comparison between cases 2 and 3 indicates an increase in the reaction zone length from 0.137 mm to 0.556 mm when the upstream normal velocity is increased from 1980 m/s to 4100 m/s. Such a comparison may not be valid, however, since the two cases belong to two distinct

regimes: one falls in the pre-cross-over regime and the other is in the post-cross-over regime. The two regimes have a very different reaction zone structure. While the temperature increases in the former, it drops in the latter.

4.2.6 Case 6

This is the first of the cases that were examined in this thesis using the free-stream initial conditions and composition presented in Dabora, Wagner, and Desbordes (15), which will be referred to in the remainder of this thesis as Dabora cases. For all the Dabora cases the free stream pressure was 0.5 atm. No free stream temperature was given, so 298.16 K was assumed, and the agreement with the reported results seems to validate this assumption. For all the Dabora cases, the free-stream composition was also the same and is listed along with the free-stream conditions in table (1) in section 3.1.

Figure (31) shows the frozen and equilibrium Hugoniots for the Dabora cases. The cross-over point corresponds to a pressure of about 38 bars and a specific volume of about 0.34 m^3/kg. The cross-over pressure ratio is therefore about 75.

The C-J velocity obtained from STANJAN is 1824.2 m/s which is in good agreement with the 1800 m/s stated in reference (15).

Figures (32) through (34) show the temperature,

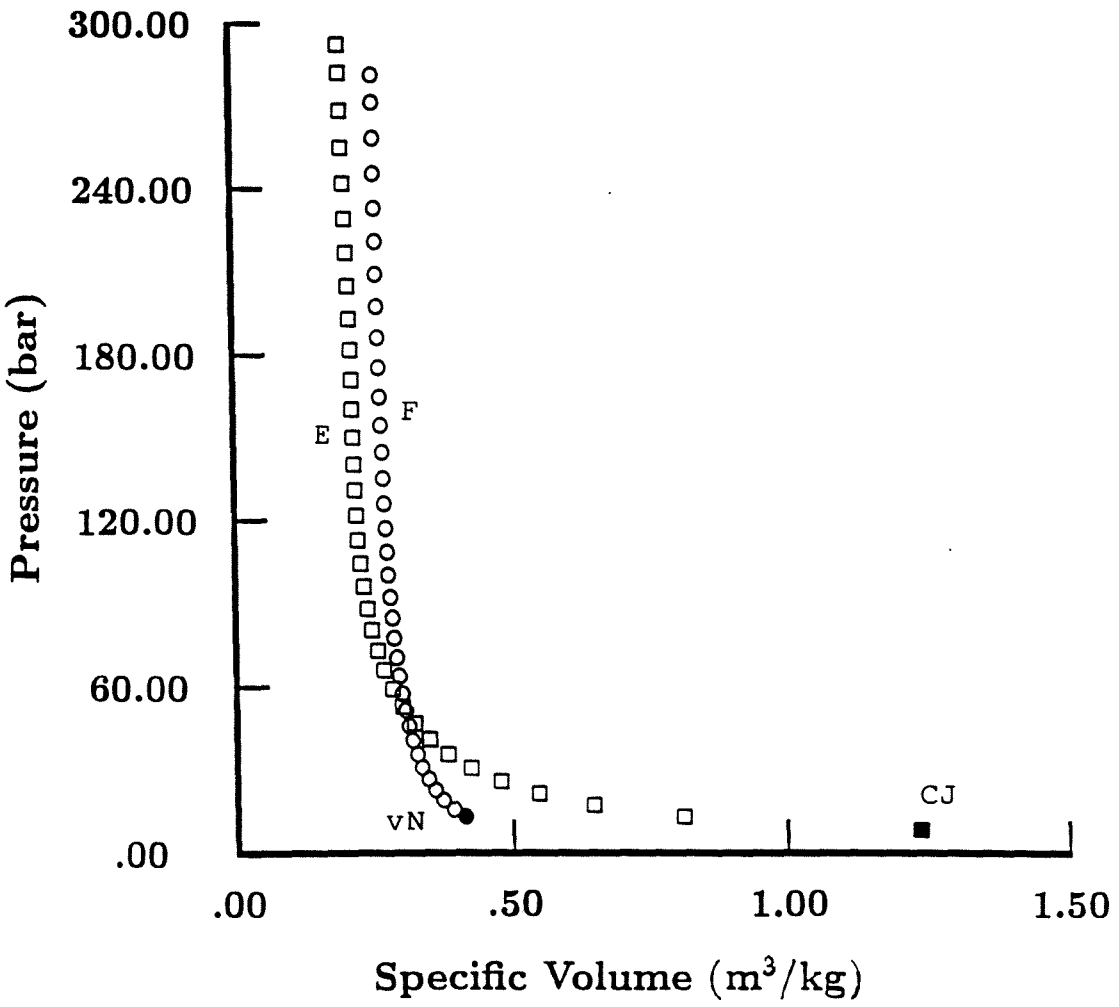

Figure 31. Frozen (F) and equilibrium (E) Hugoniots for cases 6 through 13.

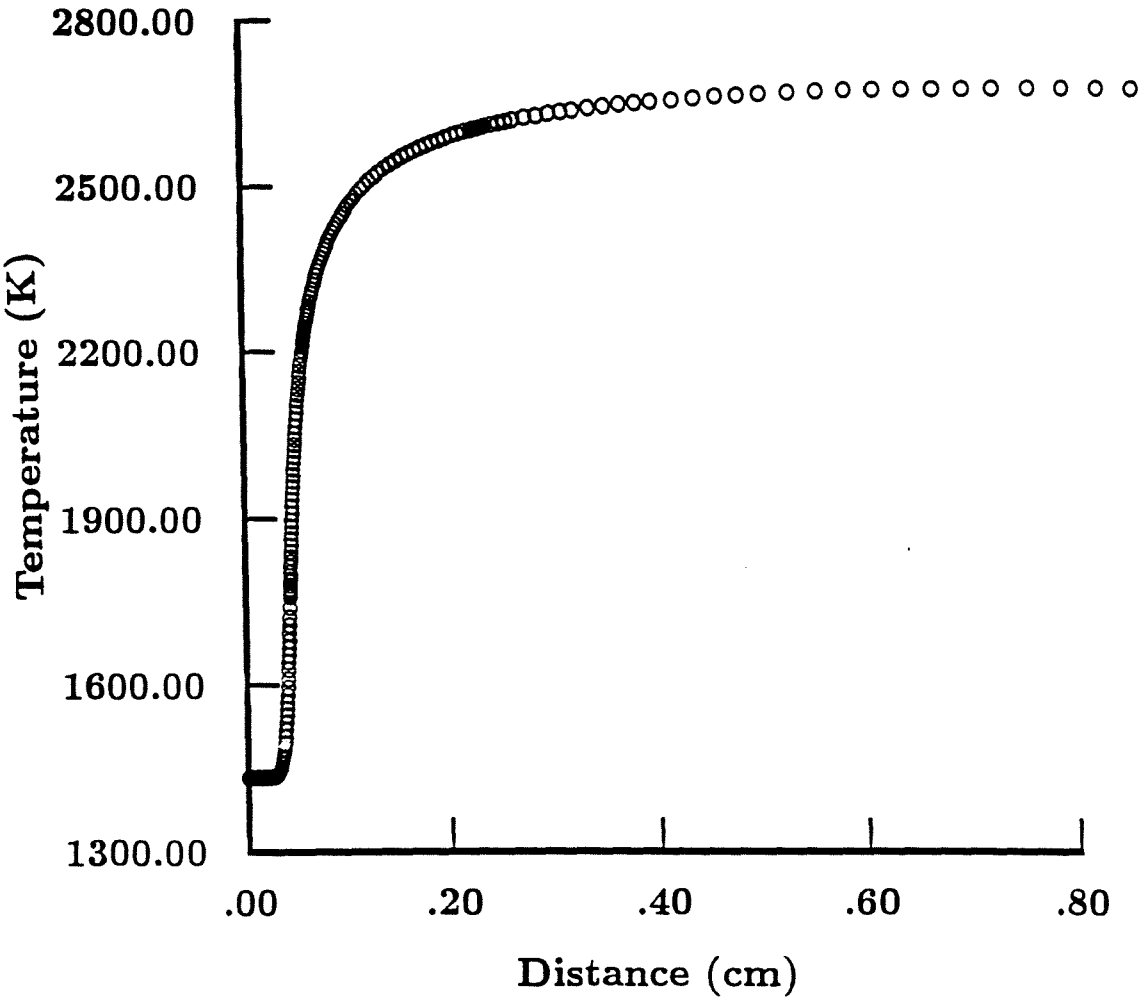

Figure 32. Temperature profile for the reaction zone of case 6.

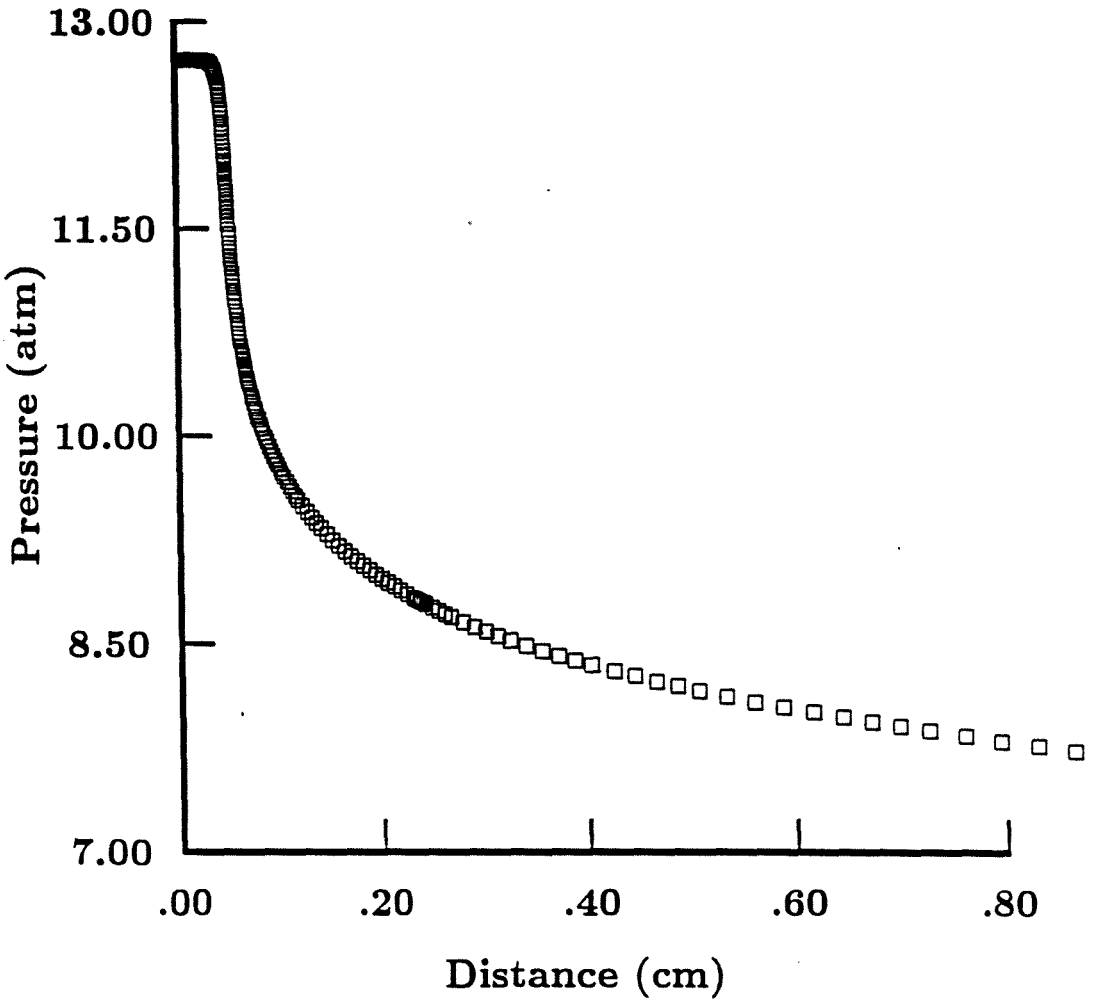

Figure 33. Pressure profile for the reaction zone of case 6.

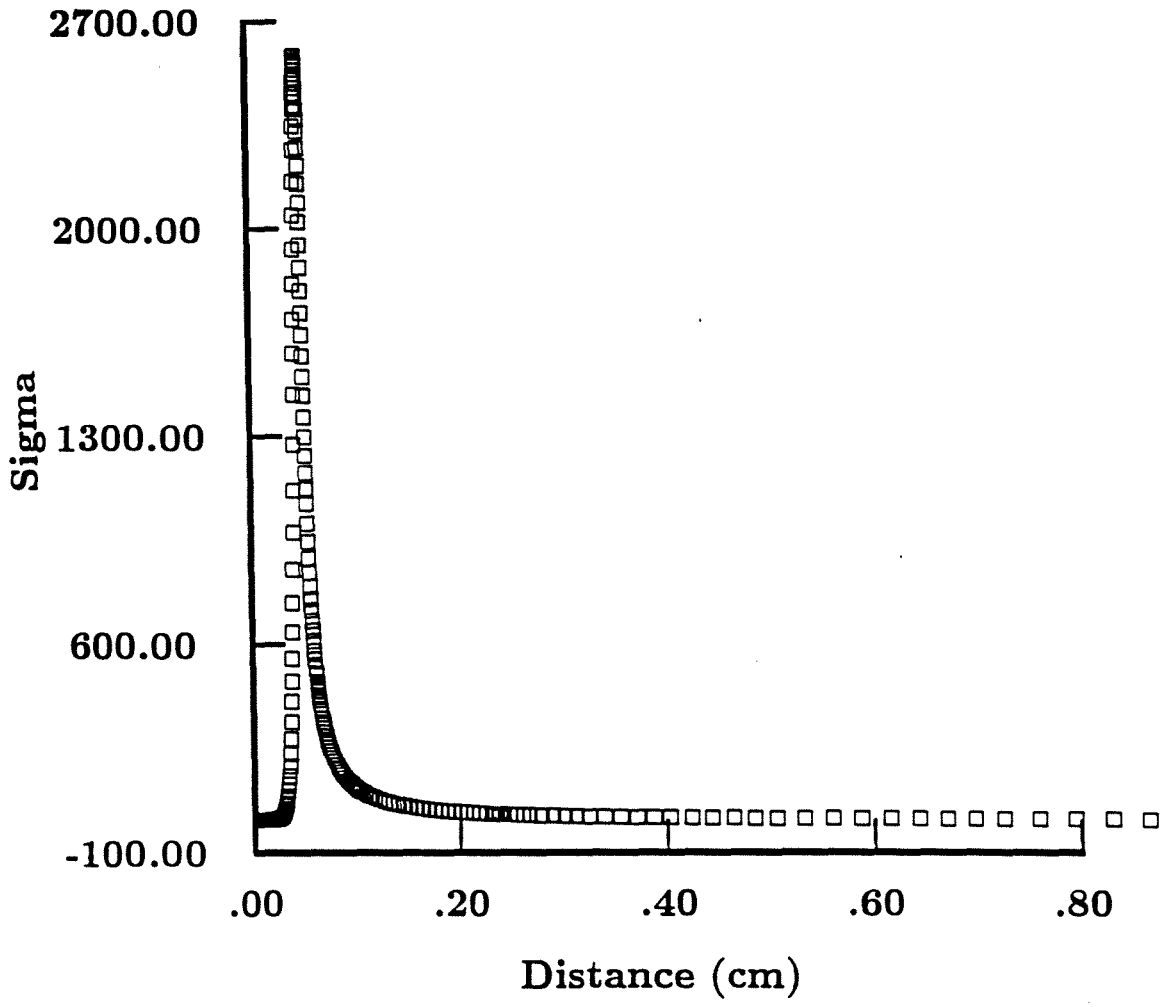

Figure 34. Sigma profile for the reaction zone of case 6.

pressure, and sigma profiles for the Dabora C-J case. Sigma is the variable which was introduced in the theory section and is a measure of the net rate of heat release. The profiles are of the typical form: a von-Neumann spike in pressure followed by a drop in pressure at a decreasing rate. The temperature jumps up after the shock, and then there is a short induction zone followed by a sharp rise in the temperature due to the termination of the reaction sequence through three-body recombination reactions. Note that neither the post-shock pressure jump nor the post-shock temperature jump are shown in the figures. The figures have horizontal ordinates which start immediately after the shock wave. Thus the reader can detect the von-Neumann spike only if he compares the pressure at a distance of zero on the figure with the free stream pressure. The maximum value of sigma corresponds to the location where the temperature profile has the largest slope. This is as expected, since sigma is a measure of the net rate of heat release. The reaction zone length based on the maximum rate of heat release (maximum sigma) was 0.440 mm. The reaction zone length is based on sigma (as opposed to leveling off of temperature, pressure or species profiles) because sigma is the critical parameter which couples the chemical kinetics and the fluid dynamics of the reactive flow.

It should be noted that since this case corresponded

to the CJ point it was not necessary to plot the frozen and equilibrium polars. The polars in this case reduce to the trivial solution: a single point with a flow deflection angle of zero.

4.2.7 Case 7

Figure (35) shows the frozen and equilibrium polars for the Dabora case with a free stream Mach number of 5.086. This yields an overdrive parameter of 1.0964. This represents very little overdrive, and so, as expected, there is no cross-over deflection angle.

The reaction zone length based on the maximum rate of heat release was 0.184 mm.

4.2.8 Case 8

Figure (36) shows the actual Dabora case polar set. This case had the same free-stream conditions and initial composition as case 6 but with a free-stream Mach number of 8.4. This corresponds to an overdrive parameter of 1.8107. This is moderately overdriven, and so the frozen and equilibrium polars approach each other very closely at the beginning of the top branch.

Figures (37) through (43) show the temperature, pressure, sigma, and species profiles for the reaction zone of the actual Dabora case. The form of the temperature, pressure, and sigma profiles is the same as that discussed above for the C-J case (case 6). This is as expected since this case and the case 6 both correspond to points below

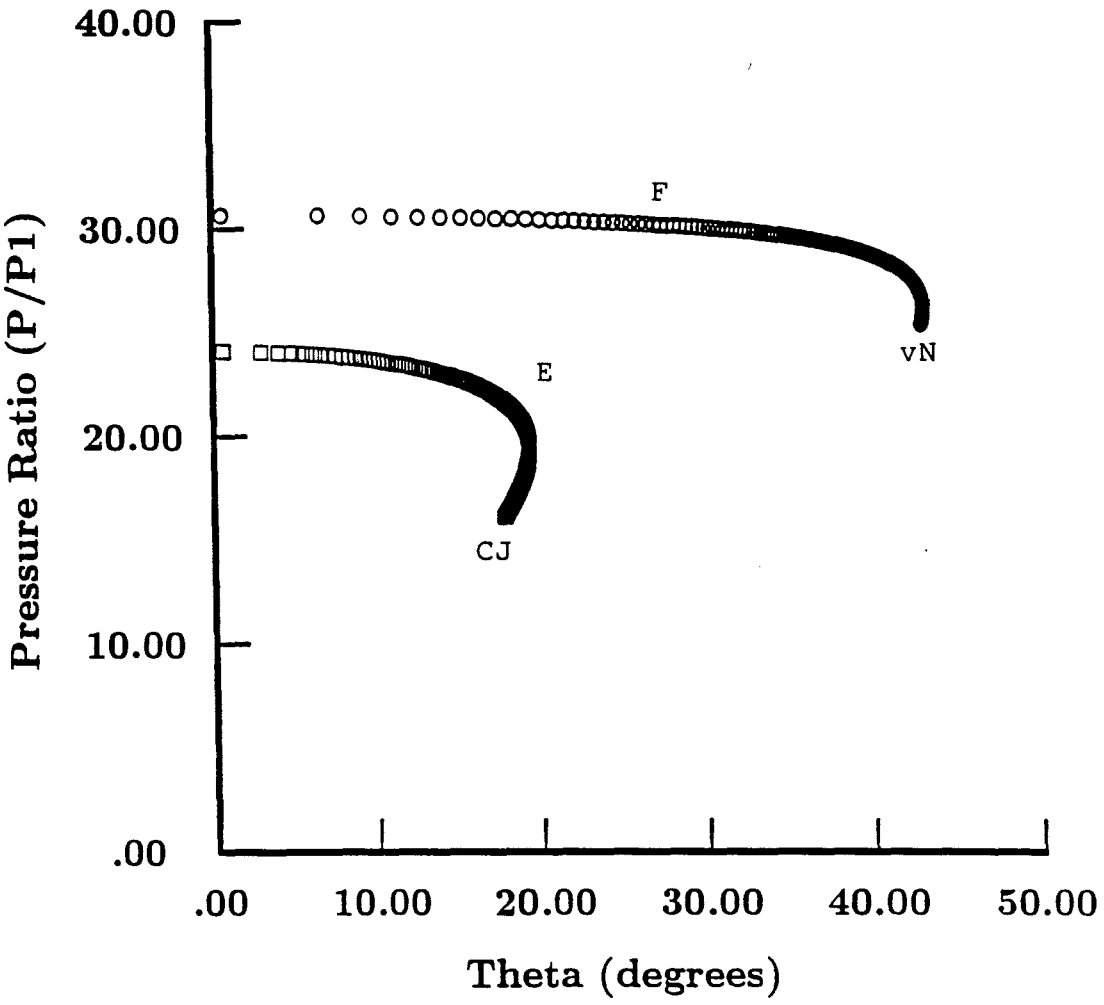

Figure 35. Frozen (F) and equilibrium (E) polars for case 7, showing the CJ point and the von-Neumann point (vN).

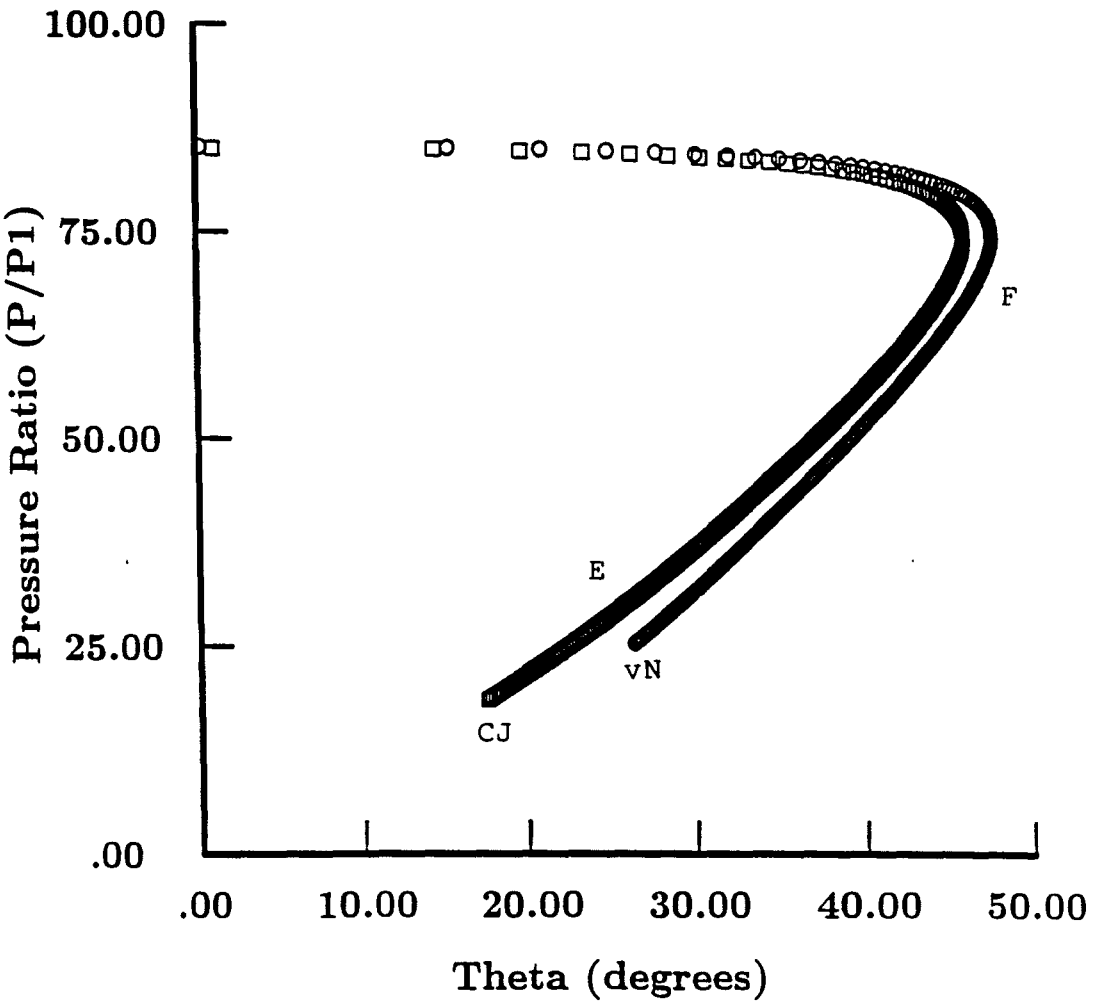

Figure 36. Frozen (F) and equilibrium (E) polars for case 8, showing the CJ point and the von-Neumann point (vN).

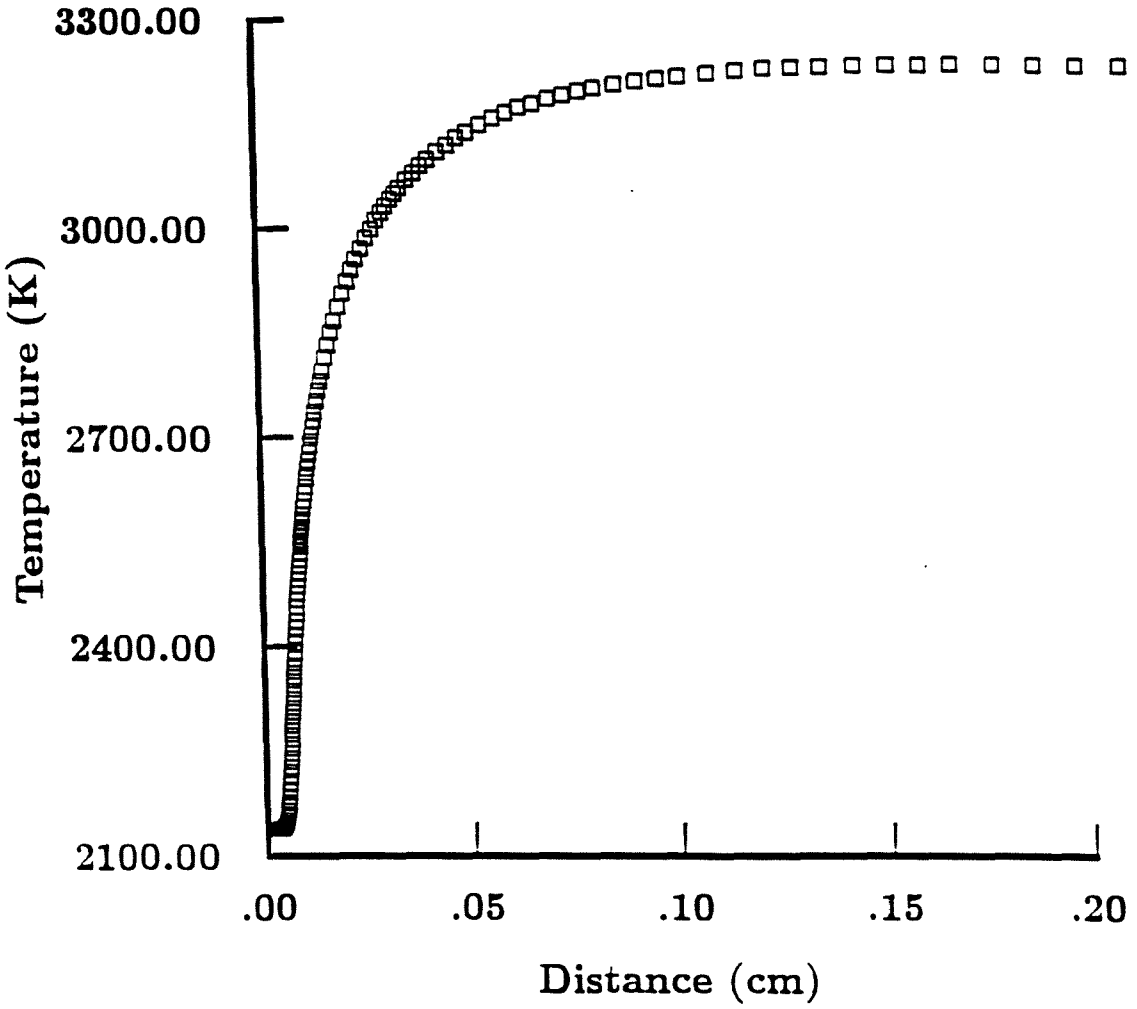

Figure 37. Temperature profile for the reaction zone of case 8.

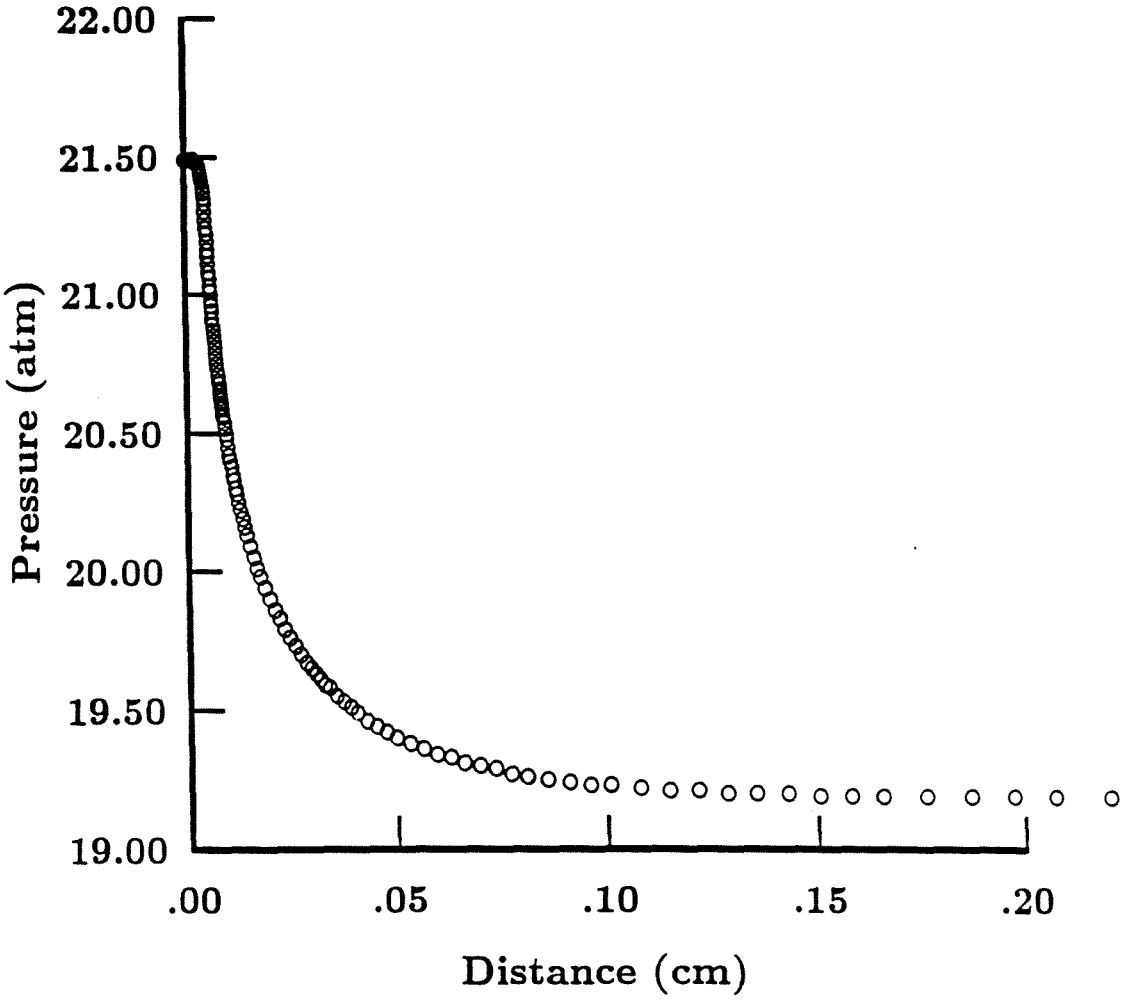

Figure 38. Pressure profile for the reaction zone of case 3.

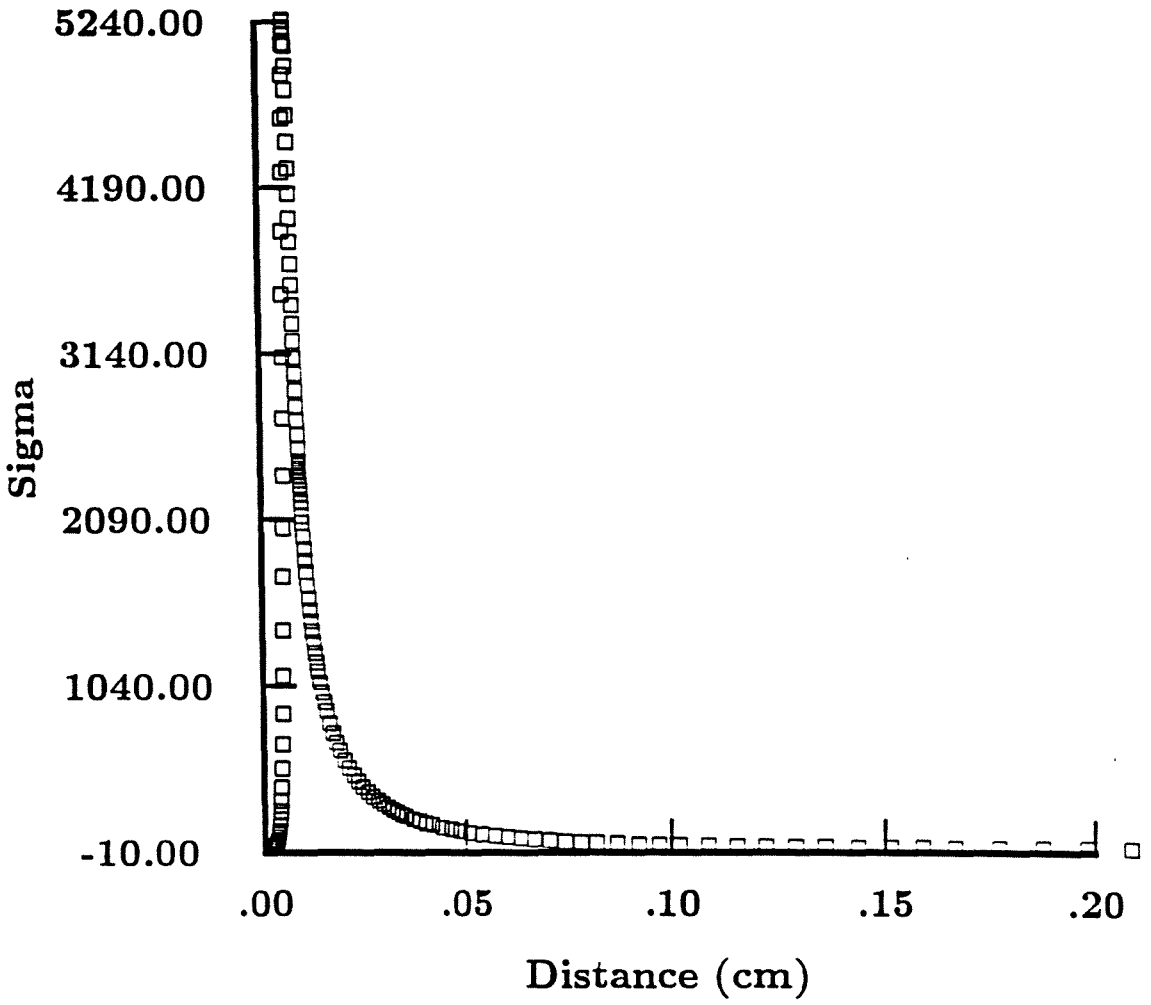

Figure 39. Sigma profile for the reaction zone of case 8.

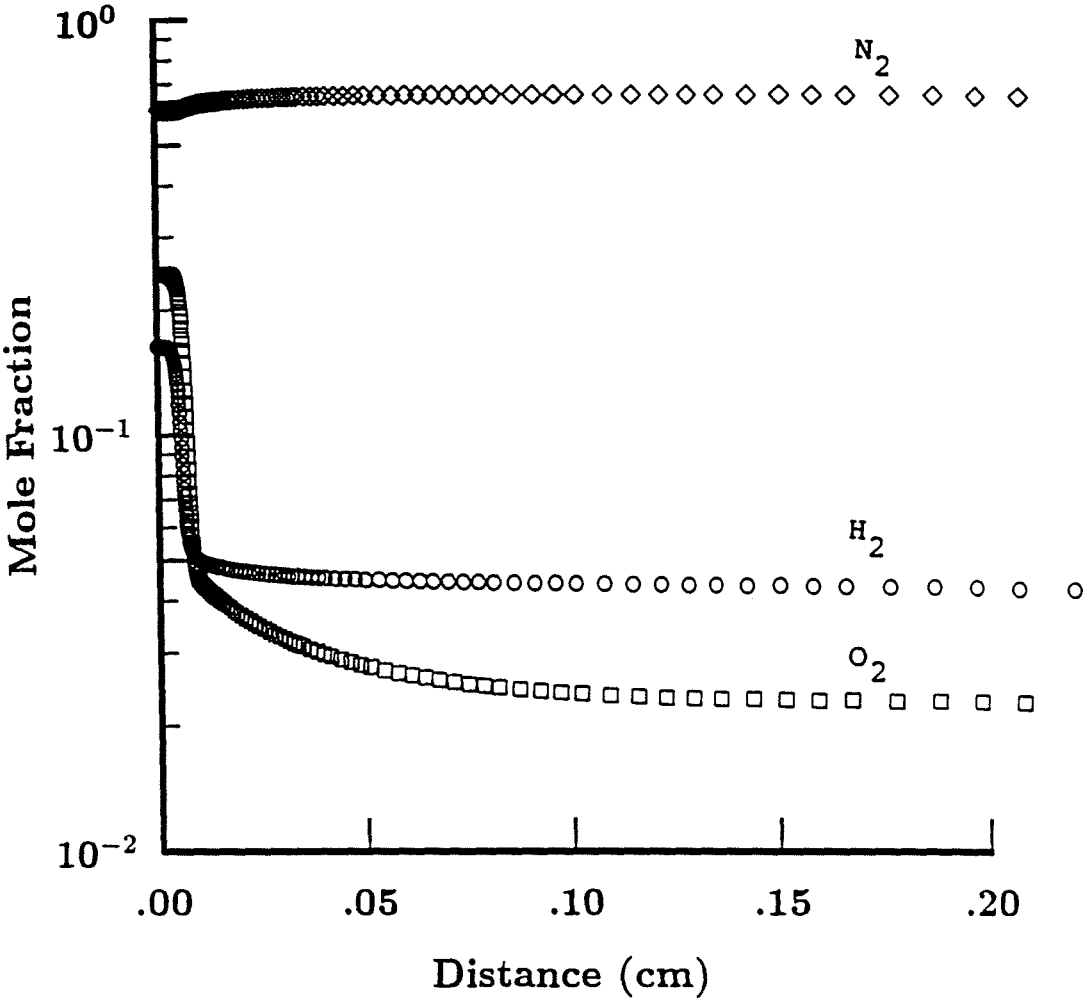

Figure 40. Mole fractions of H_2, O_2, and N_2 for the reaction zone of case 8.

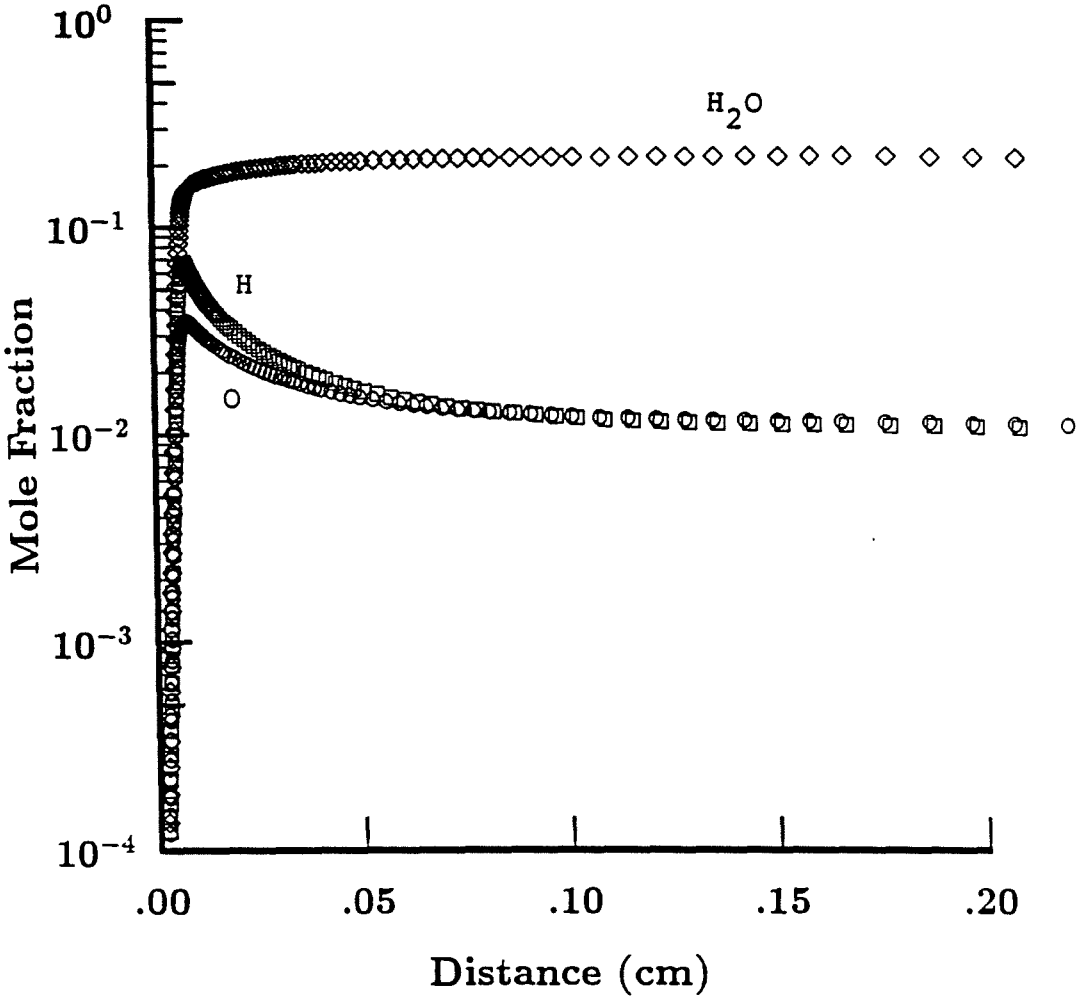

Figure 41. Mole fractions of H, O, and H_2O for the reaction zone of case 8.

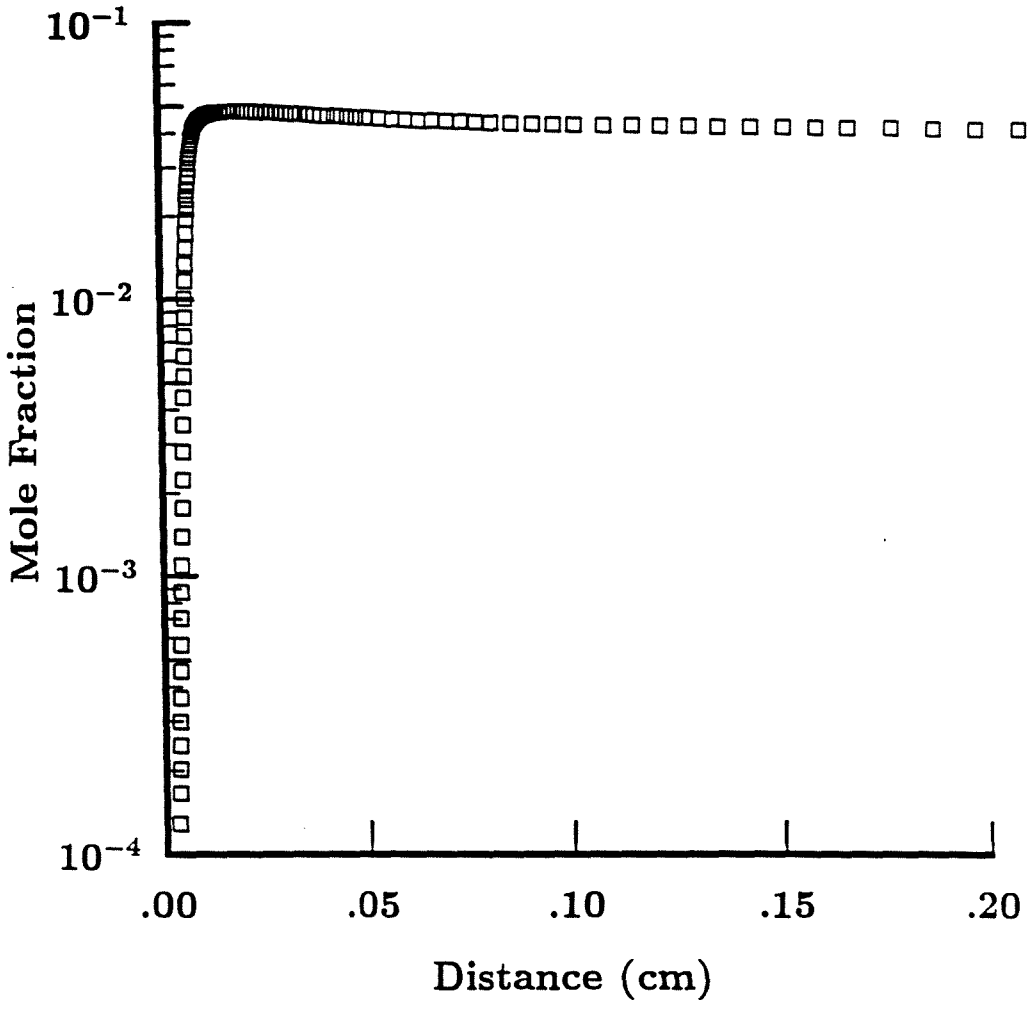

Figure 42. Mole fraction of OH for the reaction zone of case 8.

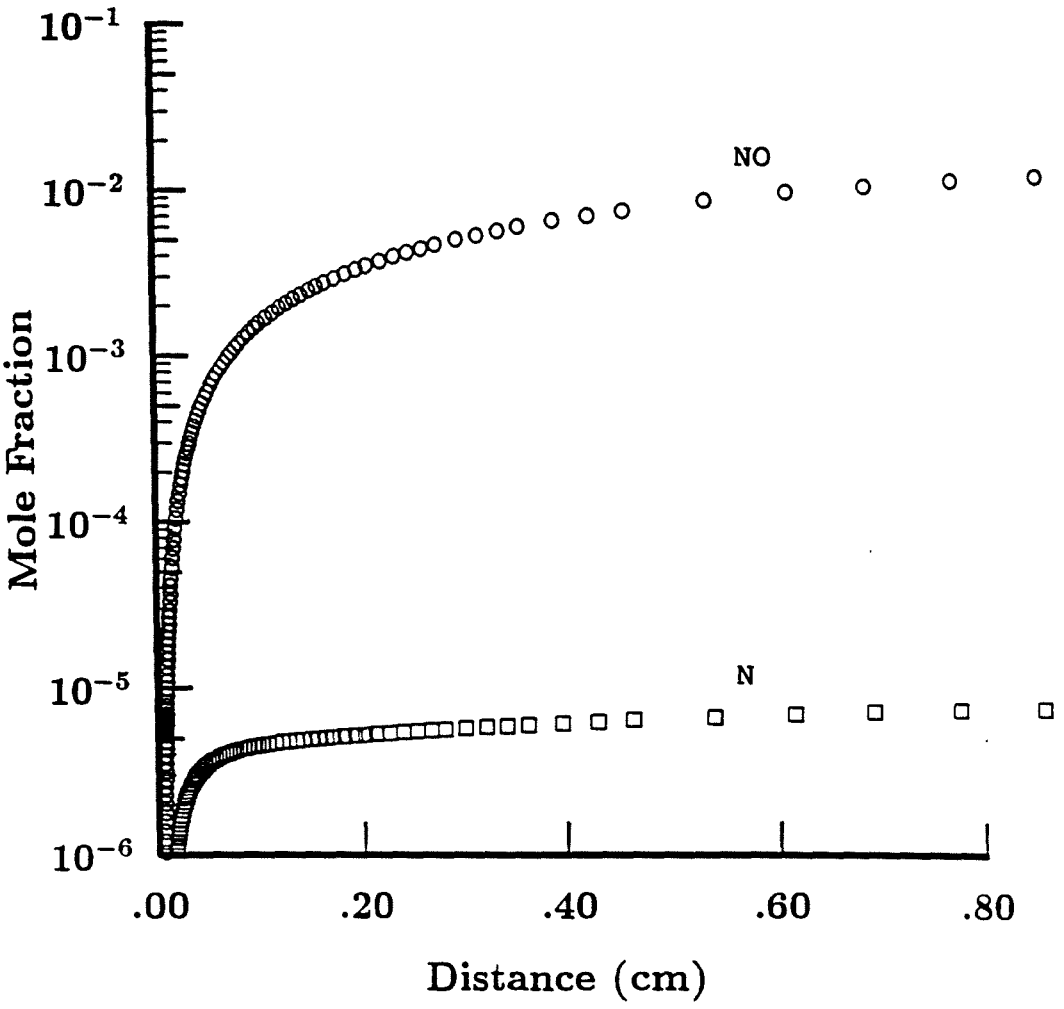

Figure 43. Mole fractions of N and NO for the reaction zone of case 8.

the cross-over point on the Hugoniots, and thus should exhibit similar behavior. The only difference is that the maximum values are higher for the case 8, and the reaction zone becomes narrower. It is worth noting that the maximum rate of heat release corresponds to the formation of the water molecules. This could be seen from a superposition of figures (37), (39), and (41). The trends for the rest of the species are the same as those discussed for the CAM cases. The reaction zone length based on the maximum rate of heat release is 0.0547 mm.

4.2.9 Case 9

Figures (44) through (51) show the temperature, pressure, sigma, and species profiles for the Dabora case where the equilibrium pressure is equal to the frozen pressure. This case corresponds to the cross-over point on the Hugoniots, and has an overdrive parameter of 1.8768. One might intuitively expect a perfectly flat pressure profile. This is not the case. The final and initial pressures on figure (44) are the same, but the profile has a double peak early on, and then dips below the cross-over value then gently rises to it again. Similar behavior is exhibited by the temperature profile, only here there is a double dip in the temperature. The sigma profile now has two peaks and a single dip, and it takes on very large negative values at the beginning of the reaction zone and at the dip. The first peak in sigma now has a relatively

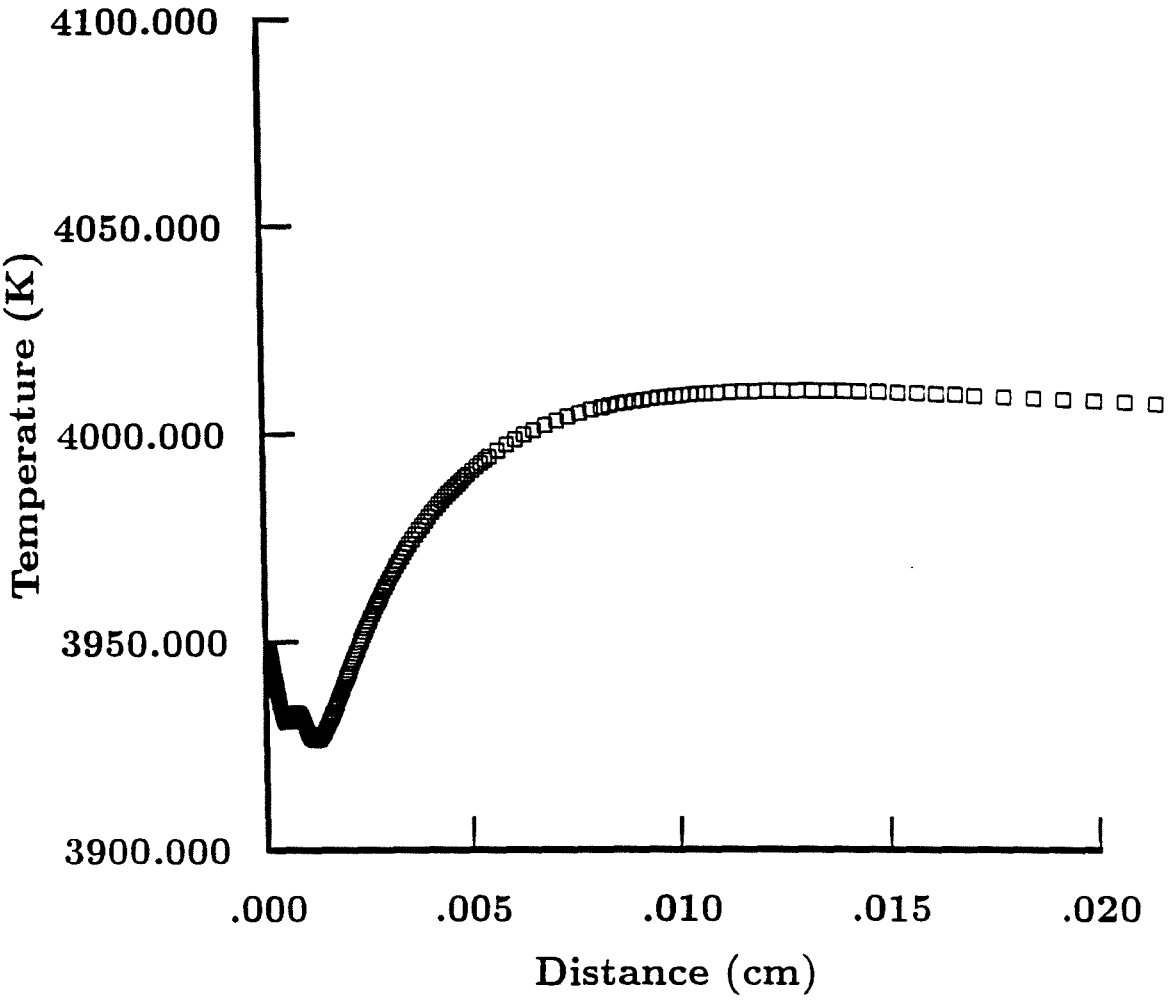

Figure 44. Temperature profile for the reaction zone of case 9.

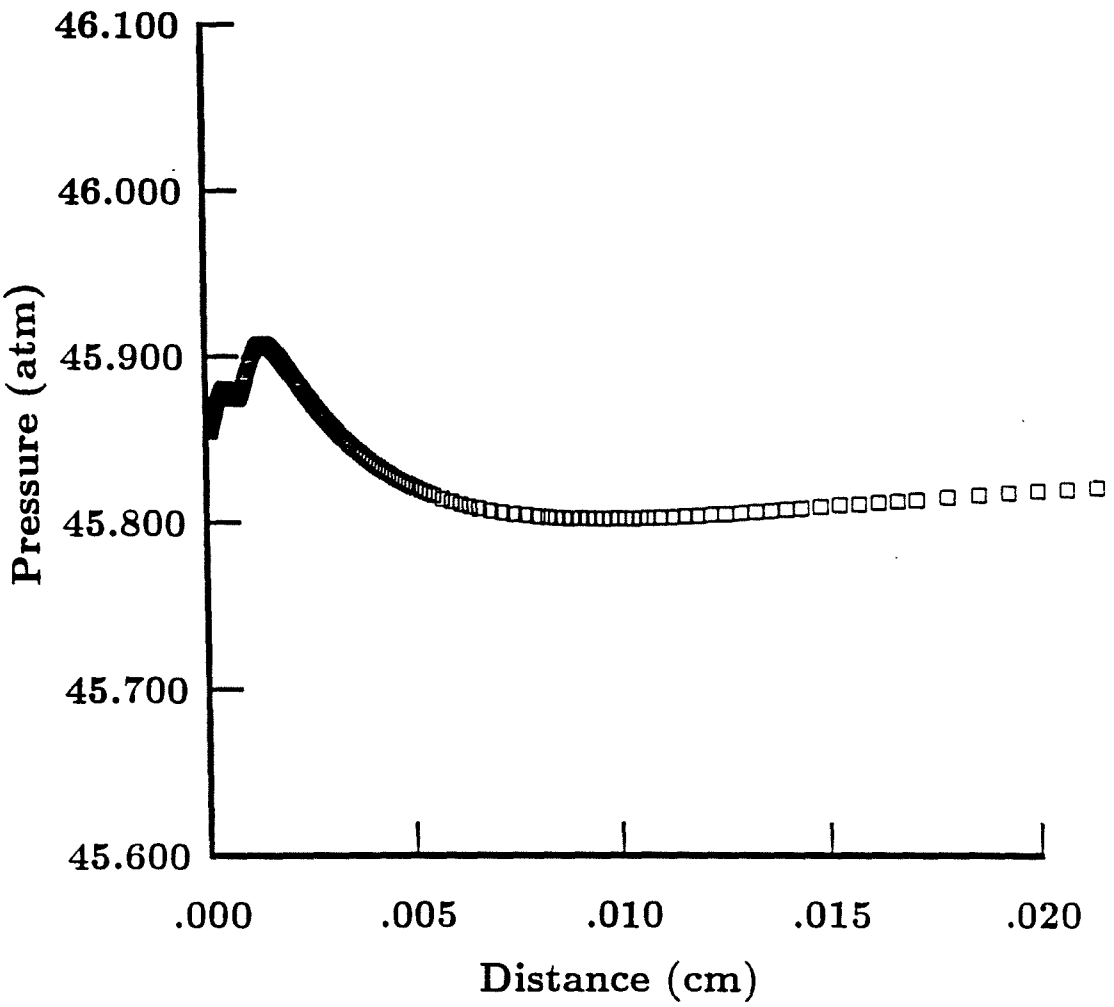

Figure 45. Pressure profile for the reaction zone of case 9.

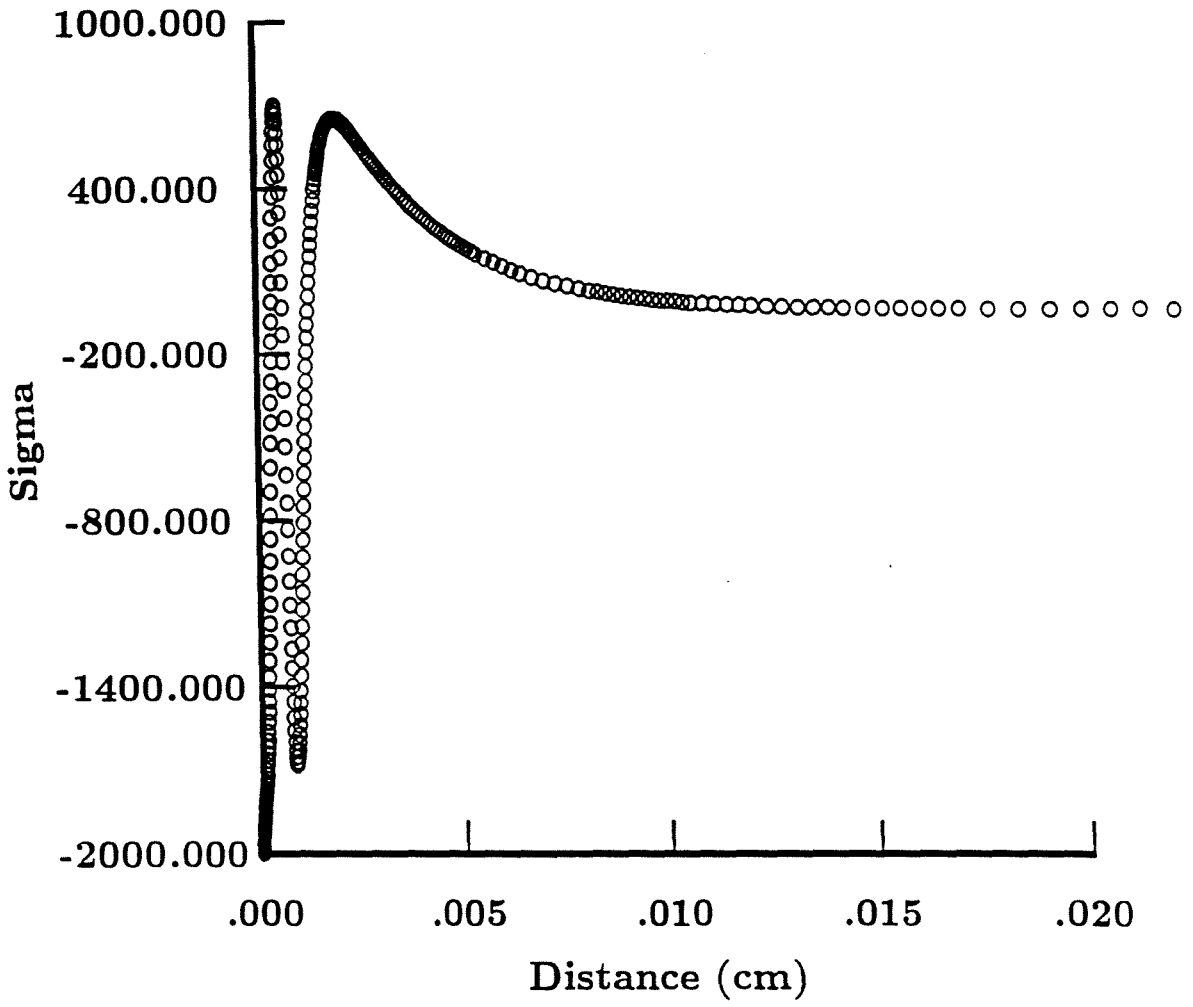

Figure 46. Sigma profile for the reaction zone of case 9.

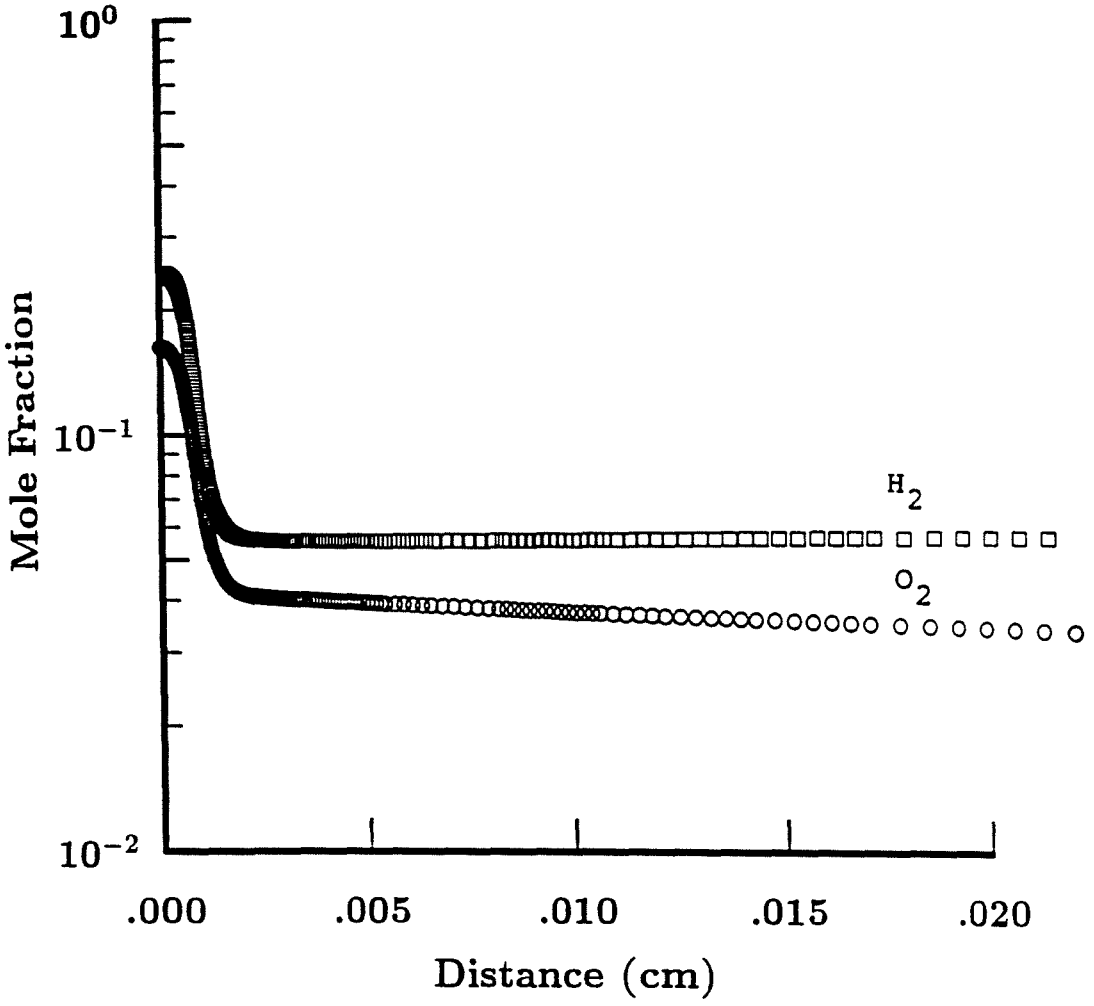

Figure 47. Mole fractions of H_2 and O_2 for the reaction zone of case 9.

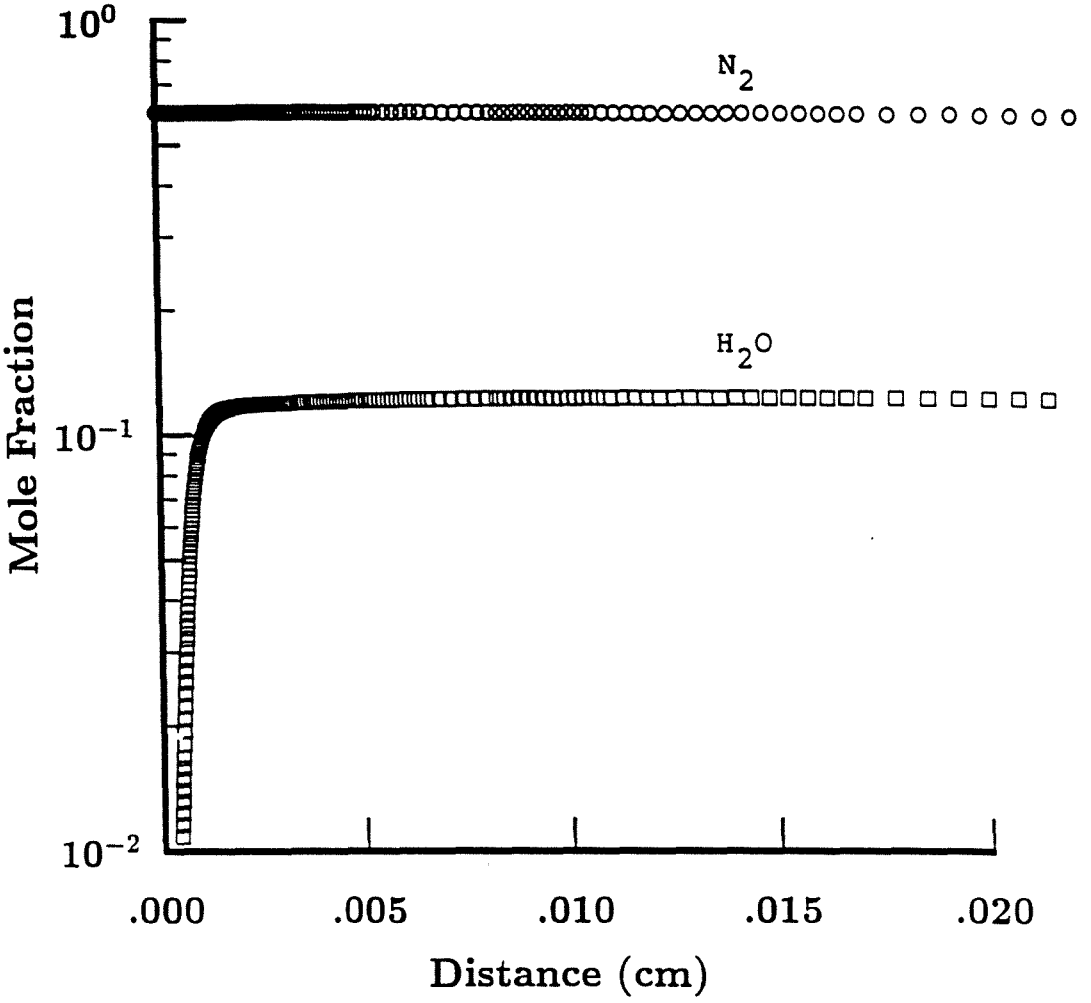

Figure 48. Mole fractions of N_2 and H_2O for the reaction zone of case 9.

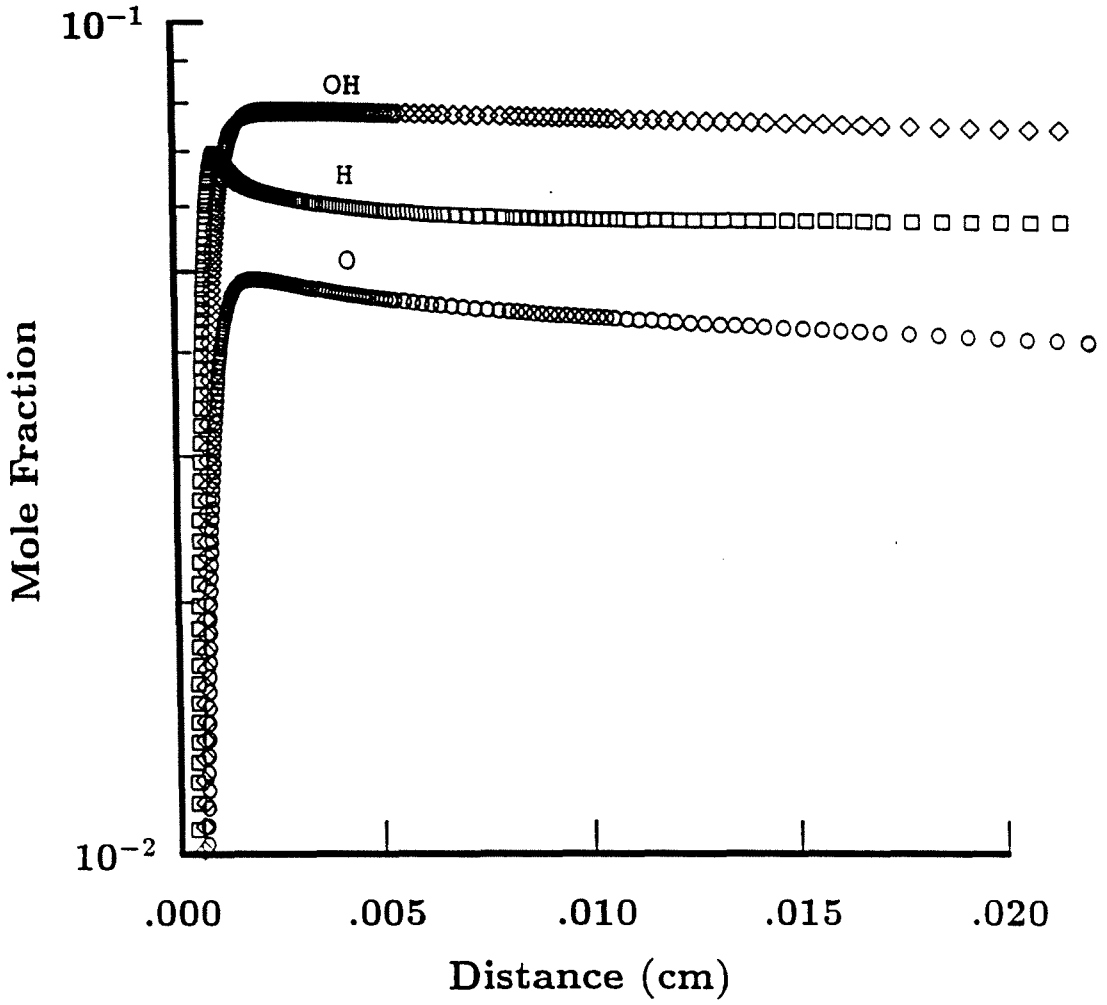

Figure 49. Mole fractions of H, O, and OH for the reaction zone of case 9.

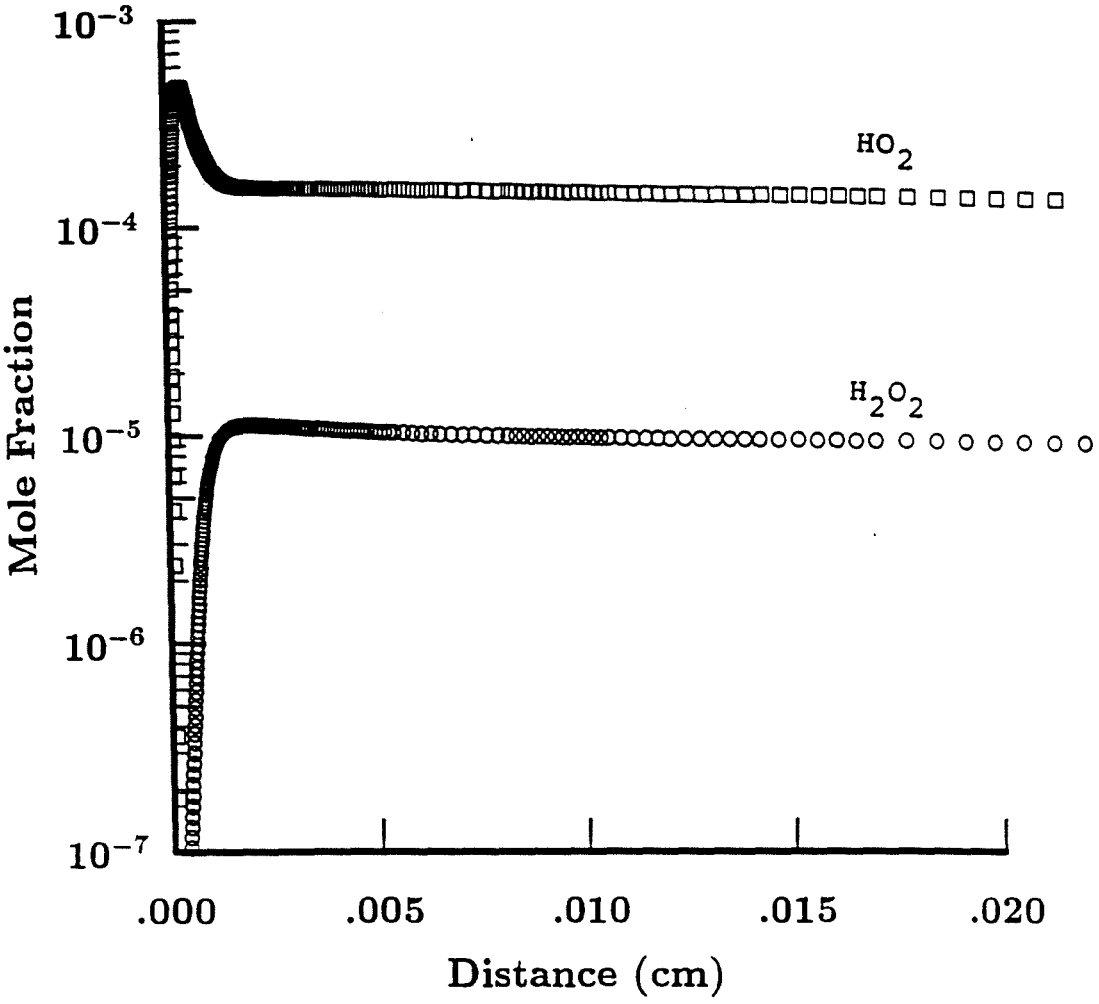

Figure 50. Mole fractions of HO_2 and H_2O_2 for the reaction zone of case 9.

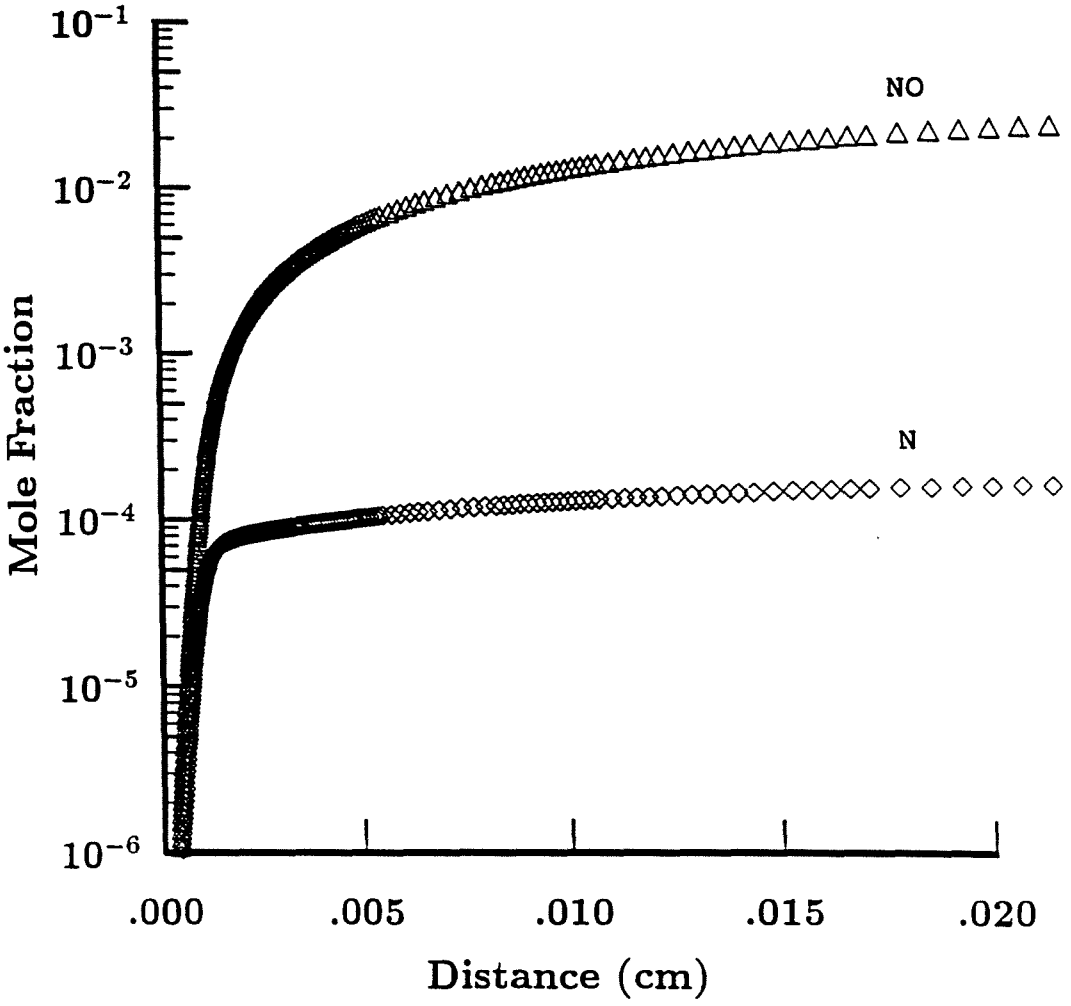

Figure 51. Mole fractions of N and NO for the reaction zone of case 9.

small positive value. The second peak is only slightly lower than the first peak. The sigma profile still drops asymptotically to its final value of zero.

By superposing the various species profiles on the sigma profile the following is observed. The first peak in the sigma profile corresponds to the largest rate of change of the mole fraction of water. It also coincides with the maximum rate of decay of H_2O_2, and the maximum rate of growth of the mole fraction of HO_2. The dip in the sigma profile corresponds to the maximum rate of decay of the H_2 and O_2 populations. It also coincides with the maximum mole fraction of H and the maximum rate of growth of the mole fraction of O. The only thing corresponding to the second peak in sigma is the leveling off of the OH mole fraction. The following is a possible explanation of these observations.

In attempting to reach chemical equilibrium, the product mixture must minimize its Gibbs free energy. The Gibbs free energy has two components: an enthalpy component which is a function of the heats of formation, and a component which is the product of the temperature and entropy.

$$G = H - T\,S \tag{39}$$

Thus, to minimize the Gibbs free energy, the flow would like to reduce the enthalpy component and increase the entropy and temperature. The enthalpy component is

minimized by producing species with low heats of formation. The entropy is maximized by producing a large number of small species with large heats of formation. Thus the two components of the Gibbs free energy work in opposing directions. Immediately behind the shock wave there are dissociation products (because of the very high temperature) which have very large positive heats of formation. Thus the temperature tends to drop so as to allow the formation of species with lower heats of formation such as water. This does reduce the entropy somewhat, but since the entropy is multiplied by such a large temperature, the entropy component of the Gibbs free energy does not drop by much. Thus, the net effect of a drop in temperature is the reduction of the Gibbs free energy, which drives the mixture towards equilibrium. This is why the temperature drops behind the non-reacting shock wave for this case. Note that the key factor is that the post-shock temperature is very high. This is why the trend is opposite for cases below the cross-over point. In such cases the post-shock temperature is not high enough to minimize the drop in entropy due to the formation of species with low heats of formation. Thus, the net effect of lowering the temperature would actually be an increase in the Gibbs free energy due to the drop in the entropy component. An increase in the Gibbs free energy implies movement away from equilibrium. This is why the flow favors

an increase in temperature behind the shock in order to minimize the Gibbs free energy.

The final rise in the temperature is due to recombination of O and H atoms to form H_2 and O_2. There is also some recombination of OH as evidenced by the fact that the peak in temperature corresponds to the point where the concentration of OH levels off to its final value. Although the drop in the O, H, and OH concentrations and the corresponding rise in the H_2 and and O_2 concentrations are both very small, the corresponding differences in heats of formation is quite large and thus results in a higher temperature.

The reaction zone length based on the maximum rate of heat release was 0.005056 mm.

4.2.10 Case 10

Figures (52) through (60) show the temperature, pressure, sigma, and species profiles for the case where the equilibrium temperature is equal to the frozen temperature. This case corresponds to an overdrive parameter of 1.8997. The same trends observed in the cross-over case (case 9) are observed in this case. The figures make it clearer that the first peak in sigma corresponds to the leveling off in temperature. The value of the first peak in sigma becomes even smaller than case 9 but still remains positive. The dip in sigma clearly corresponds to the second dip in temperature. The second

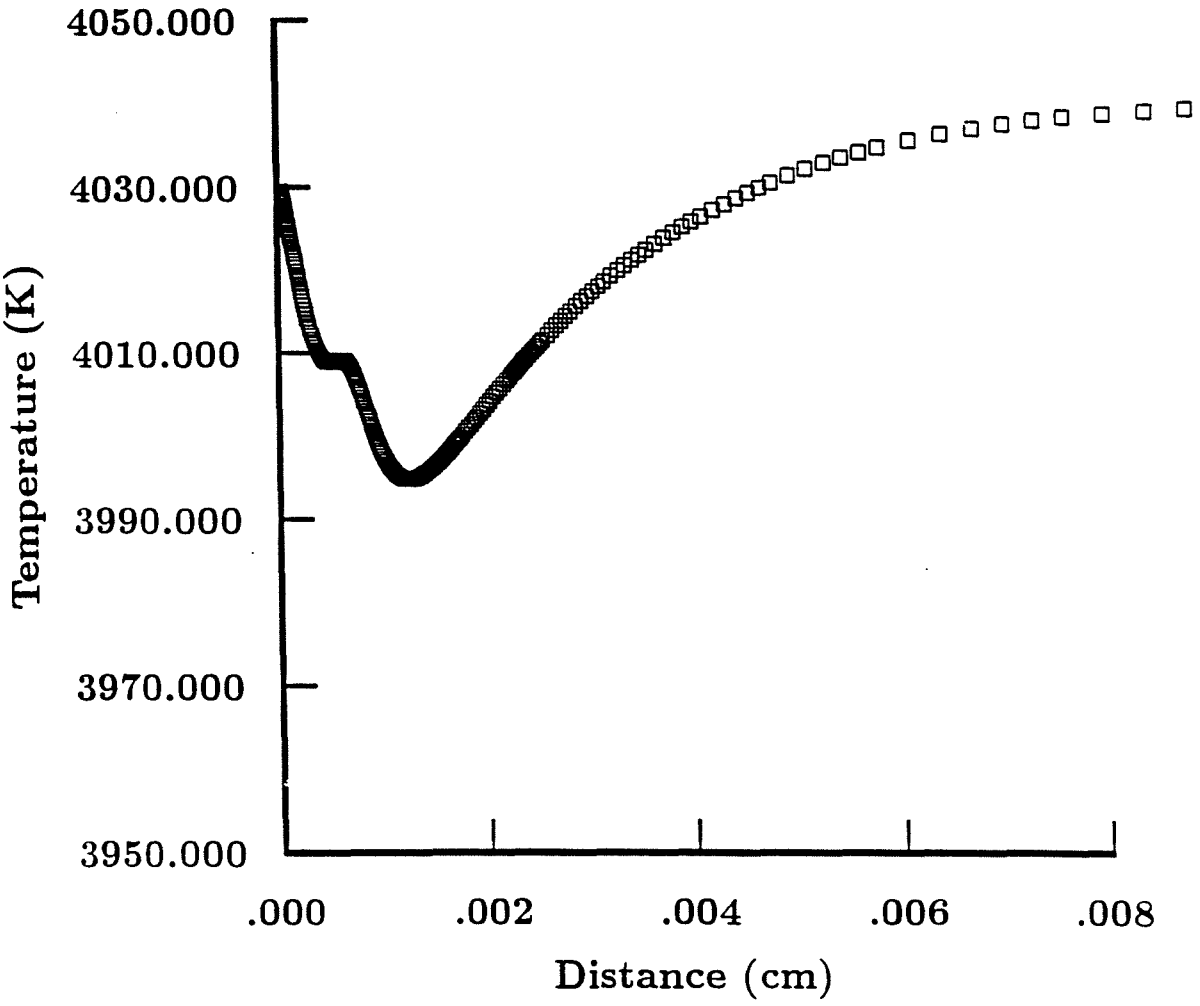

Figure 52. Temperature profile for the reaction zone of case 10.

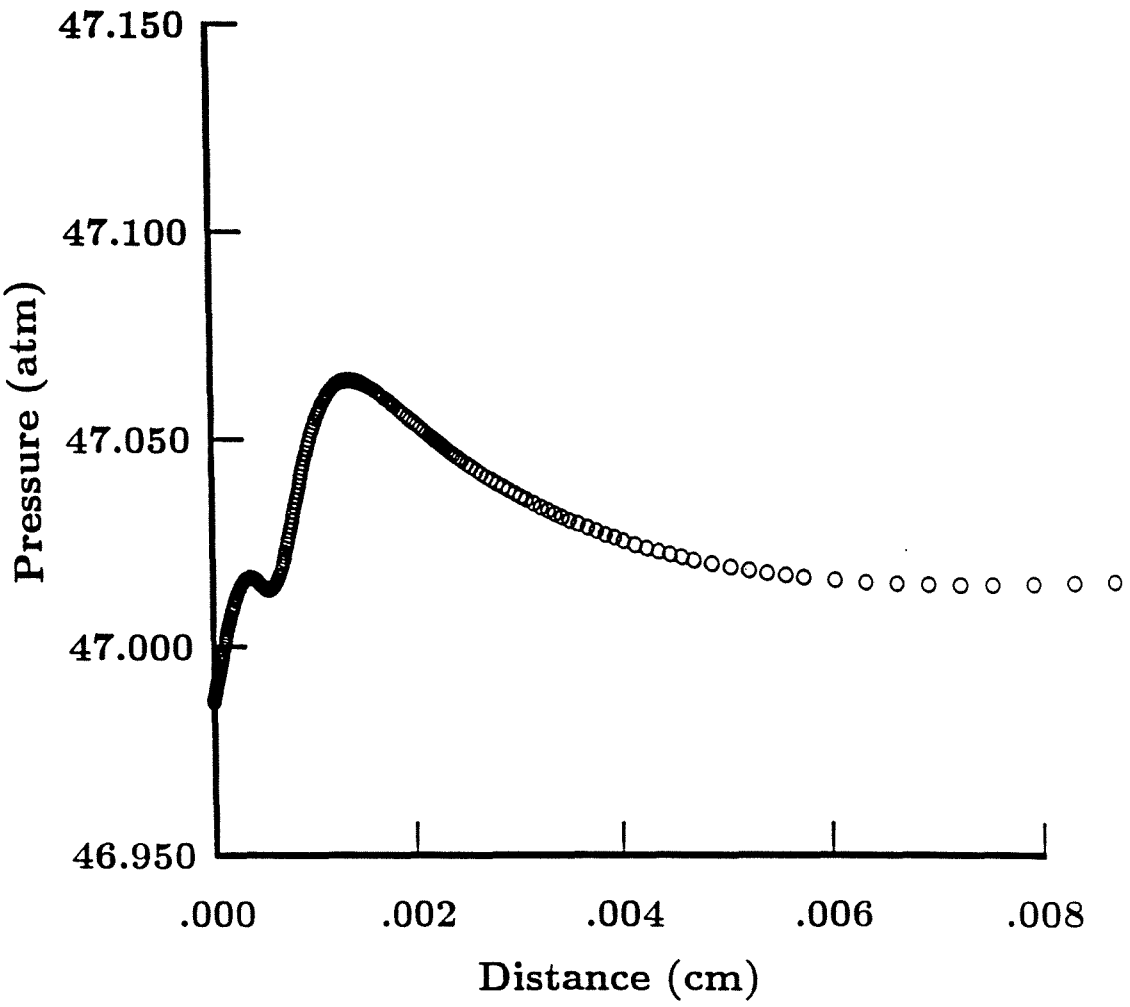

Figure 53. Pressure profile for the reaction zone of case 10.

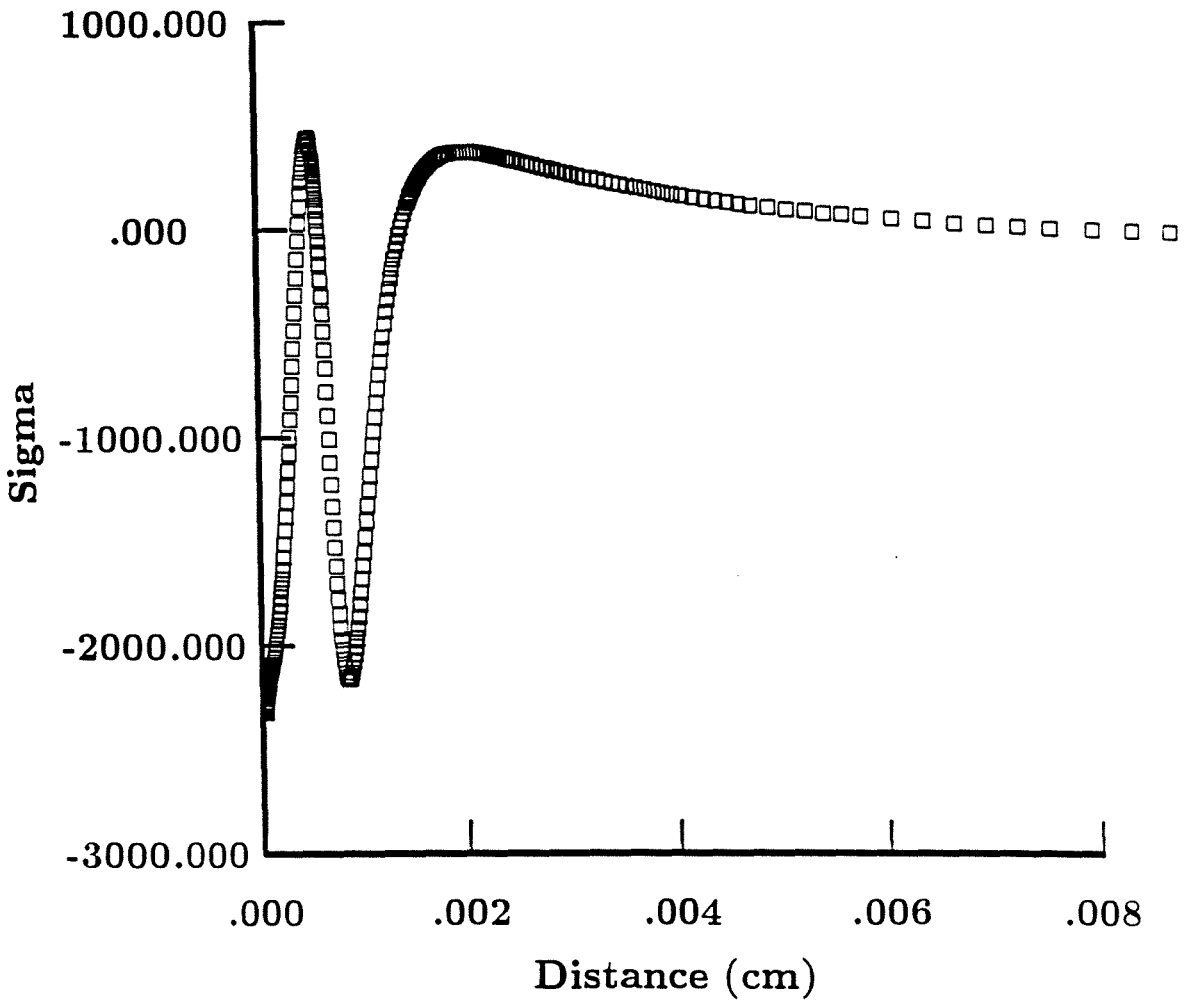

Figure 54. Sigma profile for the reaction zone of case 10.

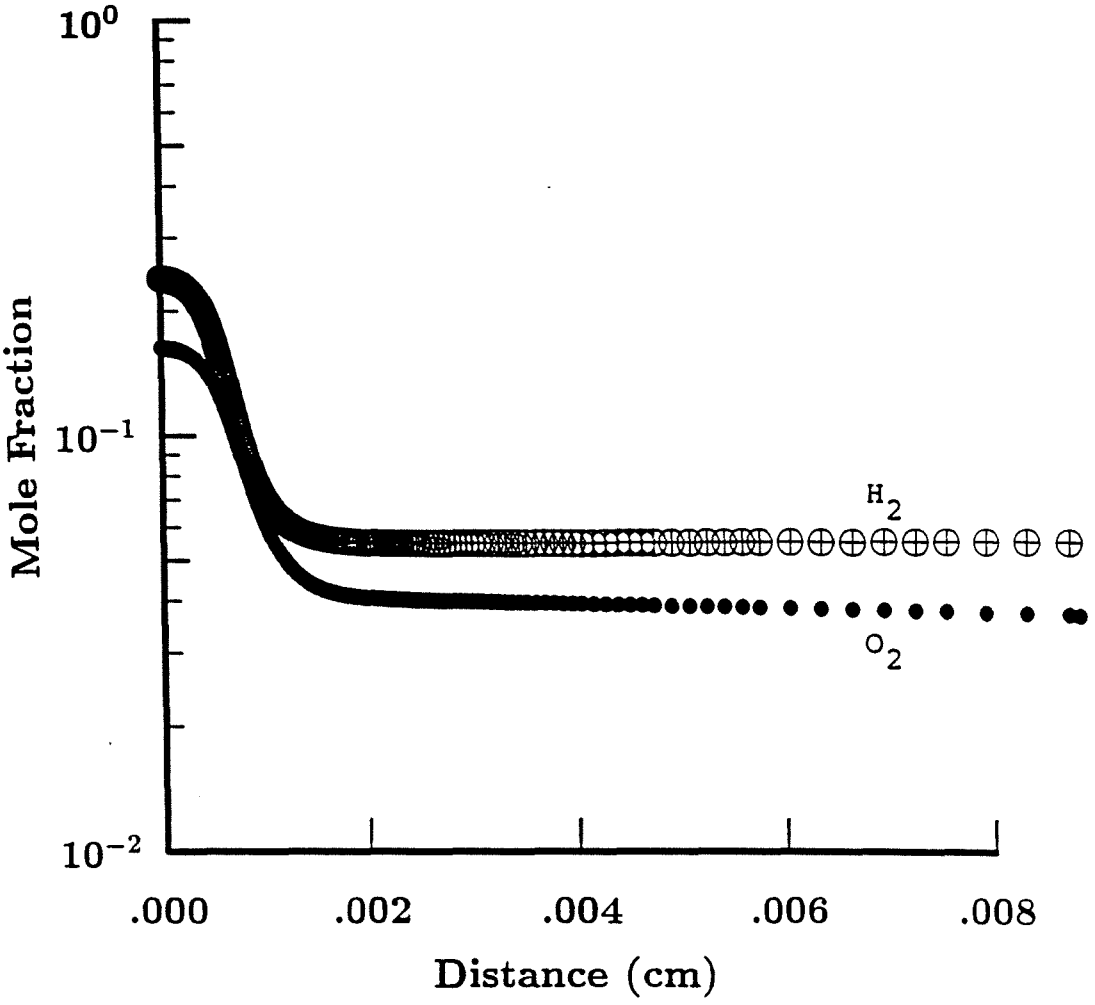

Figure 55. Mole fractions of H_2 and O_2 for the reaction zone of case 10.

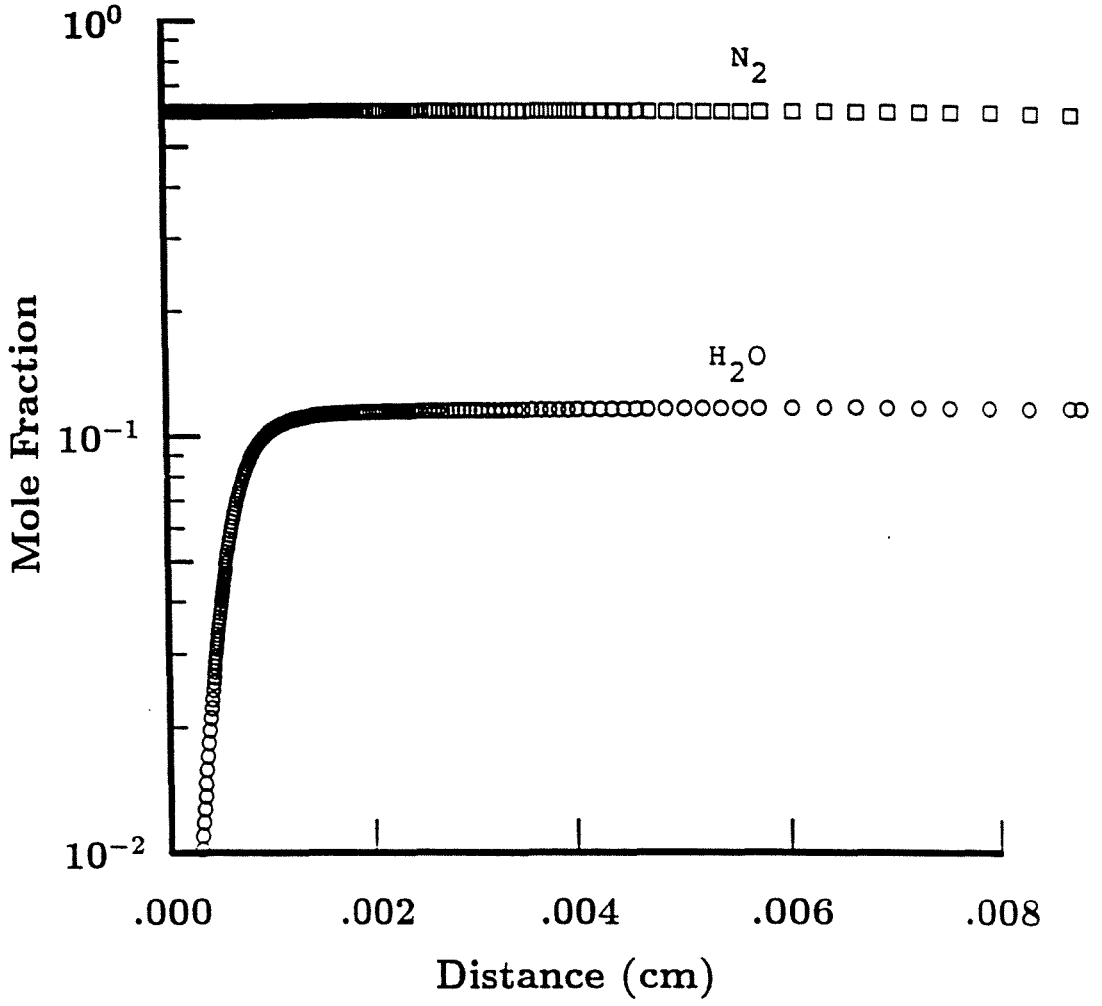

Figure 56. Mole fractions of N_2 and H_2O for the reaction zone of case 10.

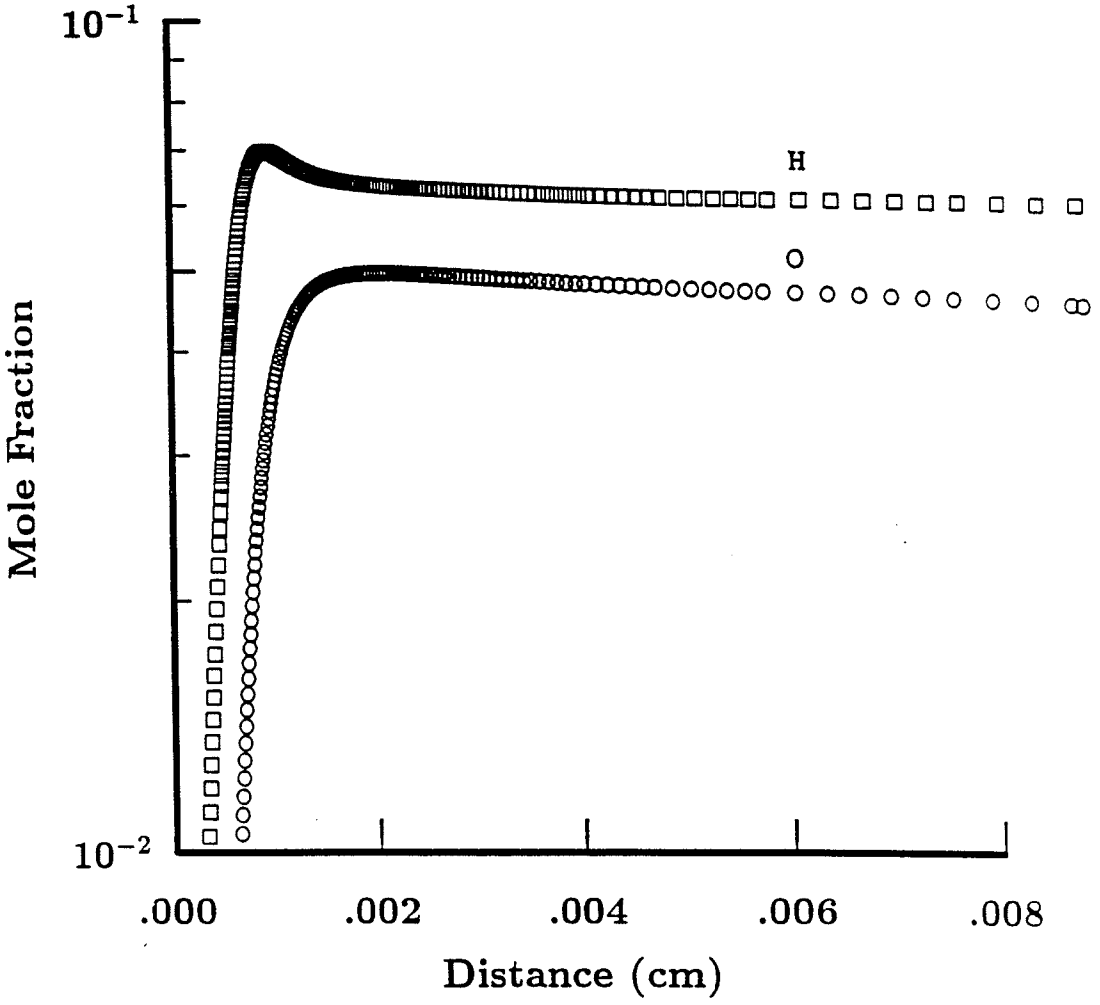

Figure 57. Mole fractions of H and O for the reaction zone of case 10.

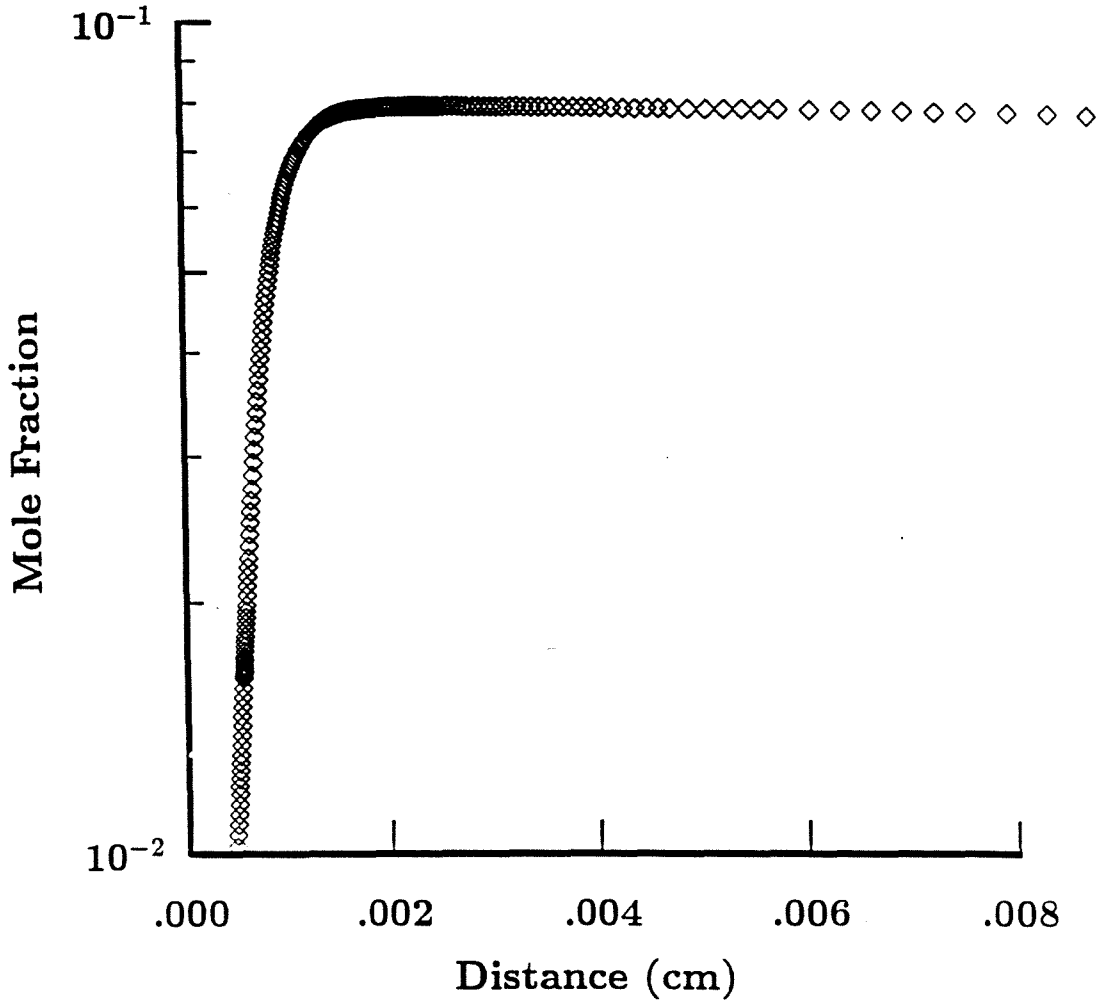

Figure 58. Mole fraction of OH for the reaction zone of case 10.

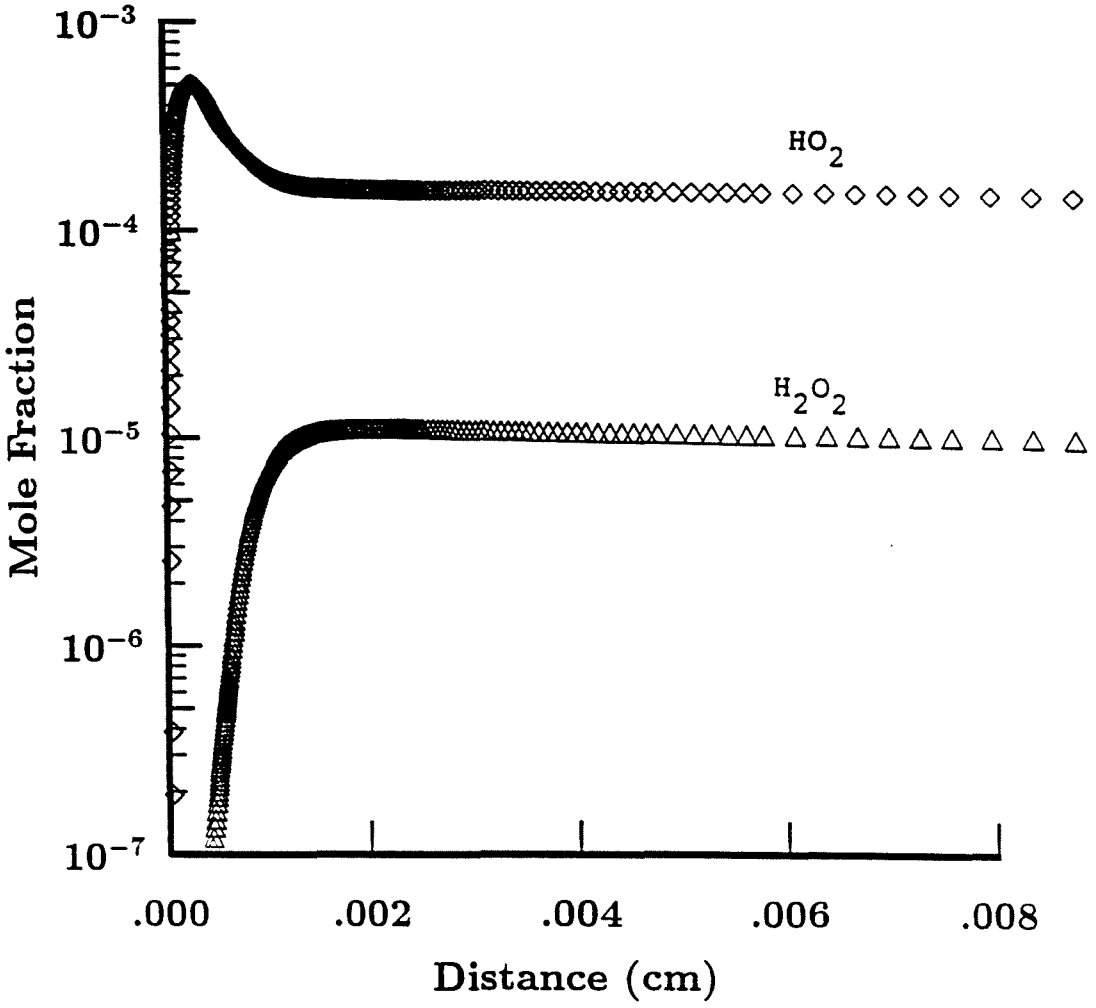

Figure 59. Mole fracions of HO_2 and H_2O_2 for the reaction zone of case 10.

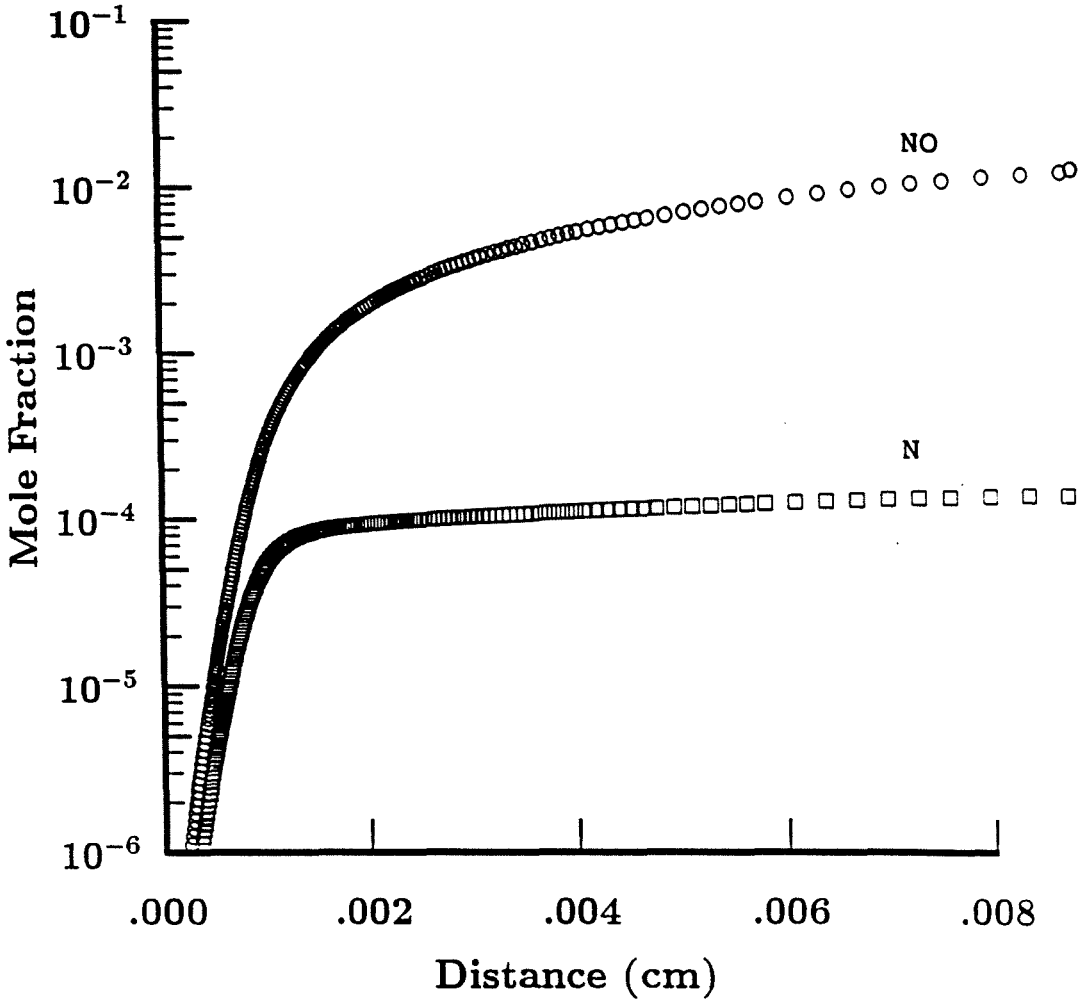

Figure 60. Mole fractions of N and NO for the reaction zone of case 10.

peak in sigma corresponds to the the final rise of the temperature to the equilibrium value, and it becomes closer in value to the first peak. The drop in sigma after the second peak is now much more shallow relative to the drop exhibited in case 9. The correlation between the various features of the species profiles and the sigma profile are the same as discussed above in case 9.

The reaction zone length based on the maximum rate of heat release is 0.00470 mm.

4.2.11 Case 11

Figures (61) through (63) show the temperature, pressure, and sigma profiles for the Dabora case with a free stream Mach number of 9.3 (overdrive parameter of 2.0047). This corresponds to a point beyond the cross-over point on the Hugoniots. The temperature and pressure trends are completely reversed from the pre-cross-over cases, just as was observed with case 3 above. There is a von-Neumann "well" instead of a von-Neumann spike. The temperature drops, instead of rising behind the shock wave and through the reaction zone. Again, this is due to the fact that in order to minimize the Gibbs free energy, the flow has to drop in temperature in order that species of lower heats of formation can be formed. In this highly overdriven case, the thermal and kinetic components of the energy of the flow are so large that the chemical contribution from the exothermic formation of water is almost negligible and

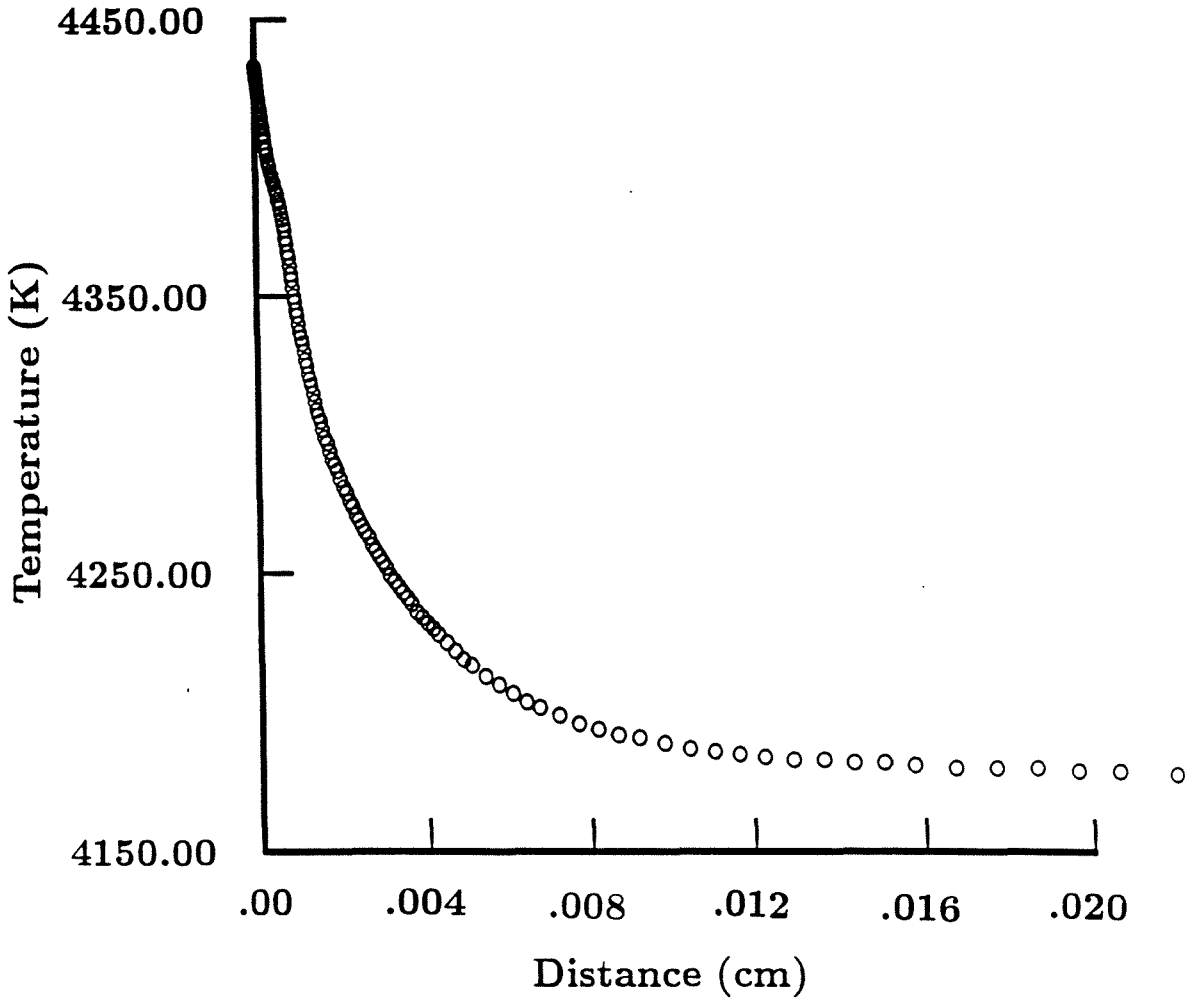

Figure 61. Temperature profile for the reaction zone of case 11.

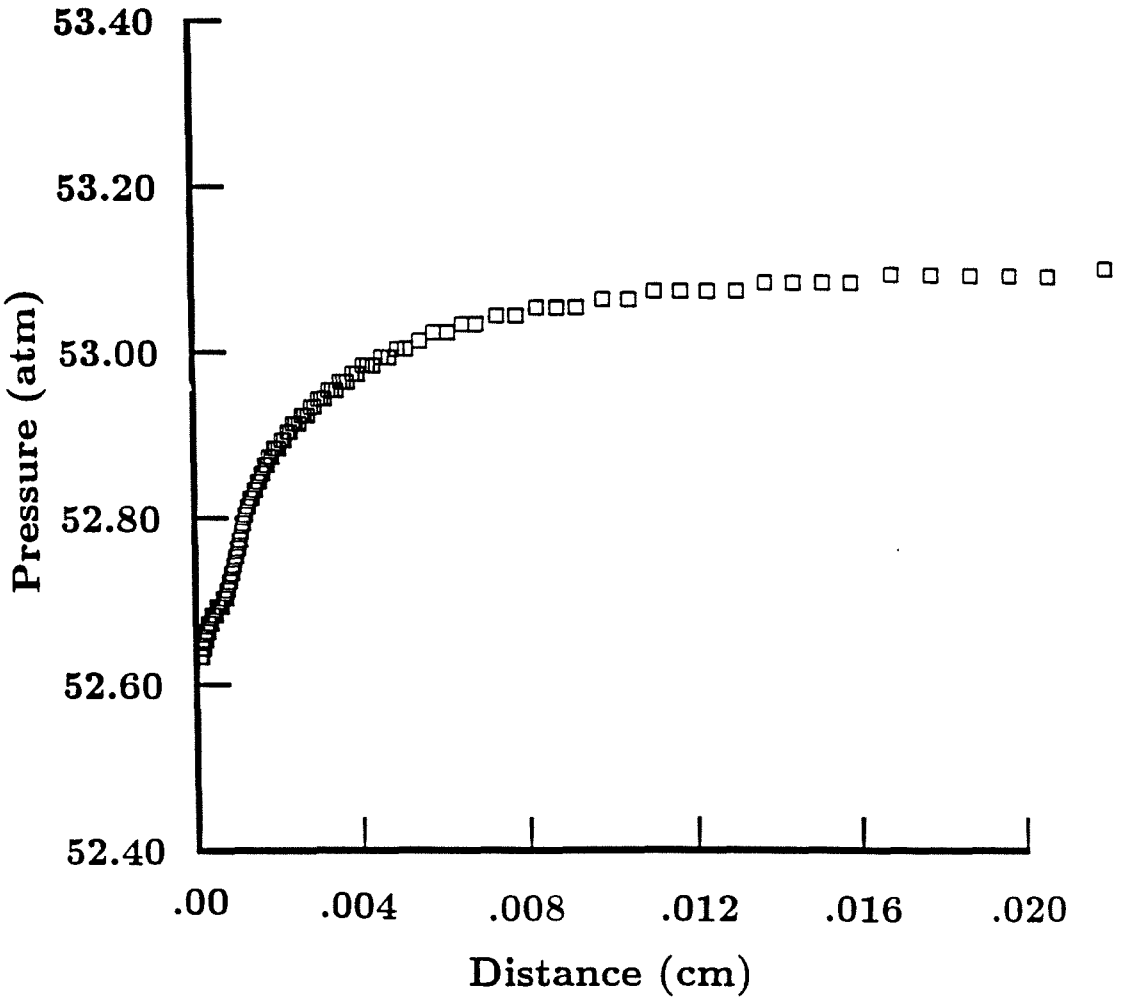

Figure 62. Pressure profile for the reaction zone of case 11.

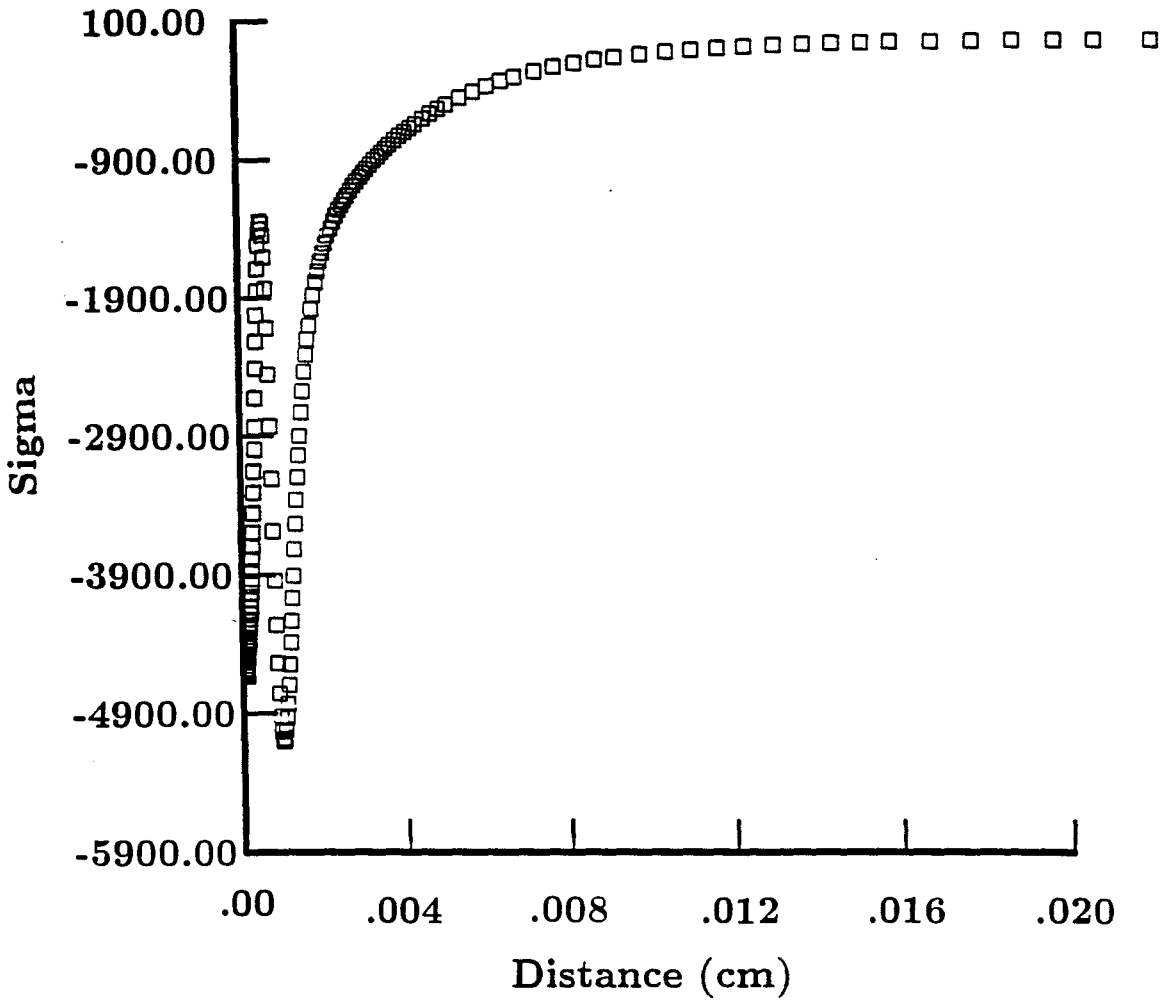

Figure 63. Sigma profile for the reaction zone of case 11.

fails to even level off the temperature. The sigma profile keeps the same shape it took for the cross-over case, except that now there is no second peak. The first peak now has a small negative value, and the profile levels off to the equilibrium value of zero from below rather from above as was observed for cases 6 through 10. This results in an asymptotic approach without overshoot.

The reaction zone length based on the maximum rate of heat release is 2.274 mm. However, this is misleading because the computer takes the maximum heat release to be zero since the first peak has a negative value. It is felt that the reaction zone should be based on the first peak in sigma which corresponds to the formation of the water molecules. Based on the first peak in sigma, the reaction zone length now becomes about 0.004 mm, continuing its downward trend with increasing overdrive.

4.2.12 Case 12

Figure (64) shows the frozen and equilibrium polars for the Dabora case with a free stream Mach number of 10.172. This corresponds to an overdrive parameter of 2.1927. Since this is a highly overdriven case, a cross-over point is obtained. The cross-over deflection angle is about 45^{o}.

The reaction zone for this case is shown in figures (65) through (73). All of the profiles have a form similar to case 11. The only difference is that the reaction zone

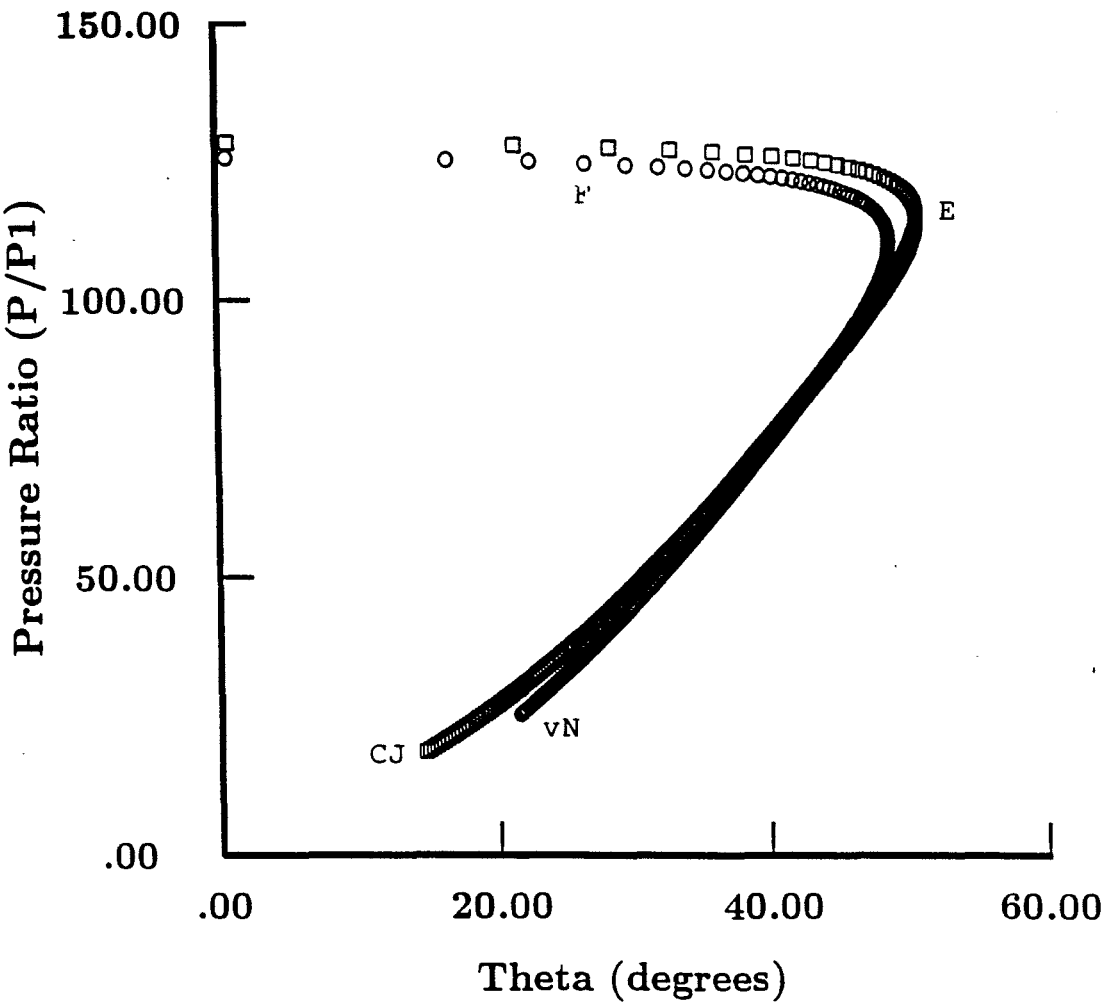

Figure 64. Frozen (F) and equilibrium (E) polars for case 12, showing the CJ point and the von-Neumann point (vN).

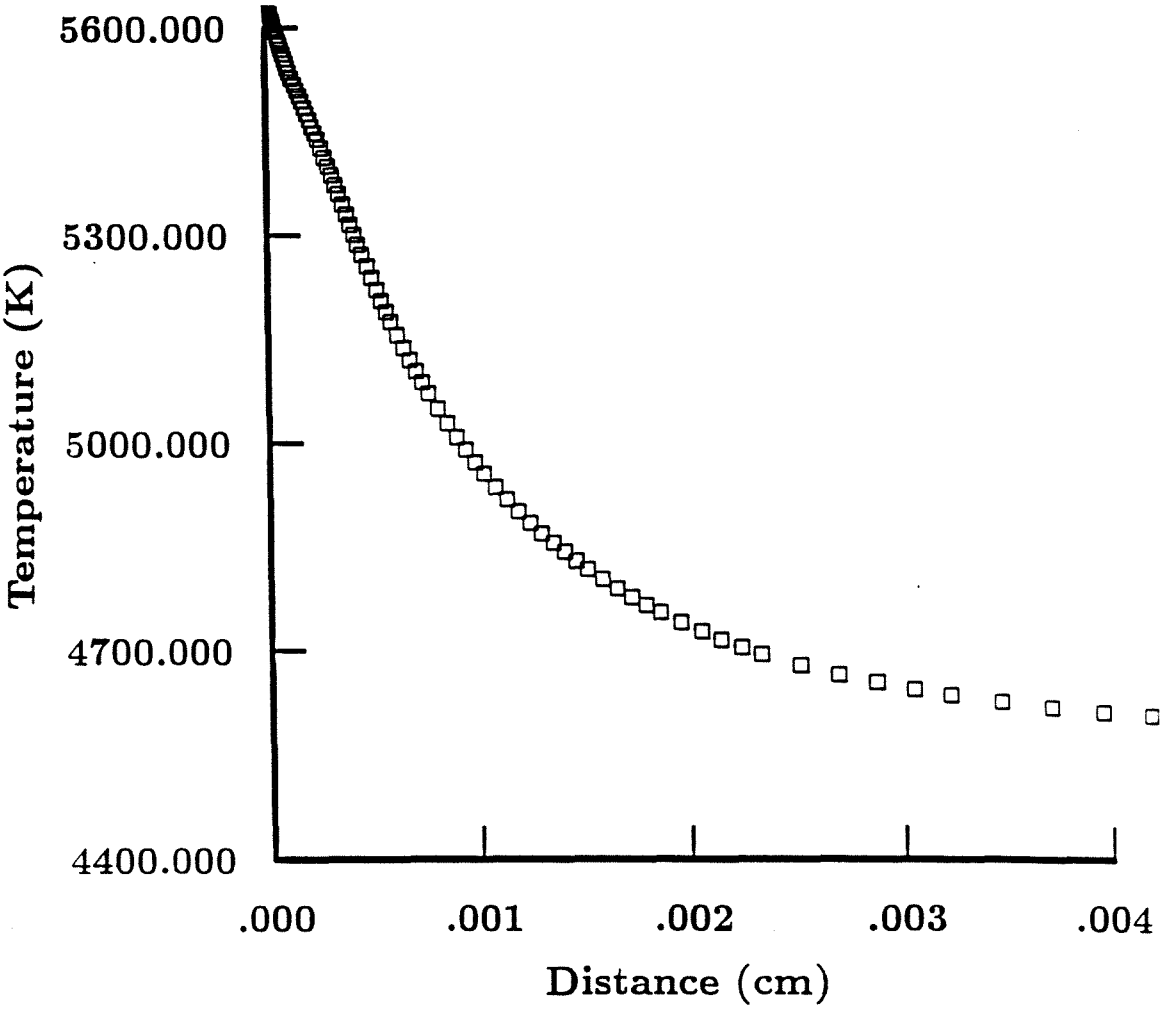

Figure 65. Temperature profile for the reaction zone of case 12.

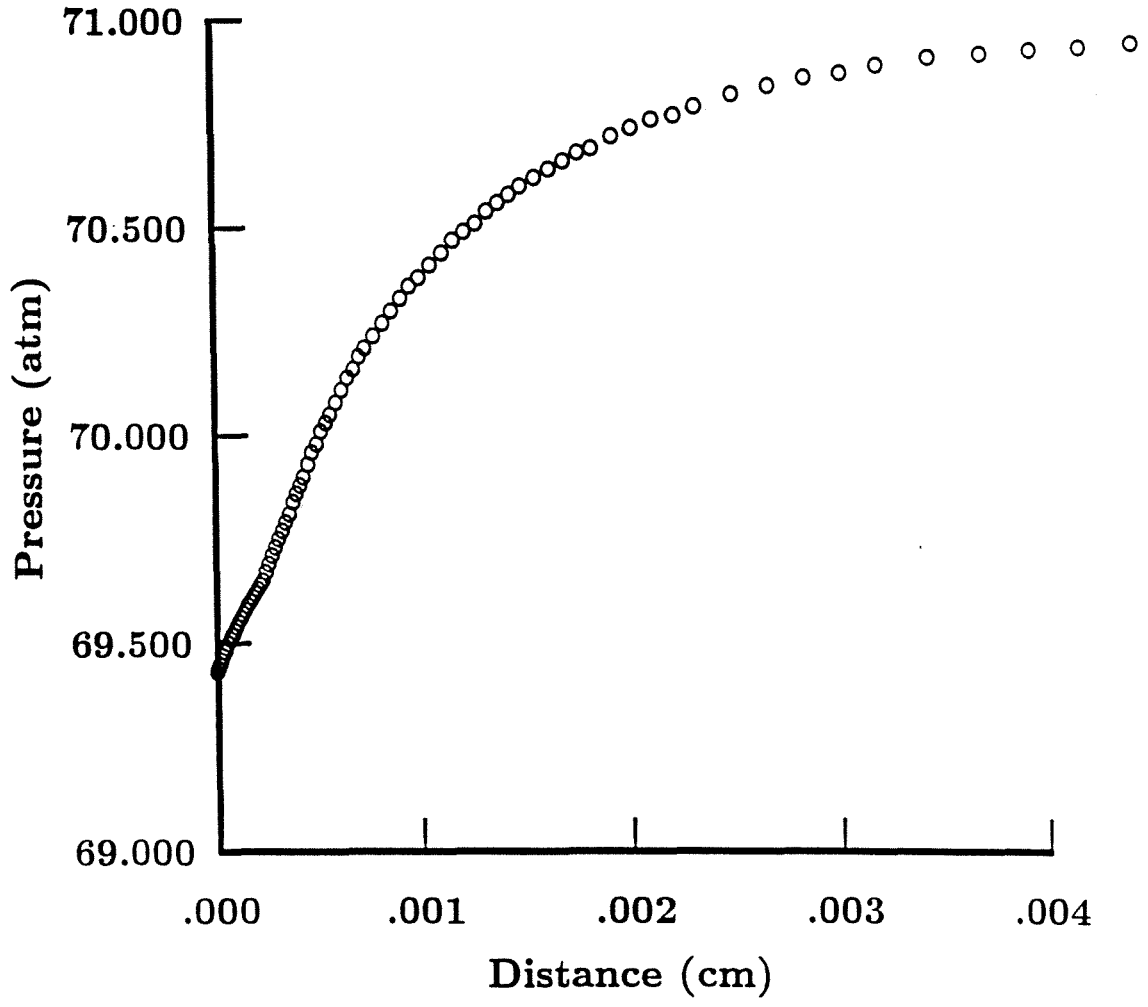

Figure 66. Pressure profile for the reaction zone of case 12.

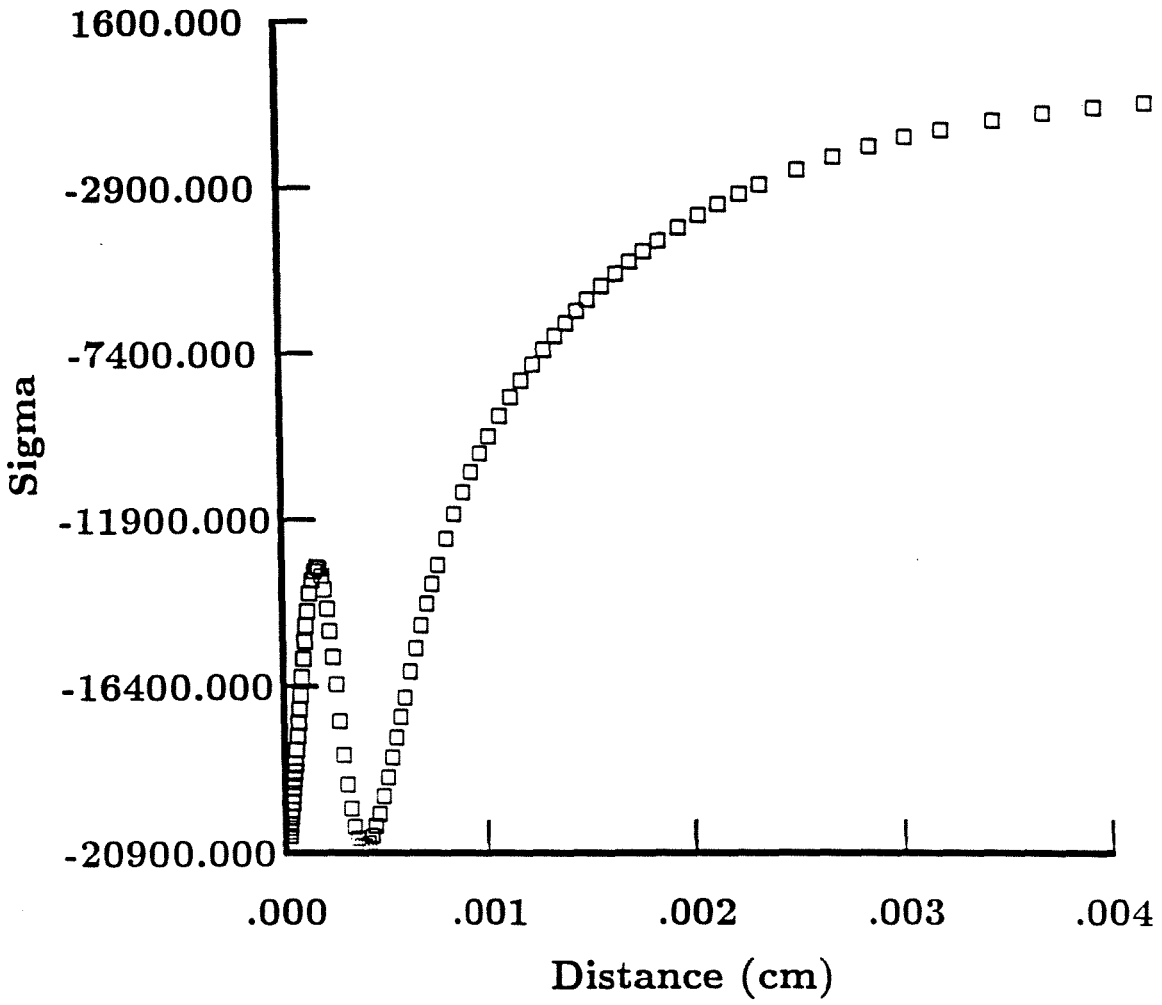

Figure 67. Sigma profile for the reaction zone of case 12.

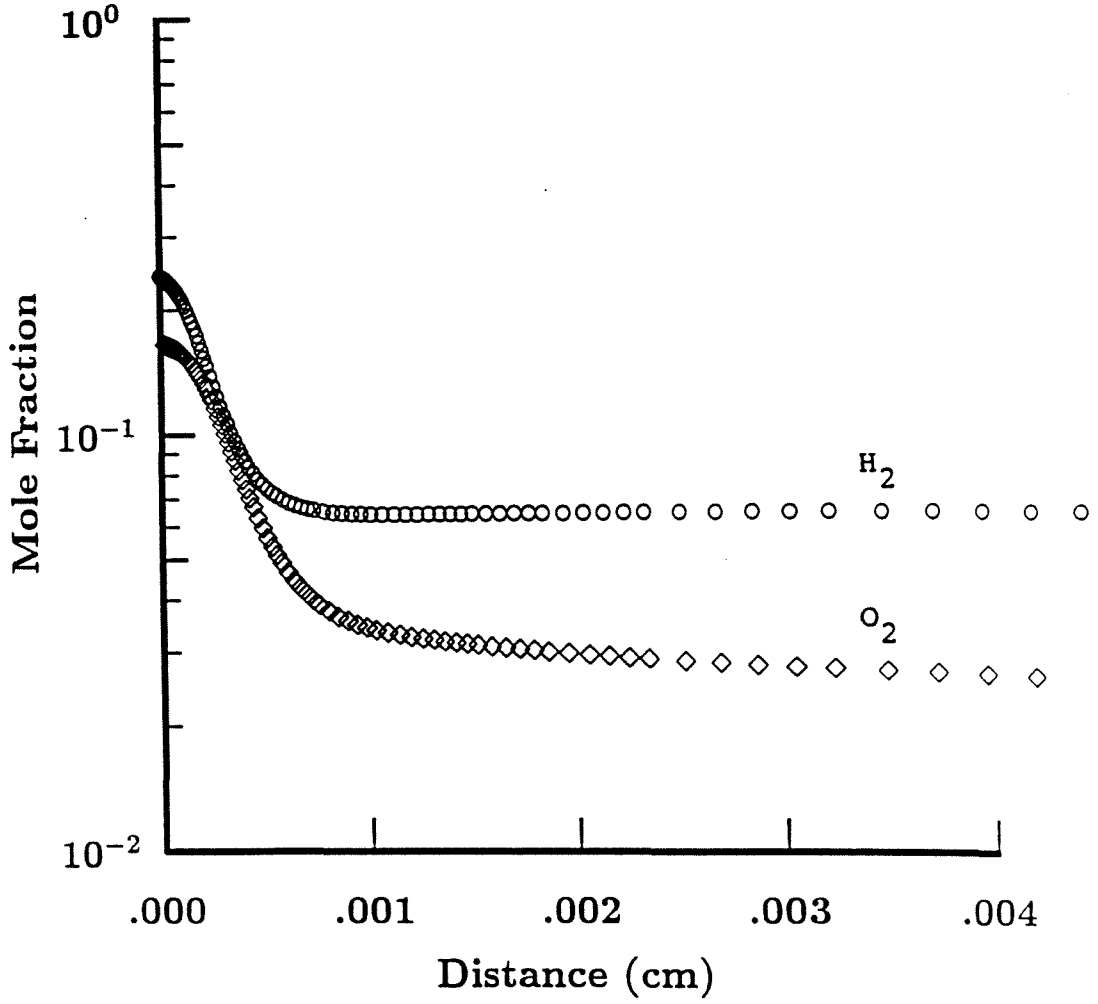

Figure 68. Mole fractions of H_2 and O_2 for the reaction zone of case 12.

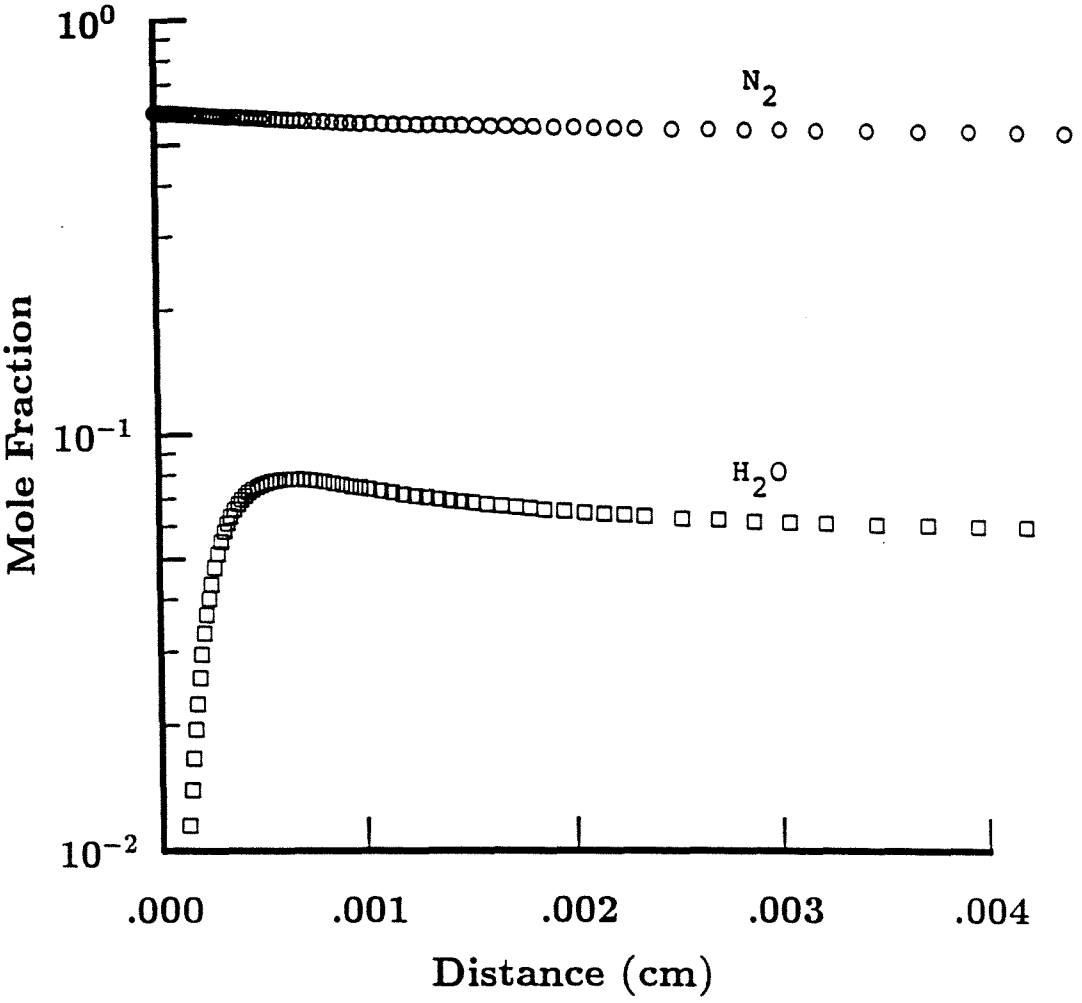

Figure 69. Mole fractions for N_2 and H_2O for the reaction zone of case 12.

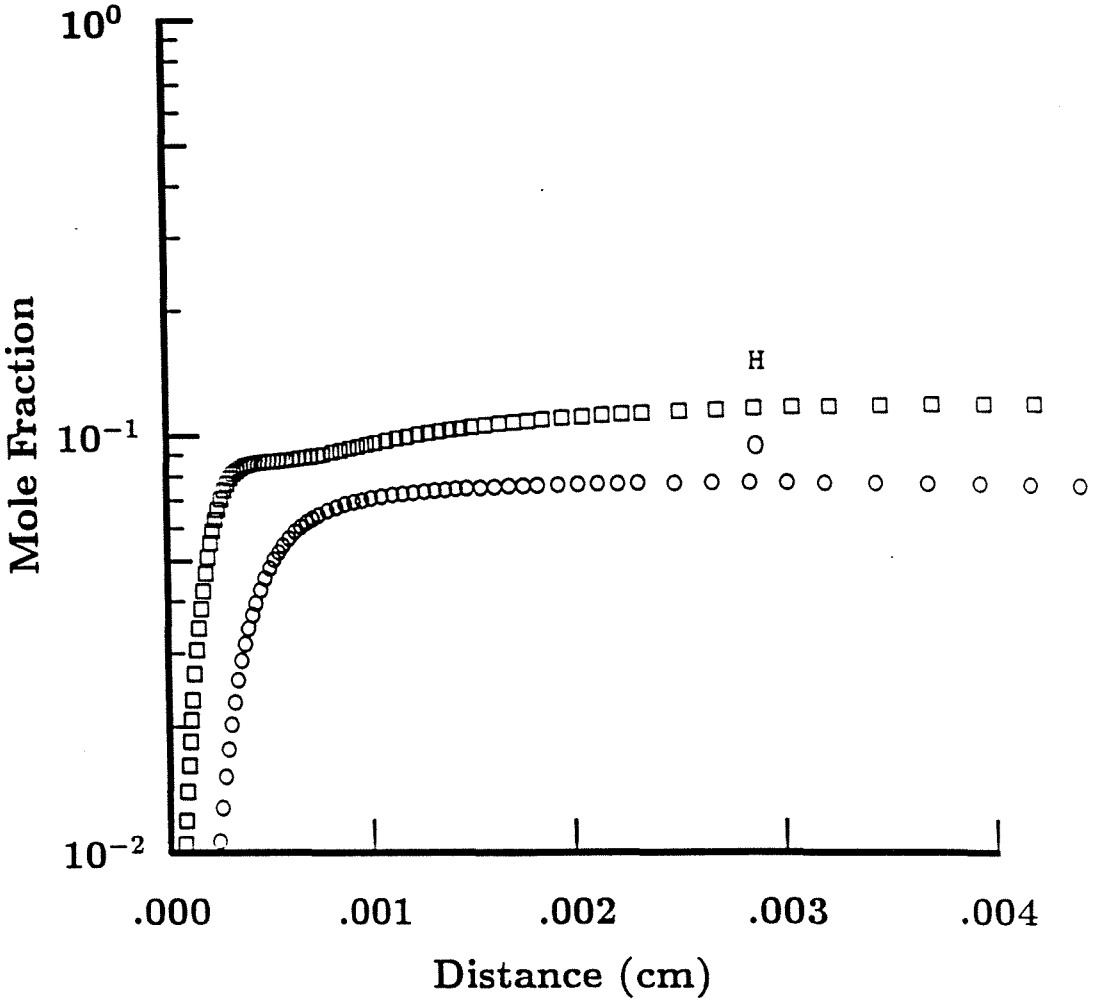

Figure 70. Mole fractions of H and O for the reaction zone of case 12.

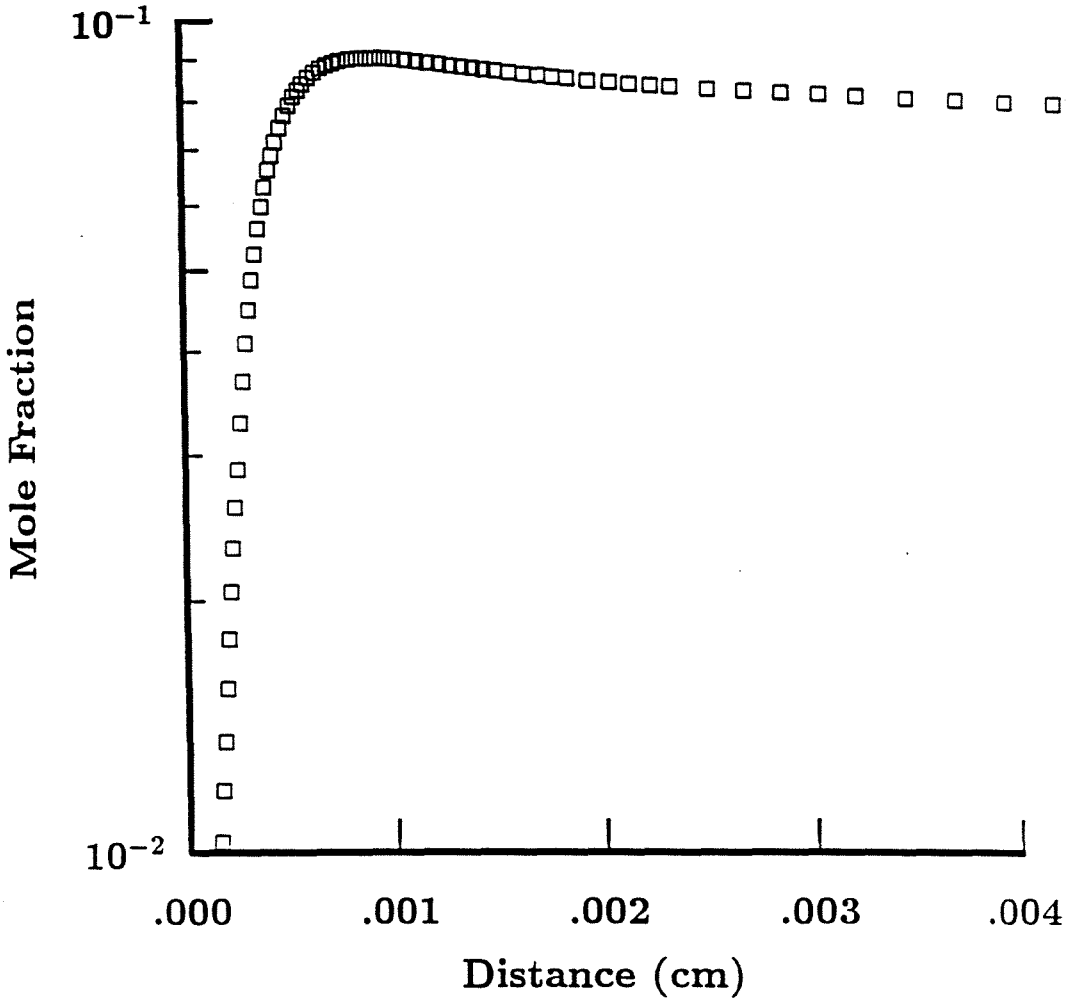

Figure 71. Mole fraction of OH for the reaction zone of case 12.

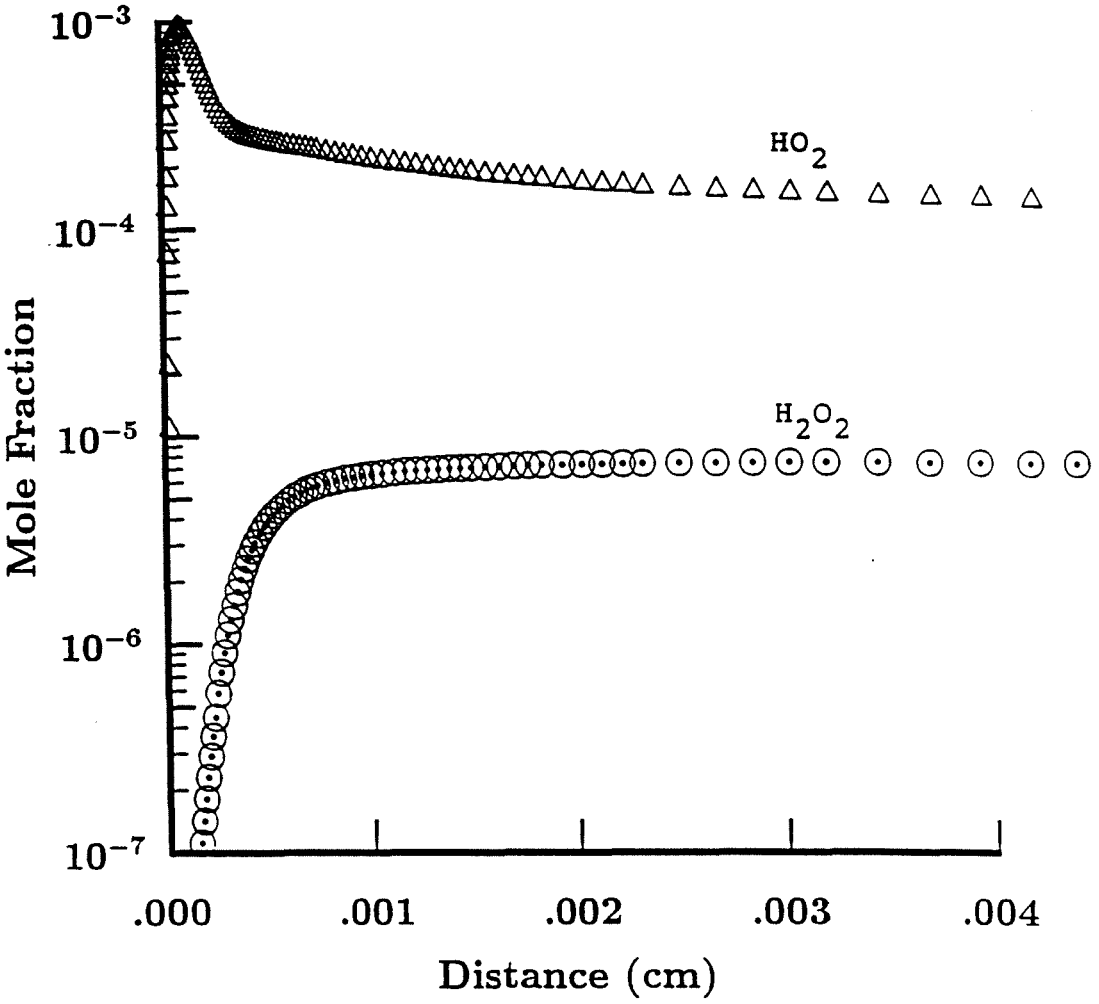

Figure 72. Mole fractions of HO_2 and H_2O_2 for the reaction zone of case 12.

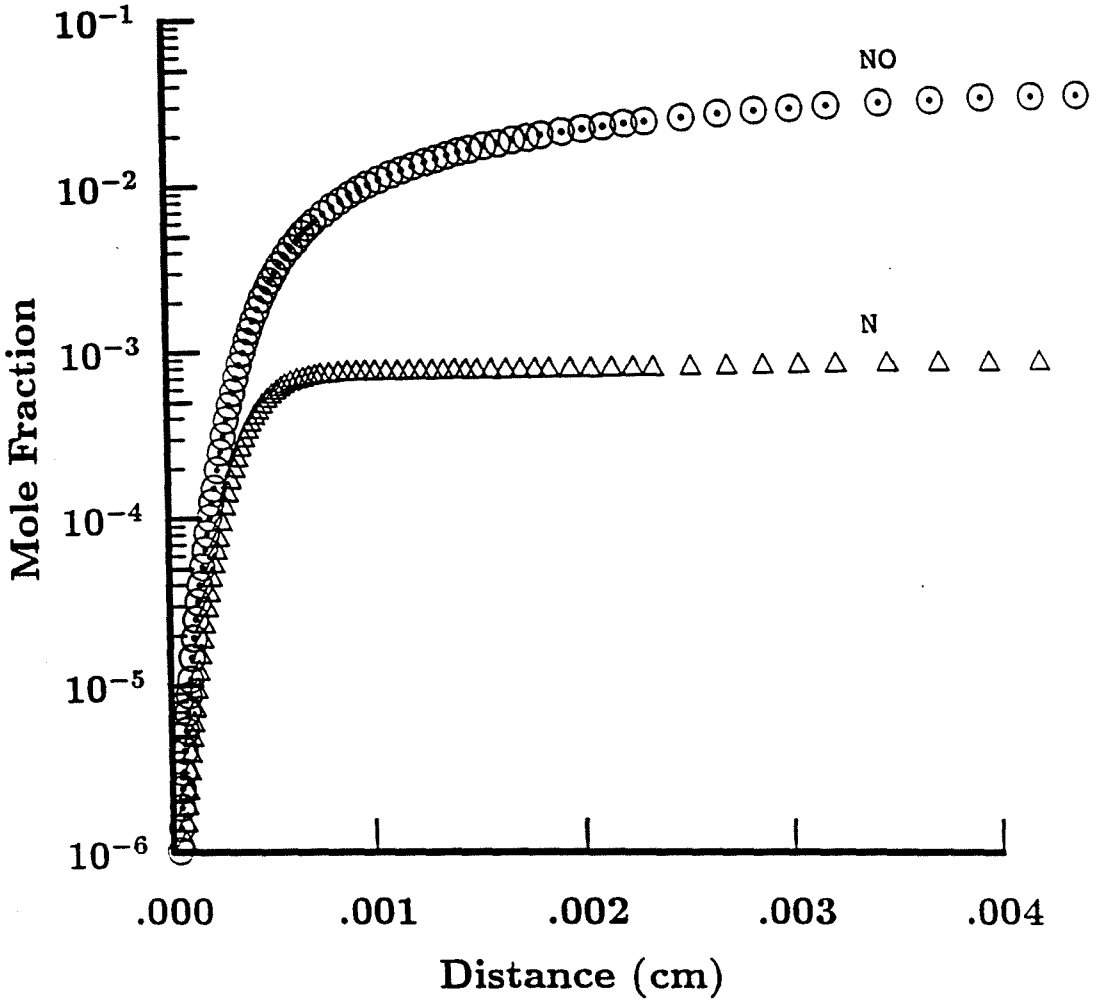

Figure 73. Mole fractions of N and NO for the reaction zone of case 12.

is thinner. The first peak in the sigma profile now has a very large negative value. Although ZND.FOR gives a reaction zone length of 2.591 mm based on the maximum rate of heat release, this should not be taken as the true reaction zone length since the first peak in sigma has a very large negative value. The reaction zone length based on the first peak in sigma is about 0.00125 mm.

4.2.13 Case 13

Figure (74) shows the equilibrium and frozen polars for the Dabora case with a free stream Mach number of 21.227. This yields an overdrive parameter of 4.5758. The same trend observed with the CAM cases is observed here. The cross-over point continues to move down along the lower branch of the polars. The cross-over flow deflection angle has now dropped to about 21^{o}. The ZND computer code failed to obtain a reaction zone structure for this case. This is because the program can only handle density jumps across the non-reacting shock wave which are below a limiting value. This is a relatively minor problem which could be fixed by assigning larger values for the limiting density ratio. A more serious problem is the 6000 K limit which is a consequence of using the JANNAF thermodynamic data. To overcome this limitation, a procedure similar to that implemented for STANJAN would have to be carried out. This involves the use of the extended thermodynamic fits provided by McBride (25) and the inclusion of ionized

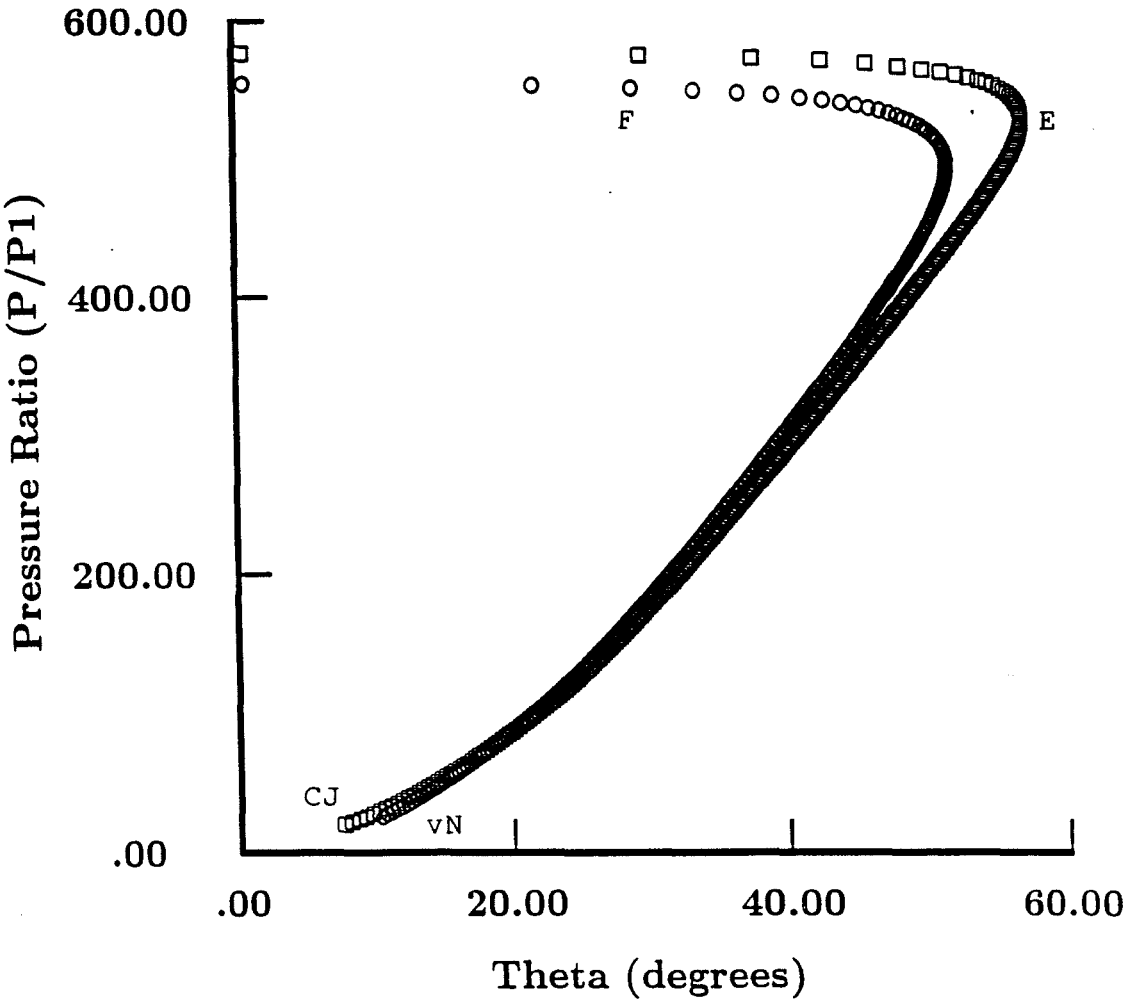

Figure 74. Frozen (F) and equilibrium (E) polars for case 13, showing the CJ point and the von-Neumann point (vN).

species in the reaction mechanism. The latter is a formidable task requiring the acquisition of reaction rate expressions for reactions of ionized species. For this case, not only was the density ratio across the shock wave larger than the upper limit, but the equilibrium temperature of 9458.80 K (from STANJAN) was far in excess of the 6000 K limit.

4.2.14 Summary of Dabora Cases

The same trends that were observed for the CAM cases concerning the variation of the equilibrium composition with the upstream normal velocity are also observed for the Dabora cases. The mole fraction of the ionized species goes up by 12 orders of magnitude as the upstream normal velocity is increased from the CJ value of 1824.2 m/s to the maximum value of 8347 m/s. However, the mole fractions of the ionized species are very small relative to the atomic species and free radicals even at the maximum upstream normal velocity. Higher upstream normal velocity favors the formation of atomic species.

Figure (75) shows the variation of the CJ, maximum, and cross-over flow deflection angles with the free stream Mach number for the Dabora cases. The curves are of identical form to those obtained for the CAM cases (figure (30)). Again, the use of the cross-over flow deflection angle as the upper bound on the utility of oblique detonation waves severely restricts the range of useful

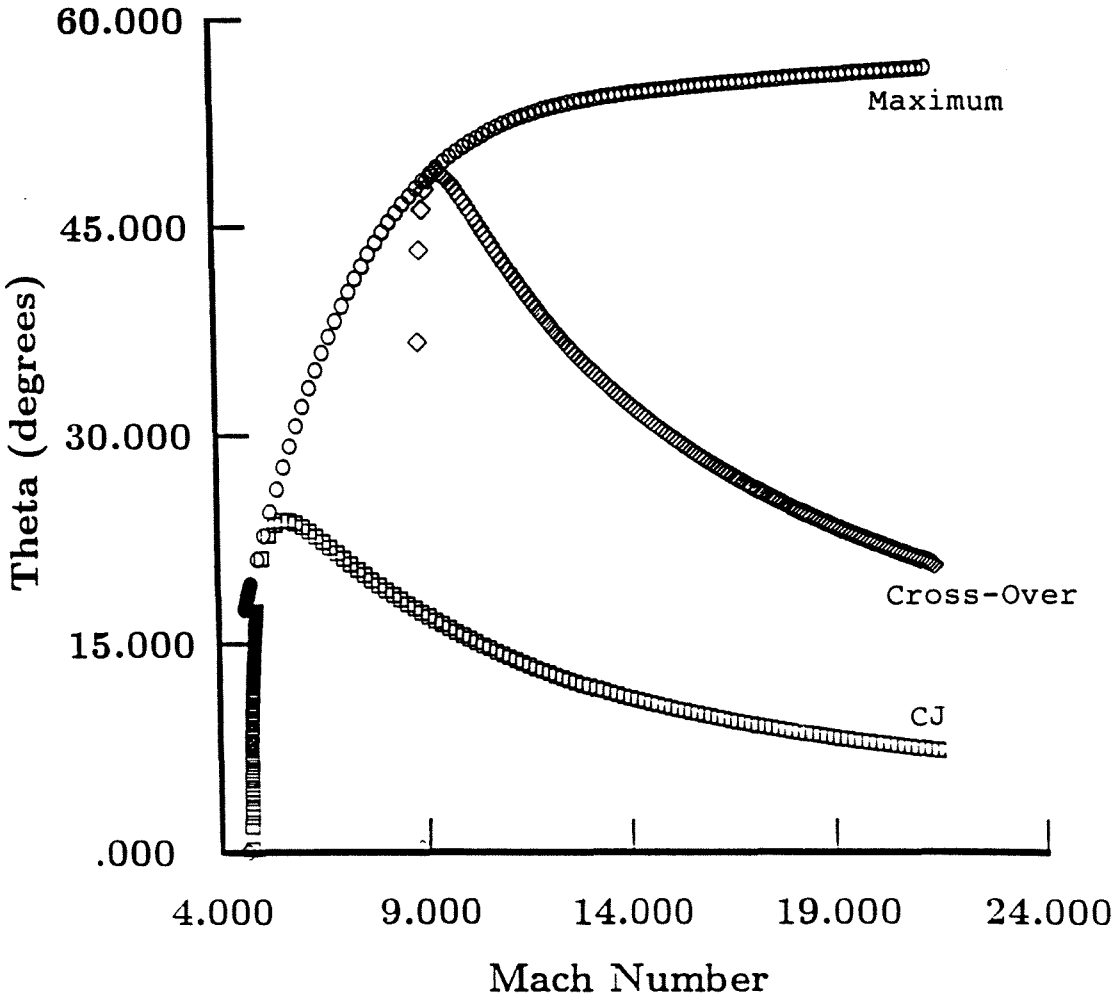

Figure 75. Maximum, CJ, and cross-over flow deflection angles versus free-stream Mach number for cases 0 through 13 (Dabora cases).

flow deflection (or wedge) angles. The maximum range of useful flow deflection angles occurs for the free-stream Mach number when the cross-over point coincides with the maximum flow deflection angle. Beyond that Mach number, the useful range of wedge angles narrows down as the Mach number is increased.

Table (4) shows the variation of the reaction zone length with the overdrive parameter. The overdrive parameter is defined as the ratio of the normal Mach number to the CJ Mach number. The table shows two reaction zone lengths: one based on the first peak in sigma, and another based on reaching a temperature within 1% of the equilibrium value. The latter shall be referred to for the remainder of this thesis as the maximum reaction zone length. The sigma profiles obtained for the post-cross-over cases make it clear that the use of the maximum sigma for the evaluation of the reaction zone length is not an acceptable procedure. This is because the sigma profiles for those cases have a negative relative maximum, and they asymptote to a value of zero. Thus the maximum sigma is zero. Basing the reaction zone length on this value of sigma would result in a reaction zone length that is too long and does not correspond to what is going on in the reaction zone. In fact, this reaction zone length corresponds to the distance required to achieve equilibrium. It is felt that the reaction zone should be

Table 4. Variation of the reaction zone length with the overdrive parameter. R_s is the reaction zone length based on the first peak in sigma, and R_T is the reaction zone length based on the temperature reaching a value within 1% of its equilibrium value.

Overdrive Parameter	R_s (mm)	R_T (mm)
1.0	0.44008	3.672
1.0964	0.18388	2.59629
1.8107	0.054711	0.055264
1.8768	0.0050559	0.128216 *
1.8997	0.0046956	0.012071 *
2.0047	0.004	0.042322
2.1927	0.00125	0.03198

* These correspond to cases very close to the cross-over point. The temperature fluctuations about the equilibrium value for these cases were less than 1%. Therefore, the location of the maximum fluctuation in temperature was used for the maximum reaction zone length of these cases.

based on the first peak in sigma, which corresponds to the formation of the water molecules which are the major product of the combustion process. A better but more involved procedure would be to evaluate the reaction zone length based on the integral of the sigma profile. This would represent the algebraic area enclosed between the sigma profile and the sigma=0 axis. One can then select the reaction zone length as the location where this area is some fraction (95-99%) of the final area. Note that the integral will be positive for pre-cross-over cases, and negative for post-cross-over cases.

The importance of the maximum reaction zone length lies in the fact that if the product gases are expanded before all the energy is released, then the enthalpy of the mixture at the beginning of the nozzle would be lower than if the equilibrium temperature was achieved. From the conservation of total energy it becomes clear that this results in a drop in the nozzle exit velocity which compromises performance. Thus, a reaction zone length based on where the temperature is within about 5% of its equilibrium value could be more useful from a propulsive standpoint. Table (4) shows that this reaction zone length is typically about one order of magnitude larger than the reaction zone length based on the first peak in sigma. Similar to the reaction zone length based on maximum sigma, the maximum reaction zone length decreases as the overdrive

parameter increases with the exception of cases very close to the cross-over point. For such cases, the temperature fluctuations about the equilibrium value are less than 1% of the equilibrium temperature. Therefore, the 1% of equilibrium temperature criterion fails to yield any useful information about the maximum reaction zone length for cases very close to the cross-over point. One could avoid this problem by basing the maximum reaction zone length on a species profile instead of temperature since the species profiles do not exhibit oscillations. The question then becomes what species to use. Furthermore, this will again be only an approximate reaction zone length. Therefore, it is felt that it is better to direct any further efforts to the reaction zone length based on the integral of sigma which promises to be the most reliable.

Similar to the behavior of the sigma profiles, the temperature and pressure profiles are very different for the pre-cross-over and post-cross-over regimes. While the temperature increases behind the non-reacting shock for the pre-cross-over cases, it drops for the post-cross-over cases. The pressure decreases behind the non-reactive shock wave for the pre-cross-over regime, and increases for the post-cross-over regime.

4.3 Total Pressure Recovery Factor

The next set of results concerns the total pressure drop across detonation waves. Table (5) shows total

Table 5. Total pressures and total pressure recovery factors for normal detonation waves with various free-stream Mach numbers. The total pressure recovery factor, P_t ratio, is defined as the ratio of P_{t2} to P_{t1}.

Upstream Composition and Conditions Same as Dabora Case			
Normal Velocity (m/s)	P_{t1} (atm)	P_{t2} (atm)	P_t Ratio ($\times 10^{-3}$)
1824.2	1873.8	12.547	6.6958
2400.0	5646.7	23.559	4.1721
3000.0	14977	37.856	2.5276
3600.0	62721	55.257	0.88100
4200.0	204460	75.241	0.36799

pressure drop across normal detonation waves of varying free stream Mach number. All of the cases have the same free stream temperature, pressure, and composition as the Dabora cases. The overdrive parameter (M_n/M_{CJ}) for these cases varies from 1.0 (the C-J case), to 2.3024. As the wave becomes more overdriven, the total pressure drop becomes more severe. The total pressure recovery factor ranges from a maximum value of 0.6696% for the C-J case, to a minimum value of 0.03680% for the Mach 10.172 case. This behavior is very similar to normal non-reacting shock waves where a stronger shock leads to a larger total pressure drop.

Table (6) shows the variation of the total pressure recovery factor with the deflection angle for a free stream Mach number of 10.172. As the deflection angle approaches zero and the oblique detonation wave approaches a normal detonation wave, the total pressure recovery factor becomes smaller. This, again, is similar to the trend observed for oblique non-reacting shock waves.

It is interesting to note that the value of the total pressure recovery factor for both normal and oblique detonation waves is lower than that for non-reacting shock waves. This raises the question as to what role does the chemical reaction play in the total pressure drop across detonation waves. Unlike non-reacting shock waves, the total temperature increases across a detonation wave. A

Table 6. Total pressure recovery factors along the equilibrium polar for the Dabora free-stream state with upto a Mach number of 10.172. The total pressure recovery factor, P_t ratio, is defined as the ratio of P_{t2} to P_{t1}.

P_{t1} = 136979.27 atm			
Normal Velocity (m/s)	Theta (deg)	P_{t2} (atm)	P_t Ratio ($\times 10^{-3}$)
1824.2	14.438	1284.2	9.3752
2000.0	18.046	1154.9	8.4311
2200.0	22.437	972.66	7.1008
2400.0	26.364	789.08	5.7606
2600.0	30.127	621.13	4.5345
2800.0	33.837	476.91	3.4816
3000.0	37.546	358.40	2.6165
3200.0	41.277	264.60	1.9317
3400.0	44.994	192.34	1.4042
3600.0	48.482	137.87	1.0065
3800.0	50.520	97.964	0.71517
4000.0	0.0000	87.781	0.64083

simplistic analysis assuming frozen composition across the detonation (a constant gamma model) would indicate that the total pressure downstream of the wave should increase as the total temperature increases. Such an analysis is in error because the composition changes across the detonation wave. The main effect of the chemical reaction (for pre-cross-over cases) is to decrease the static pressure behind the detonation wave. This decrease in the static pressure seems to outweigh the increase in the total temperature, which results in a net drop in total pressure across the detonation wave which is larger than that across non-reacting shock waves. This type of analysis is based on the typical entropy-temperature-pressure relations for stagnation states. Although such an analysis gives a reasonable explanation of what happens, it is felt that it is more appropriate to investigate the stagnation state downstream of the detonation wave using the Gibbs free energy instead of just the entropy. This is because the Gibbs free energy includes both an entropy component and an enthalpy component. It is felt that the enthalpy must be taken into consideration since the wave is no longer adiabatic and the composition across it is no longer frozen. It was decided that such an analysis was beyond the scope of this thesis, and thus it was left as an area for future investigation.

4.4 The Scramjet Model

The last phase of this thesis was to design a scramjet using an oblique detonation wave for a combustor. The design point was an altitude of 150000 feet, and a flight Mach number of 20. At this altitude the ambient temperature and pressure are 232.66 K and 1105.18 Pa, respectively. All ambient conditions for this part of the thesis were obtained from Oates (28). The reader is referred to figure (7) in section 3.4 for the location of the various engine stations.

For the design point, the inlet had a deflection angle of 9.576°, and the cowl further deflected the flow by 7.990°. Since the deflection angles are quite small, very little total pressure drop is incurred through the inlet. The post-inlet temperature, pressure, and velocity are 1789.9 K, 13.996 kPa, and 6414.96 m/s respectively.

Using the post-inlet conditions, it was possible to determine the corresponding C-J and cross-over points. The C-J velocity was 1675.7 m/s, while the cross-over velocity was 2319.6 m/s. It was thus decided to use a normal velocity component of 1997.65 m/s (the average of the above two velocities) for safe, stable operation as discussed above in the theory section. This normal velocity component yields a wave angle of 18.144°, and a deflection angle of 11.185°. The design of the inlet and combustor was thus complete. The product gases had a temperature of 3093.91 K,

a pressure of 63.260 kPa, a specific volume of 18.935 m^3/kg, a static enthalpy of 4.023 MJ/kg, an entropy of 12.68 kJ/kg-K, a C_p of 9.5102 kJ/kg-K, and a ratio of specific heats of 1.1867. It was found that the total pressure recovery factor across the oblique detonation wave was 37.65%, which is quite low compared to a non-reacting oblique shock wave, but is much higher than the values shown in Table (6). The reason why the total pressure recovery factor is much higher than the values of Table (6) lies in the fact that the operating point used corresponds to a constant normal upstream Mach number. This is because for a given set of initial conditions and composition the CJ Mach number and the cross-over Mach number are both fixed. Since the operating normal Mach number is the average of the CJ and cross-over Mach numbers, it too must be fixed. Another factor is the fact that the wedge angle used is quite small. This results in a small wave angle which results in a very small normal Mach number. Thus, not only is the normal upstream Mach number fixed but it is also very small. Thus, as the Mach number upstream of the detonation wave is increased, the normal Mach number stays constant while the tangential Mach number increases substantially. Since the tangential component of the Mach number has no total pressure loss associated with it, this results in a much higher total pressure recovery factor.

An isentropic expansion of the product gases to

ambient pressure was then carried out. It was felt that it was necessary to treat the flow through the nozzle as an equilibrium flow because experience from reference (29) had shown that the drop in temperature through the nozzle could lead to recombination reactions, and thus the flow in the nozzle cannot be assumed frozen. Treating the flow in the nozzle as in equilibrium would result in the maximum possible length for the nozzle. The other extreme is to treat the flow in the nozzle as frozen (reference (17)). Such an analysis assumes that the nozzle is quite short and thus the residence time of the flow in the nozzle is short enough to permit the use of a frozen analysis. It was finally decided to carry out both types of analyses as bounding cases on the flow within the nozzle. Note that accounting for chemical kinetics within the nozzle would result in a flow that is in between the two extremes of frozen flow and equilibrium flow. Although including chemical kinetics would result in the most accurate modeling of the flow in the nozzle, it would require the modification of the ZND program to handle variable area flow. This was left as an area for future work.

For equilibrium flow the conditions at the exit of the nozzle were: a temperature of 1709.54 K, a specific volume of 4248.6 m^3/kg, and a static enthalpy of -1.320 MJ/kg. Having obtained the state at the exit of the nozzle, it was then possible to compute the nozzle exit velocity

from conservation of total enthalpy between the detonation wave and the nozzle exit. The exit velocity was 6957.07 m/s. From this an exit-to-throat area ratio of 196.07 is obtained. The nozzle exit velocity also yields a specific thrust of 274.67 m/s, where specific thrust is defined as the difference between the nozzle exit and free-stream velocities. The air specific impulse (defined as specific thrust divided by the gravitational acceleration) was found to be 28.01 sec.

For frozen flow the conditions at the exit of the nozzle were: a temperature of 715.51 K, a specific volume of 2025.9 m^3/kg, and a static enthalpy of 58.66 kJ/kg. This resulted in a nozzle exit velocity of 6755.99 m/s, which yields a specific thrust of 73.604 m/s, an air specific impulse of 7.506 sec, and a nozzle exit-to-throat area ratio of 97.257. Thus, the frozen flow analysis results in a much lower specific thrust than the equilibrium analysis (about one fourth). It also results in a lower area ratio. This clearly indicates that frozen flow in the nozzle represents the lower bound on the performance of the engine.

Both specific thrust and air specific impulse are quite low even for the equilibrium analysis. This indicates that in order to obtain any useful thrust out of this engine, very large mass flow rates would have to be employed, which implies a very large engine. Large engines

are not only heavy, but they also incur a substantial drag penalty. However, it is felt that the use of a fuel-rich mixture would result in substantial increases in thrust. This is because a hydrogen-rich mixture would result in a product mixture with a much lower molecular weight. The nozzle exit velocity is roughly proportional to the square root of the ratio of the combustor total temperature to the molecular weight. Thus, the net effect of decreasing the molecular weight of the product gases is an increase in the nozzle exit velocity. Using a rich mixture does not result in a lower combustor temperature for the case of hydrogen because the maximum adiabatic flame temperature for hydrogen-air mixtures is obtained with a rich mixture (about 20% mole percent excess hydrogen).

Several off design points were investigated. Since they all have nozzles that expand the product gases to ambient pressure, they are not really off-design points. Rather, they are alternate design-points. The states at each station within the engine for each of these design points are shown in Appendix F. The appendix shows both the frozen as well as the equilibrium result for the nozzle exit state. For the M=10 and an altitude of 50000 feet case, the total velocity downstream of the detonation wave is subsonic. The general trend is that as both the flight Mach number and altitude increase, both the specific thrust

and air specific impulse drop. The largest exit-to-throat area ratio is for the original design point of M=20 and an altitude of 150000 feet. As the flight Mach number increases, the total pressure recovery factor across the detonation wave increases from 1.2% for the M=10 case, to 53.3% for the M=25 case. This is as expected, since as the flight Mach number increases, the tangential component of velocity increases while the normal component stays constant. Since there is no total pressure drop associated with the tangential velocity, the net effect is a reduction in the total pressure loss across the detonation wave.

The entropy rise across the inlet increases with flight Mach number. The entropy increase across the inlet rises from 2.203 kJ/kg-K for the M=10 case, to 4.088 kJ/kg-K for the M=25 case. This is to be expected. Since the wave angles of the inlet are held constant, a higher free stream Mach number results in a higher normal Mach number and thus in a stronger shock with a higher entropy rise.

A parametric study of the effect of varying each of the altitude and the flight Mach number while keeping the other constant was beyond the scope of this thesis. A single trajectory was investigated, and figure (76) shows the variation of the specific thrust with altitude for that particular trajectory for the assumption of equilibrium flow in the nozzle. The specific thrust drops with

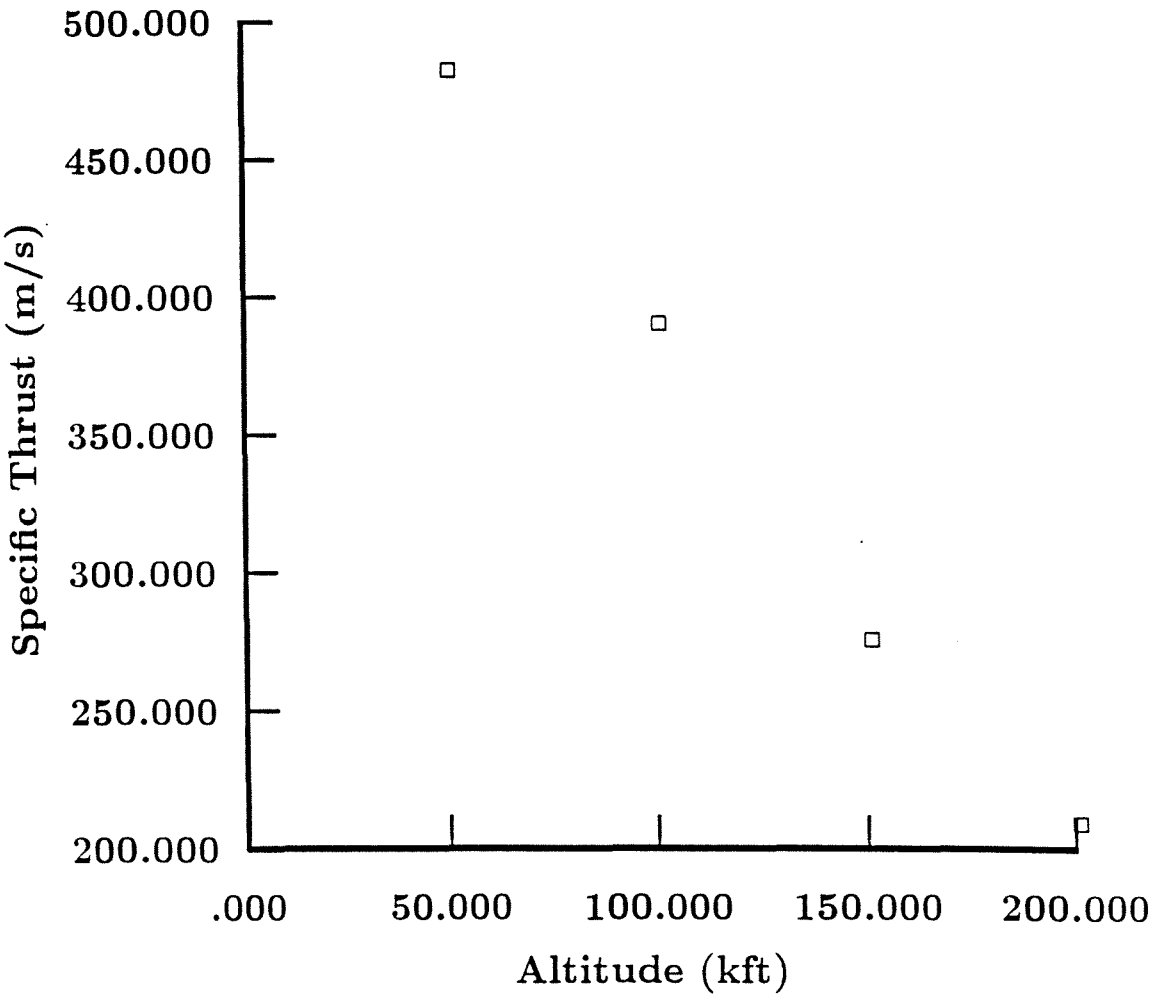

Figure 76. Specific thrust as a function of altitude along the selected trajectory.

increasing altitude. However, the figure does not permit any generalizations about the effect of increasing the altitude while keeping the flight Mach number constant.

It is more meaningful to relate the specific thrust to a more general quantity that is a function of both altitude and flight Mach number and is approximately the same for similar types of trajectories. The loading factor is such a quantity, and it is defined as the product of half the density and the square of the flight velocity. Since this quantity multiplied by the drag coefficient and the reference area yields the net drag, the loading factor is a useful measure of the aerodynamic loading to which the engine will be subjected. Since the drag coefficient drops slightly with flight Mach number for hypersonic flight, and the exit area increases drastically with increasing flight Mach number, it was felt that the loading factor should drop with increasing flight Mach number. This was the rationale behind the selection of the various design points. Figure (77) shows the variation of specific thrust with the loading factor for equilibrium nozzle flow. The specific thrust increases with increasing loading factor. This makes sense since a higher loading factor implies a larger drag force, and therefore a larger specific thrust is required to propel the engine forward.

An analysis was made with the original design point but with a combustion wedge that would set up a detonation

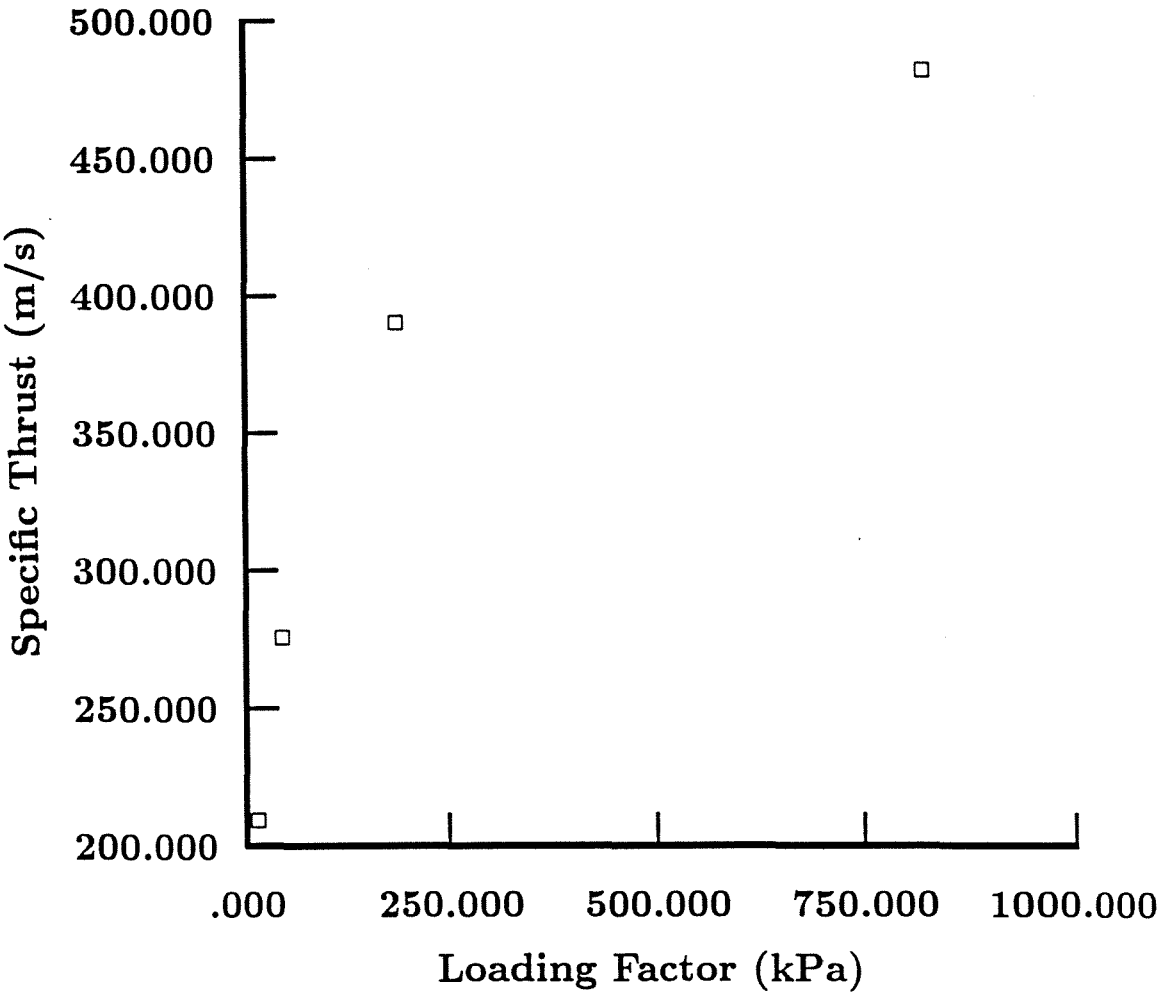

Figure 77. Specific thrust as a function of the loading factor, Q, along the selected trajectory.

at or beyond the cross-over point. The thermodynamic variables at each station in the engine for this analysis are shown in Appendix G. Again, the appendix shows the nozzle exit state for both the equilibrium and frozen flow assumptions. Figures (78) and (79) show the variation of the specific thrust with the overdrive parameter for equilibrium and frozen nozzle flows, respectively. The cross-over point corresponds to an overdrive parameter of 1.3843. As expected, the maximum specific thrust is obtained for the CJ case where the overdrive parameter is equal to 1.0. The specific thrust drops with increasing overdrive. The drop is gentle at first but then becomes quite steep. The specific thrust becomes negative for an overdrive parameter of about 2.3 for equilibrium nozzle flow. For frozen nozzle flow, the specific thrust becomes negative at a lower overdrive parameter of 1.3940. This confirms the doubts raised earlier in this thesis about the useful upper limit on the overdrive of oblique detonation waves for propulsion purposes. Figure (78) also seems to justify the selection of a point between the C-J point and the cross-over point for the operation of the engine since the drop in specific thrust is not that drastic when the overdrive parameter is increased from 1.0 to 1.3843.

It is interesting to note that although the cross-over point constitutes the upper limit on the overdrive for the frozen nozzle flow, this is not the case for

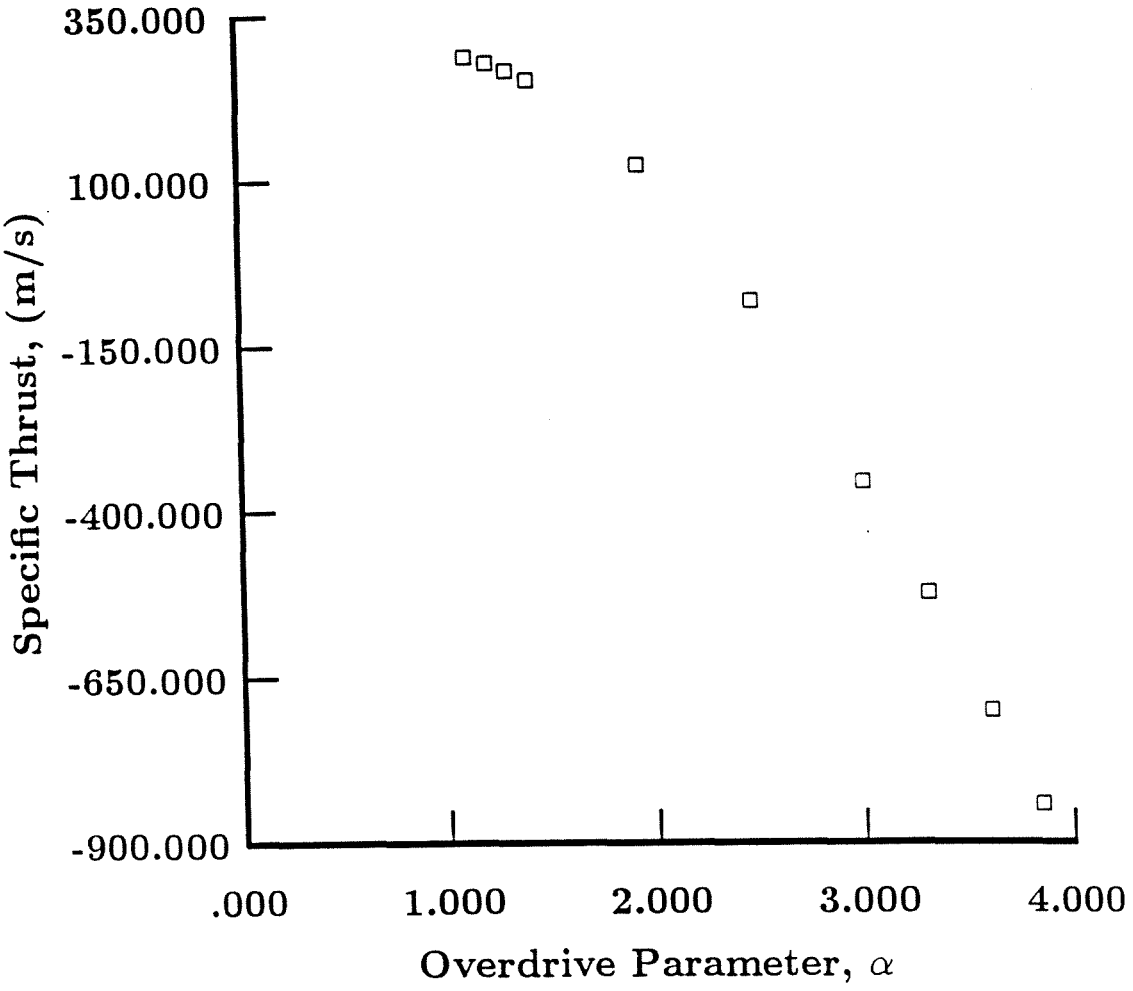

Figure 78. Variation of specific thrust with the overdrive parameter for the design point with a free-stream Mach number of 20 and an altitude of 150 kft.

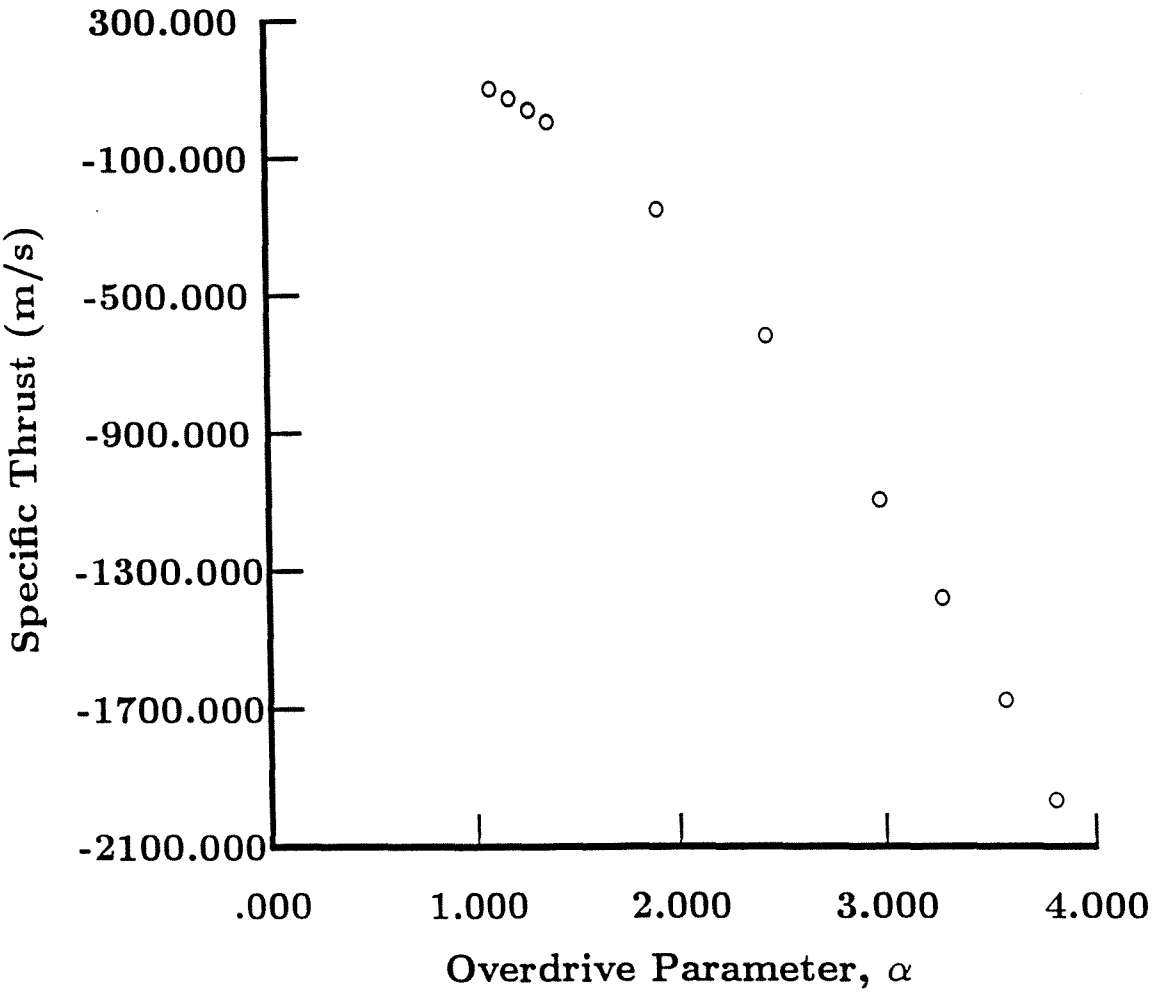

Figure 79. Variation of specific thrust with the overdrive parameter for the design point with a free-stream Mach number of 20 and an altitude of 150 kft, assuming frozen flow in the nozzle.

equilibrium nozzle flow. For the latter it is possible to obtain positive specific thrust upto an overdrive parameter of 2.3. The fact that the temperature drops instead of increases within the reaction zone could lead to the initial conclusion that the addition of fuel to this hypersonic flow does not yield anything useful from a propulsive standpoint. This would imply that the detonation wave could just as well be replaced by a non-reacting shock wave. However, the positive specific thrust obtained beyond the cross-over point clearly shows that this argument is in error. The detonation wave plays a very important role in conjunction with the nozzle. The detonation wave provides the dissociated species which could then recombine to form stable products and release energy. Such species cannot be produced unless fuel is added to the flow. However, since the temperature downstream of the detonation wave is so high, the recombination reactions do not take place except in the nozzle when the temperature drops low enough due to the expansion of the product gases. The recombination reactions result in species with large negative heats of formation (mainly water molecules) which results in a lower enthalpy, and thus in a higher exit velocity which in turn results in a positive specific thrust. In a sense, the nozzle comprises a substantial portion of the reaction zone for post-cross-over detonative scramjets. The specific thrust does not become negative until the detonation wave

becomes so overdriven that the nozzle inlet temperature becomes too high and never drops low enough within the nozzle to allow for recombination reactions.

Thus, the cross-over point costitutes the limit on overdrive only for scramjets with frozen nozzle flow. Thus, it is possible to obtain positive specific thrust for chemically reacting nozzle flow even beyond the cross-over point up to a critical value of the overdrive parameter.

PART 5

DISCUSSION AND CONCLUSIONS

Frozen and equilibrium Hugoniots were obtained for a variety of hydrogen-air detonations corresponding to different free stream compositions, temperatures and pressures. The cross-over points were identified for each set of Hugoniots. For each set of Hugoniots, oblique detonation polars were generated which corresponded to various free stream Mach numbers. If possible, the deflection angle corresponding to the cross-over point was identified. The importance of the cross-over point lies in the fact that the pressure and specific volume after the non-reactive shock wave are the same as those downstream of the reaction zone of the detonation wave. It also roughly corresponds to the overdrive parameter at which a detonative scramjet with frozen nozzle flow would have a specific thrust of zero. Beyond the cross-over point, the fluid has to cool down behind the shock wave since the post shock temperature is too high. This results in a von-Neumann "well" rather than a von-Neumann spike.

The comparison between the generated detonation wave polars and reaction zone structures on the one hand and those found in reference (10) on the other clearly shows a serious discrepancy. Such discrepancies could have been easily detected by the authors if they bothered to make equilibrium computations. This tendency of rushing to

conclusions without attempting to make sure that they agree with the most basic conditions is becoming all too common in the field of computational analyses. The main cause of the discrepancy in the case of reference (10) probably lies in the fact that the reaction zone was not modeled with a fine enough resolution. Since very rapid energy release occurs in the reaction zone, poor resolution could lead to inaccurate temperature values. Since the reaction rates are strong functions of temperature, the error in temperature leads to an error in the heat release which in turn leads to further error in temperature. This cycle leads to non-physical results.

Some general conclusions can be made about the effect of increasing the free stream Mach number for a given upstream state. The effect on the polars is that a cross-over point appears at the beginning of the top branch. As the free stream Mach number is increased further, the cross-over point rapidly moves along the top branch and then, more slowly, down the lower branch.

Increasing the free stream Mach number for a given wedge angle corresponds to moving down the equilibrium Hugoniot. A reaction zone structure similar to that of a C-J detonation is maintained until the cross-over point is reached. This structure consists of a post-shock von-Neumann spike followed by a drop in pressure at a decreasing rate. This is accompanied by a post-shock jump

in temperature followed by a short induction zone, then a rapid increase in temperature through the reaction zone, and finally a leveling off of temperature. The rapid increase in temperature corresponds to the maximum rate of heat release which is mainly due to the formation of the water molecules.

For the cross-over point, the reaction zone structure is significantly different. The rate of heat release has two peaks and a dip. The first peak corresponds to a leveling off in temperature which is due mostly to the formation of the water molecules. The formation of water in this case does not increase the temperature since the thermal and kinetic components of the energy of the flow are so large that the chemical heat release becomes negligible by comparison.

The dip in the rate of heat release corresponds to the continuing decline in temperature. This is caused by the leveling off of the formation of the free radicals which have large positive heats of formation.

The water formed for the cross-over point is a small quantity compared to pre-cross-over reaction zones. This is due to the fact that the very high temperature does not favor exothermic reactions. Instead, endothermic reactions like the dissociation of H_2 and O_2 into H and O are what predominate until the temperature drops low enough.

The second peak in sigma corresponds to the final

rise of temperature. This corresponds to the leveling off of the mole fraction of OH radical, and a slight decrease in the concentration of the H and O atoms. It also corresponds to a slight rise in the concentrations of H_2 and O_2. Since the hydrogen and oxygen molecules have much lower heats of formation than the free radicals, the net result is an increase in temperature.

For post-cross-over points the reaction zone structure is of the same form as for the cross-over point. The only difference is that there is no second peak in either the temperature or sigma. Both profiles asymptotically approach their equilibrium values without overshoot.

The maximum value of sigma should not be used as the criterion for evaluating the reaction zone length. This is because for post-cross-over cases the maximum value of sigma is zero which corresponds to the length required to achieve equilibrium. The first peak in sigma or the integral of sigma should be used for the determination of the reaction zone length. To determine the maximum reaction zone length (which is critical for combustor design), the location at which the temperature is within 1% of the equilibrium value (or some other value based on approaching equilibrium) should be used.

The total pressure recovery factor for detonation waves behaves in the same manner as for non-reacting shock

waves. The total pressure recovery factor becomes smaller for stronger waves (higher upstream normal Mach number). This is true for both normal waves with increasing free stream Mach number, or oblique waves with constant free stream Mach number and increasing wedge angle. The only difference between the shock waves and detonation waves is that the total pressure recovery factor for detonations is lower than for shock waves. This is due to the fact that the although the chemical reaction results in a rise in the total temperature it also results in a drop in the static pressure downstream of the detonation wave. The drop in the static pressure more than offsets the increase in the total temperature and thus the net result is a larger drop in the total pressure. It is felt that a rigorous analysis of the stagnation state downstream of a detonation wave must make use of the Gibbs free energy instead of just the entropy. This is because the flow across the detonation wave is neither adiabatic nor frozen. Thus both the chemical and thermal components of the enthalpy will change across the wave. This means that a thermodynamic variable that includes both enthalpy and entropy changes is required for a proper analysis. The Gibbs free energy is precisely such a variable.

The total pressure drops across detonation waves cast serious doubt over the use of such waves for propulsion. Such total pressure losses more than offset any increases

in the total pressure recovery factor for the inlet diffuser which result from the elimination of the need to drastically decelerate the incoming flow before it enters the combustor.

If a detonative scramjet is to be produced, it will most likely require the use of variable geometry for both the inlet diffuser as well as the detonation wedge. Variable geometry for the latter is particularly important since the CJ detonation and cross-over velocities are both quite sensitive to the conditions upstream of the wave. The operating normal velocity component (which is determined by the wedge angle) could be taken as the average of the CJ detonation velocity and the cross-over velocity. Thus, the upstream normal velocity component can be adjusted only by adjusting the wedge angle so as to achieve the desired operating point. Operating the engine at a point beyond the cross over point results in lower specific thrust. In fact, if the flow within the nozzle is assumed to be frozen, the specific thrust will become zero very slightly above the cross-over point. For equilibrium nozzle flow, the range of operation is considerably extended (upto an overdrive parameter of about 2.3 for stoichiometric hydrogen-air mixtures). The addition of fuel to the flow plays an important role even for post-cross-over cases. The addition of fuel permits the formation of dissociation products which later recombine in the nozzle to form products with

low heats of formation. This reduces the enthalpy of the flow and thus increases the nozzle exit velocity and specific thrust. The recombination reactions take place in the nozzle because the temperature downstream of the detonation wave is too high and remains so until it drops within the nozzle due to expansion. If the operating point is far enough from the cross-over point (an overdrive parameter larger than about 2.3 for stoichiometric hydrogen-air mixtures) then the specific thrust will become negative.

The specific thrust developed by a scramjet using an oblique detonation wave for a combustor is quite low, even if the flow within the nozzle is assumed to be in equilibrium. There is concern that the specific thrust is so low that the engine will not be able to overcome its own drag, let alone propel a vehicle. However, it is possible that the use of a hydrogen-rich mixture might result in a higher nozzle exit velocity which in turn results in a higher specific thrust. The specific thrust decreases as the loading factor decreases. Accompanying trends are an increase in the total pressure recovery factor across the detonation wave, and an increase in the entropy rise across the inlet.

PART 6

RECOMMENDATIONS FOR FUTURE WORK

The nature of this thesis work was mostly exploratory. A future step might be a more systematic effort to obtain Hugoniots and polars for specified ranges of initial conditions and compiling the results in graphical form. This would be done by means of a parametric study, in which one variable at a time is changed while the other variables are held constant. The variables would include the pre-detonation temperature, pressure, and Mach number, the type of combustible mixture, and the equivalence ratio. Such a parametric study could also be useful for the analysis of the individual effects of increasing the altitude and flight Mach number on the performance of a detonative scramjet.

Another area for future work is the off-design performance of the detonative scramjet. Such work would involve the computation of the inlet diffuser angles, the detonation wedge angle, and the nozzle exit-to-throat area ratio for optimum performance at various points along the trajectory of the vehicle using such an engine. Four such points have been obtained in this thesis, but many more points are required to compile correlations that could be programmed into an on-board computer which would adjust the geometries to obtain the desired performance.

Another interesting area would be the investigation

of the effect of various equivalence ratios and fuels on engine performance. For hydrogen fuel, the equivalence ratio is particularly important since it is felt that the use of a hydrogen-rich mixture could result in higher nozzle exit velocities and thus in higher specific thrust.

A more rigorous analysis of the total pressure recovery factor for reacting flows should be carried out using the change in the Gibbs free energy across detonation waves.

The computer code ZND.FOR should be modified to handle varying area reacting flow so as to obtain a more realistic model of the flow within the nozzle instead of dealing with the two extremes of frozen and equilibrium flows.

It is also important to carry out an analysis of the stability characteristics of oblique detonation waves. Unlike normal detonation waves, the characteristics for oblique detonation waves are skewed instead of parallel behind the reaction zone which could result in instability.

Finally, and perhaps most important, an analysis should be carried out to investigate the interaction between the detonation wave and boundary layers on the walls of the wedge. Since viscous effects drastically affect the characteristics of non-reacting shock waves, one might suspect that viscous effects cannot be neglected in the case of detonation waves either.

PART 7

LITERATURE CITED

1. Chapman, D. L.; Philos. Mag. **47**, p.90; 1899.

2. Jouget, E.; "Mechanique des Esplosifs"; Dorn; Paris; 1917.

3. Fletcher, E. A.; Dorsch, R. G.; and Gerstein, M.; "Combustion of Aluminum Borohydride in a Supersonic Wind Tunnel"; NACA RM E55D07a, June, 1955; declassified April, 1958.

4. Nicholls, J. A., Dabora, E. K., and Gealer, R. L.; "Studies in Connection with Stabilized Gaseous Detonation Waves"; Seventh Symposium on Combustion; pp. 144-150; Butterworths Scientific Publications; London; 1958.

5. Gross, R. A., and Chinitz, W.; " A Study of Supersonic Combustion"; J. of Aero/Space Sci.; July 1960.

6. Liu, J. C.; Liou, J. J.; Sichel, M. ; and Kauffman, C. W.; "Diffraction and Transmission of a Detonation into a Bounding Explosive Layer"; 21st Symposium (International) on Combustion; The Combustion Institue; 1986; pp.1639-1647.

7. Ficket, W. and Davis, W. C.; Detonation; University of California Press; Berkley, California; 1979.

8. Liou, J. J.; "Analysis of the Wave Interaction between a Propagating Gaseous Detonation and a Bounding Explosive Layer"; PhD Thesis at the University of Michigan; 1986.

9. Pratt, D. T.; Humphrey, J. W.; and Glenn, D. E.; "Morphology of a Standing Oblique Detonation Wave"; AIAA-87-1785; AIAA/SAE/ASME/ASEE 23rd Joint Propulsion Conference; San Diego, California; June 29-July 2, 1987.

10. Cambier, J., Adelman, H. G., and Menees, G. P.; "Numerical Simulations of Oblique Detonations in Supersonic Combustion Chambers"; J. Propulsion; 5 No. 4; pp. 482-491; July-August 1989.

11. Chuck, C., and Eberhardt, S.; "Numerical Simulation of Hypersonic Oblique Shock-Wave / Laminar Boundary-Layer Interaction with Shock Induced Combustion";

AIAA-90-0149; 28th Aerospace Sciences Meeting; Reno, Nevada; January 8-11, 1990.

12. Fort, J., and Pratt, D.; "Supersonic Flameholding by Attached Oblique Shock Waves"; AIAA-90-0735; 28th Aerospace Sciences Meeting; Reno, Nevada; January 8-11, 1990.

13. Eidelman, S., Grossman, W., and Lottati, I; "Computational Analysis of Pulsed Detonation Engines and Applications"; AIAA-90-0460; 28th Aerospace Sciences Meeting; Reno, Nevada; January 8-11, 1990.

14. Hertzberg, A.; Bruckner, A. P.; and Bogdanoff, D. W.; "Ram Accelerator: A New Chemical Method for Accelerating Projectiles to Ultrahigh Velocities"; AIAA Journal; **26** No.2; February 1988; pp.195-203.

15. Dabora, E. K., Wagner, H. Gg., and Desbordes, D.; "Oblique Detonations at Hypersonic Velocities"; December, 1988.

16. Dabora, E. K., and Wagner, H. Gg.; "A Technique for Establishing Oblique Detonations"; Max-Planck-Institut Für Strömungsforschung; Bericht 102/1988; March, 1988; Göttingen.

17. Sargent, W. H., and Gross, R. A.; "A Detonation Wave Hypersonic Ramjet"; ARS Journal; June 1960; pp. 543-549.

18. Lee, J. H.; "Parameters of Gaseous Detonation"; Ann. Rev. of Fluid Mech. **16**; 1984; pp.311-336.

19. Edwards, D. H.; Walker, J. R.; and Nettleton, M.A.; "On the Propagation of Detonation Waves Along Wedges"; Arch. Comb.; **4**; 1984; p.197.

20. Strehlow, R. A.; Fundamentals of Combustion; Robert E. Kreiger Publishing Co.; New York; 1979.

21. Shepherd, J. E.; Notes on Two-Dimensional Steady Reaction Zone Equations; Rensselaer Polytechnic Institute; Troy, New York; 1988.

22. Liepman, H. W. and Roshko, A.; Elements of Gasdynamics; John Wiley; New York; 1957.

23. Shepherd, J. E. and Westbrook, C. K.; "Detailed Chemical Kinetic Models"; Unpublished Notes on Fuel-Air Detonations; September, 1986.

24. Reynolds, W. C.; "The Element Potential Method for Chemical Equilibrium Analysis: Implementation in the Interactive Program STANJAN; Version 3"; Department of Mechanical Engineering, Stanford University; January, 1986.

25. McBride, B.; NASA-Lewis; Personal communication with Shepherd, J. E.; December, 1989.

26. Kee, R. J.; Rupley, F. M.; and Miller, J. A.; "CHEMKIN II: A FORTRAN Chemical Kinetics Package for the Analysis of Gas-Phase Chemical Kinetics"; Sandia National Laboratories Report SAND90-8009.

27. Hindmarsh, A. C.; "ODEPACK, A Systemized Collection of ODE Solvers"; Vol.1; IMACS Trans. on Scientific Computation; North-Holland, Amsterdam; 1983; pp. 55-64.

28. Oates, G. C.; Aerothermodynamics of Gas Turbine and Rocket Propulsion; Revised and Enlarged; AIAA Education Series; 1988.

29. Sabet, A., and Wong, K.; "Design of the Nozzle and Combustor for a Supersonic Combustion Ramjet Using Concepts of Finite Rate Combustion of Hydrogen and Air"; Capstone Senior Mechanical Design Project; The Albert Nerken School of Engineering; The Cooper Union; New York; May, 1989.